

(NASA-CR-169478) *FINITE ELEMENT MODELS, FOR
PREDICTING CRACK GROWTH CHARACTERISTICS IN
COMPOSITE MATERIALS (Virginia Polytechnic
Inst. and State Univ.) 141 p HC AC7/ME A01

83-12213

Unclas
00818

CSCI 11F G3/26

COLLEGE
ENGINEERING

DISTRIBUTION STATEMENT A

Approved for public release
Distribution Unlimited

19960318 007

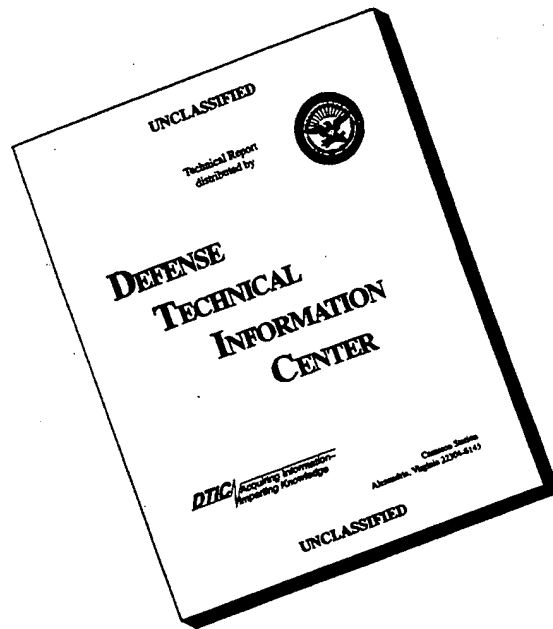


DEPARTMENT OF DEFENSE
CASTIC TECHNICAL EVALUATION CENTER
WASHINGTON, D.C. 20315

PLASTED 443945

DTIC QUALITY INSPECTED 1

DISCLAIMER NOTICE



THIS DOCUMENT IS BEST QUALITY AVAILABLE. THE COPY FURNISHED TO DTIC CONTAINED A SIGNIFICANT NUMBER OF PAGES WHICH DO NOT REPRODUCE LEGIBLY.

College of Engineering
Virginia Polytechnic Institute and State University
Blacksburg, VA 24061

VPI-E-82-29

October, 1982

Finite Element Models for Predicting Crack Growth
Characteristics in Composite Materials

Matthew B. Buczek¹
Carl T. Herakovich²

Department of Engineering Science & Mechanics

Interim Report 31
The NASA-Virginia Tech Composites Program

NASA Cooperative Agreement NCC1-15

Prepared for: Materials Processing and Applications Branch
National Aeronautics & Space Administration
Langley Research Center
Hampton, VA 23665

¹Graduate student
²Professor of Engineering Science & Mechanics

BIBLIOGRAPHIC DATA SHEET		1. Report No. VPI-E-82-29	2.	3. Recipient's Accession No.
4. Title and Subtitle FINITE ELEMENT MODELS FOR PREDICTING CRACK GROWTH CHARACTERISTICS IN COMPOSITE MATERIALS			5. Report Date October 1982	
			6.	
7. Author(s) M. B. Buczek and C. T. Herakovich			8. Performing Organization Rept. No. VPI-E-82-29	
9. Performing Organization Name and Address Virginia Polytechnic Institute & State University Engineering Science & Mechanics Blacksburg, Virginia 24061			10. Project/Task/Work Unit No.	
			11. Contract/Grant No. CA NCC1-15	
12. Sponsoring Organization Name and Address National Aeronautics & Space Administration Langley Research Center Hampton, Virginia 23665			13. Type of Report & Period Covered	
			14.	
15. Supplementary Notes				
16. Abstracts				
<p>② Two dimensional and quasi-three dimensional, linear elastic finite element models for the prediction of crack growth characteristics, including crack growth direction, in laminated composite materials are presented. Mixed-mode crack growth in isotropic materials, unidirectional and laminated composites is considered.</p> <p>The modified crack closure method is used to predict the applied load level for crack extension and two new failure theories, modifications of the point stress and the Hashin failure criteria, are proposed to predict the direction of crack extension in composites. Comparisons are made with the Tsai-Wu failure criterion and the Sih strain energy density criterion as well as with experimental results. It is shown that the modified versions of point stress and Hashin criteria compare well with experiment.</p> <p style="text-align: right;"><i>Author, modified</i></p>				
17. Key Words and Document Analysis. 17a. Descriptors				
composites, fracture, finite elements, crack direction, strain energy release rate				
17b. Identifiers/Open-Ended Terms				
17c. COSATI Field/Group				
18. Availability Statement Distribution Unlimited			19. Security Class (This Report) UNCLASSIFIED	
			21. No. of Pages 131	
			20. Security Class (This Page) UNCLASSIFIED	
			22. Price	

ACKNOWLEDGEMENTS

This work was supported by the NASA-Virginia Tech Composites Program under NASA Grant CA-NCC1-15. Dr. John G. Davis, Jr. was the technical monitor.

The authors want to express their thanks to professors J. N. Reddy and C. W. Smith for their assistance and advice.

This work constitutes the thesis of the first author for a Master of Science Degree in Engineering Mechanics at Virginia Tech.

TABLE OF CONTENTS

ACKNOWLEDGEMENTS.....	ii
LIST OF TABLES.....	v
LIST OF FIGURES.....	vi
<u>CHAPTER</u>	
1. INTRODUCTION.....	1
1.1 Motivation.....	1
1.2 Literature Review.....	1
1.3 Purpose of the Present Study.....	4
1.4 Basic Assumptions.....	5
1.5 Description of the Finite Element Model.....	5
1.6 Problems Considered.....	6
2. THEORETICAL BACKGROUND.....	10
2.1 Criterion for Crack Extension.....	10
2.1.1 Energy Release Rate Concept.....	10
2.1.2 Modified Crack Closure Approach.....	11
2.1.3 Finite Element Considerations in Computing the Energy Release Rate.....	15
2.2 Criteria for Predicting the Direction of Crack Extension.....	18
2.2.1 Modified Griffith Criterion.....	18
2.2.2 Sih Strain Energy Density Criterion.....	21
2.2.3 Tsai-Wu Failure Criterion.....	27
2.2.4 Modified Point Stress and Hashin Criteria.....	29
2.2.4.1 Modified Point Stress Criterion.....	29
2.2.4.2 Strength, $T_{\phi\phi}$, Along a Given Plane in Anisotropic Materials.....	31
2.2.4.3 Modified Hashin Criterion.....	42
2.2.4.4 Finite Element Considerations in Implementing the Modified Point Stress and Hashin Criteria.....	51
3. RESULTS.....	52
3.1 Isotropic Cases.....	52
3.1.1 Mode-I Crack in an Infinite Plate.....	52

3.1.2	Mixed-Mode Fracture of an Infinite Isotropic Plate.....	58
3.2	Off-Axis, Unidirectional Composite Tension Specimens....	62
3.2.1	Comparison of the Crack-Extension Direction Theories for a 30° Lamina.....	63
3.2.2	Variation of the Modified Point Stress and Hashin Functions for a 30° Lamina.....	65
3.2.3	Crack Extension in Unidirectional Laminates.....	70
3.2.4	Effects of Crack Orientation on the Fracture Characteristics of Unidirectional Laminates.....	72
3.3	Free Edge Crack Growth in Laminated Composite Tensile Specimens.....	77
4.	CONCLUSIONS.....	88
	REFERENCES.....	90
<u>APPENDIX</u>		
A	Linear Elastic Finite Element Relations.....	93
B	Constitutive Relations.....	104
C	Material Properties.....	112
D	Finite Element Meshes.....	113
E	On the Relationship between the Free Edge Stresses and Direction of Crack Extension for Angle Ply Laminates.....	117
F	CLFM2D Input Data Sequence.....	120

~~PRECEDING PAGE BLANK NOT FILMED~~

LIST OF TABLES

<u>Table</u>		<u>Page</u>
3.1	Finite Element Energy Release Rate Predictions for a Mode-I Crack in an Infinite Plate.....	56
3.2	Comparisons of the Theoretical and Finite Element Predicted Stress Intensity Factors for a Mode-I Crack in an Infinite Plate.....	57
3.3	Finite Element Crack Extension Predictions for Unidirectional Laminates.....	71
3.4	Influence of Crack Position on the Fracture Characteristics of 30° Unidirectional Laminates.....	74
3.5	Influence of Specimen Aspect Ratio on the Fracture of 30° Unidirectional Laminates.....	75
3.6	Influence of crack Orientation on the Fracture Characteristics of 30° Unidirectional Laminates.....	76

LIST OF FIGURES

<u>Figure</u>		<u>Page</u>
1.1	Edge Replica of a $[(\pm 30)_2]_S$, Tensile Specimen.....	2
1.2	Isotropic Crack Problems Considered.....	7
	a. Mode-I Crack in an Infinite Plate	
	b. Mixed-Mode Crack in an Infinite Plate	
1.3	Composite Crack Problems	9
	a. Crack in a Unidirectional Tensile Specimen	
	b. Transverse Crack in a Laminated Tensile Specimen	
2.1	States of Crack Closure.....	12
	a. State 1	
	b. State 2	
	c. State 3	
2.2	Crack Coordinate System.....	14
2.3	Mode-I Cracks in a Fibrous Material.....	20
	a. Extension Parallel to Fibers	
	b. Extension Perpendicular to Fibers	
2.4	Finite Element Representation of a Crack with Seven Possible Extension Directions.....	22
2.5	Crack Tip Coordinate System of the Strain Energy Density Theor.....	23
2.6	Modified Point Stress Parameters.....	30
2.7	Unidirectional Laminate with an Arbitrary Crack Present.....	33
2.8	Infinitesimal Stress Elements at (r_0, ϕ)	34
	a. Defined Angles	
	b. Rotation into Material Coordinates	
2.9	Plane Stress $T_{\phi\phi}$ vs. ϕ for Various Values of θ	36
2.10	Free Edge Crack in a Laminated Composite.....	38
2.11	Local to Global Strength Transformations.....	39
2.12	Free Edge Crack Strength Transformation.....	40
	a. Free Edge Crack with Arbitrary Orientation	
	b. Stress Element at (r_0, ϕ)	

2.13	Free Edge $T_{\phi\phi}$ vs. ϕ for various values of θ'	43
2.14	Composite Laminate with Modified Hashin Parameters.....	45
2.15	Two Dimensional Stress Transformations.....	48
3.1	Finite Element Crack Models.....	53
	a. Full Crack Model	
	b. Mid-Plane Symmetry Model	
3.2	Crack Extension Angle, $-\theta_0$, vs. Crack Inclination Angle, β , for Isotropic Mixed Mode Fracture.....	60
3.3	Predicted and Expected Crack Extensions for a 30° Unidirectional Laminate.....	64
	a. Modified Griffith	
	b. Strain Energy Density	
	c. Tsai-Wu	
	d. Modified Point Stress	
	e. Modified Hashin	
	f. Experimental	
3.4	Normalized Modified Point Stress Ratio vs. ϕ for a 30° Unidirectional Laminate.....	67
3.5	Normalized Modified Hashin function vs. ϕ for a 30° Unidirectional Laminate.....	68
3.6	Laminate Geometry.....	79
	a. Front Face	
	b. Free Edge	
3.7	Possible Crack Types on the Free Edge of a Cross-Ply Laminate.....	82
3.8	Delamination Crack Growth Model.....	83
3.9	Cross-Ply Transverse Crack Growth Sequence.....	84
3.10	G vs. α Curve for Transverse Crack Growth in a Cross-Ply Laminate.....	86
A.1	Global and Local Coordinate Systems - 4 Node, Isoparametric Element.....	94
B.1	Material and Global Coordinate Systems for a General Laminate.....	105
B.2	Material and Global Coordinate Systems for a Two- Dimensional Lamina.....	109

D.1	306 Element x 338 Node Finite Element Mesh.....	114
D.2	68 Element x 82 Node Finite Element Mesh.....	115
D.3	132 Element x 150 Node Finite Element Mesh.....	116
E.1	Principal Plane Orientation vs. Plane of Crack Extension for Angle-Ply Laminates.....	119
	a. $[90_2/0_2]_s$	
	b. $[10_2/-10_2]_s$	
	c. $[30_2/-30_2]_s$	
	d. $[45_2/-45_2]_s$	
F.1	Local Node Numbers and Stress-Strain Output Locations...	125
F.2	Coordinate System and Orientation of Material Principal System.....	126
F.3	Nodes Defining Crack Tip.....	129

Chapter 1

INTRODUCTION

1.1 Motivation

A problem of considerable and increasing importance within the field of composite materials is the fracture of laminated composite structures. The anisotropy of the material greatly complicates even the simplest of problems. An example of a complicated problem is the edge replica of Fig. (1.1); it demonstrates the crack types present on the free edge of a $[+30_2/-30_2]_s$ tensile coupon. From Fig. (1.1) it is apparent that a crack can start out in a transverse mode and turn into a delamination within its growing length. Complexities such as this require in-depth fracture mechanics models which not only predict at what load a crack will extend but also the direction of crack extension. This study was undertaken in an attempt to develop a model with the capability of describing the characteristics of crack growth in composites.

1.2 Literature Review

Smith [1] has discussed limitations of some of the current analytical models for predicting crack growth characteristics in composite materials. Likewise, most of the previous finite element models either involve complex computational procedures or suffer from serious limitations. Some models distinguish between fiber and matrix [2, 3], others use hybrid or singular finite elements [4, 5], and still others assume a

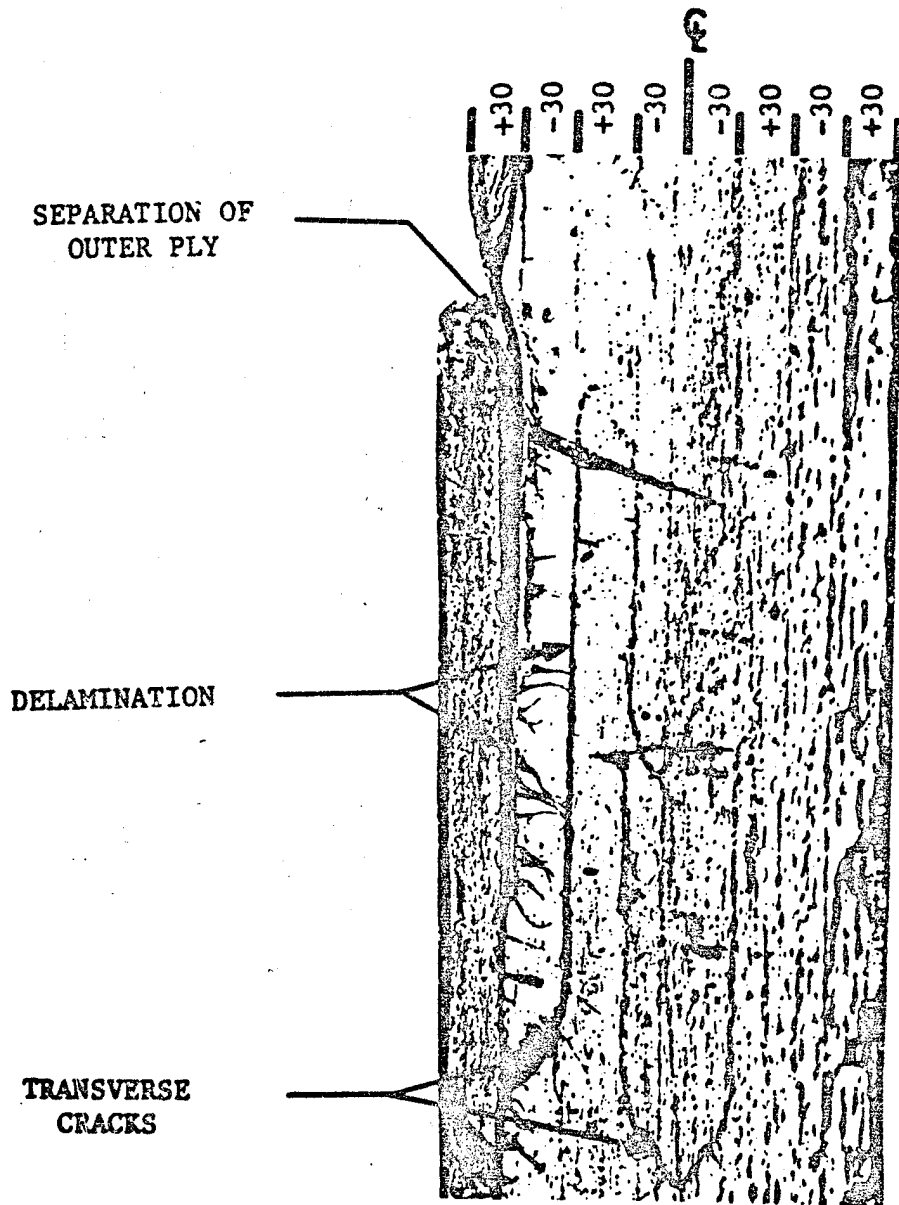


Figure 1.1 Edge Replica Of A $[(\pm 30)_2]_5$ Celson 6000/PMR-15 Graphite-Polyimide Laminate

direction of crack growth [6]. Finite element analyses which require a distinction between the fiber and matrix materials are impractical for most real life situations since the number of degrees of freedom required in such an analysis could easily exceed the capacity of most computers currently available. While the use of singular or hybrid finite elements may give a good representation of the stresses, strains and displacements near a crack tip, they generally require more computation time and they are not well suited to explaining large scale crack growth characteristics. Experimental results [7, 8] have shown that the direction of crack extension can change significantly during crack growth in a laminated composite material. These results limit analyses which assume a direction of crack growth to specialized cases or to small increments of crack growth.

There are many different finite element models that do not require specialized elements. Two such models are the failed element approach of Adams [3], and the modified crack closure approach of Rybicki and Kannien [9]. The failed element approach assumes that when an element in an area of high stress exhausts its strain energy capacity, it fails. From this, it is assumed that a "crack" has formed and has the dimensions of the failed element. This approach has two implications, the most important of which is that a finite amount of material is removed from the system, which in an actual material is not the case. The other is that the crack is not likely to close up on itself in subsequent loading because of its exaggerated width. The modified crack closure technique is based on the crack closure integral and can be used

within the framework of a linear elastic analysis with a relatively coarse mesh. In the modified crack closure technique, the crack closure integral is evaluated directly from the nodal forces and displacements required to close a virtual crack of extension, Δa . The modified crack closure technique also has the advantage of obtaining mode-I, mode-II, and mode-III results in a single analysis.

Few fracture theories predict the direction of crack extension [2], as well as the external load level which causes crack extension. Hashin [10] suggested that a failure criterion could be constructed which would include the plane on which failure would occur. Some of the many fracture/failure criteria which have been used to predict fracture/failure of composite materials include the Sih strain energy density criterion [2], the Tsai-Wu failure criterion [11], the Whitney-Nuismer point stress criterion [12], and the Hashin failure criterion [10]. Of the criteria listed, only the strain energy density criterion [2] and the point stress criterion [12] are readily capable of predicting the direction of crack extension. However, without modification, their use is limited to special cases.

1.3 Purpose of the Present Study

The purpose of this study was to develop a finite element model capable of predicting crack growth characteristics in composite materials. It was desired to develop a model which not only could determine what applied load level would cause crack extension but one which could also determine the direction of crack extension.

1.4 Basic Assumptions

Unless otherwise stated, the model developed was based on the following assumptions:

- (i) Linear elastic, homogeneous isotropic or homogenous orthotropic fibrous composites
- (ii) small displacement theory
- (iii) a crack extends from one end only - one crack at a time
- (iv) no variation of geometry in one of the coordinate directions (i.e., plane stress, plane strain and generalized plane strain problems).

1.5 Description of the Finite Element Model

The finite element model developed uses a two dimensional mesh of four node, linear, isoparametric elements. The model has the capabilities of obtaining either plane strain, plane stress or generalized plane strain solutions. (Refer to Appendix A for a description of the finite element method as it applies to this study.) The material models available include isotropic, orthotropic and laminated orthotropic, (off-axis), materials. (See Appendix B for an explanation of the constitutive relations for the respective material models.)

The approach taken to the solution of the crack problem was to separate the analysis into two main parts. In the first part of the solution the direction of crack growth was determined and in the second part the load level which would cause crack extension was determined.

The crack growth direction was determined through the use of several fracture/failure theories. The theories considered include a modified version of the Griffith criterion [13], the Sih strain energy density criterion [2], the Tsai-Wu failure criterion [11], and modified versions of the Whitney and Nuismer point stress theory [12], and Hashin failure criteria [10]. The failure criteria are described in Chapter 2 and the results are compared with theory and experiment in Chapter 3.

The determination of the load level which would cause crack extension was made through the use of the modified crack closure method [9]. The modified crack closure method, as it applied to this study, is presented in Chapter 2.

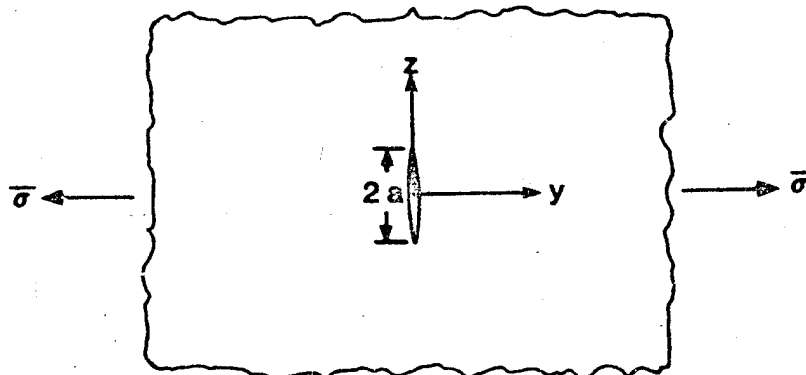
The main reasons behind the choice of this solution approach was that it could be used with a linear elastic analysis, that it could be used with a relatively coarse mesh and that it required a minimum of computer time.

1.6 Problems Considered

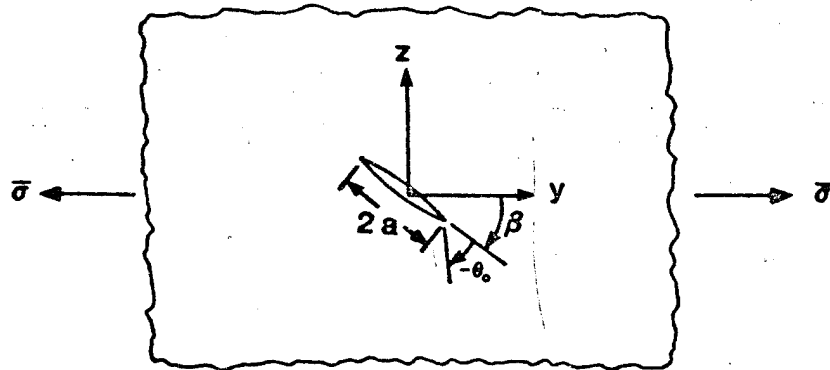
The problems considered in this study were:

- (i) A mode-I crack in an infinite isotropic plate with remote loading of $\bar{\sigma}$, Fig. (1.2a), was considered as a test of the crack closure technique.
- (ii) Mixed mode cracks in infinite plates of isotropic materials, Fig. (1.2b), were analyzed as a test of the crack growth direction, $-\theta_0$, for various angles of crack inclination, β .

ORIGINAL PAGE IS
OF POOR QUALITY



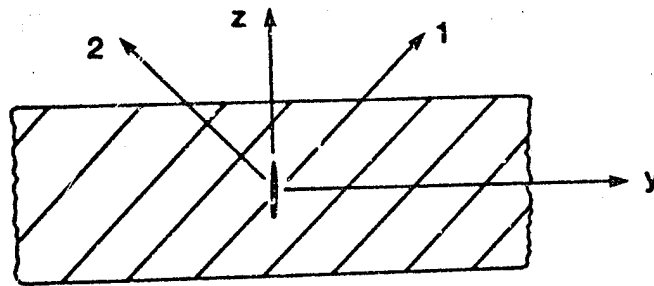
a. Mode-I Crack In An Infinite Plate



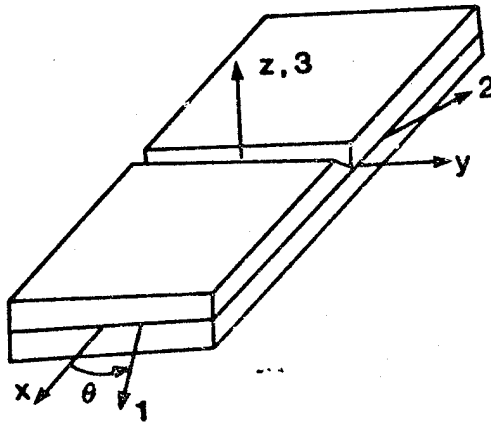
b. Mixed Mode Crack In An Infinite Plate

Figure 1.2 Isotropic Crack Problems Considered

- (iii) Off-axis, unidirectional, orthotropic tensile specimens, Fig. (1.3a), were analyzed for the direction of crack extension in fibrous composites and the results were compared with available experimental results.
- (iv) Transverse cracks were introduced on the free edge of a laminated composite tension specimen, Fig. (1.3b), and the predicted crack paths were compared against available experimental results.



a. Crack In A Unidirectional
Tensile Specimen



b. Transverse Crack In A Laminated
Tensile Specimen

Figure 1.3 Composite Crack Problems
Considered

Chapter 2

THEORETICAL BACKGROUND

2.1 Criterion for Crack Extension

2.1.1 Energy Release Rate Concept

In the Griffith theory of classical fracture mechanics [13], it is assumed that strain energy is released when a crack surface is created in a stressed body. The rate of energy release when a crack extends stably in a body is known as the critical energy release rate, G_c . The critical energy release rate, G_c , can be determined experimentally by a procedure which allows for stable, slow crack extension, (see Ref. [17] for isotropic materials and [6] for composites).

For structures, such as a composite laminate, an existing crack may or may not grow under a given state of stress. To determine whether or not an existing crack will extend, it is necessary to calculate the available energy release rate, $G(a)$, associated with a crack of length a . If the available energy release rate, $G(a)$, is equal to the critical energy release rate, G_c the crack will grow in a stable fashion. If the available energy release rate, $G(a)$, is greater than the critical energy release rate, G_c , the crack grows unstably and if the available energy release rate, $G(a)$, is less than the critical energy release rate, G_c , the crack does not extend. Similarly, the external load which first causes the available energy release rate, $G(a)$, to reach the critical energy release rate value, G_c , is the critical load and loads greater

than the critical load level result in unstable growth while loads less than the critical load level do not extend the crack.

Mathematically, the energy release rate, $G(a)$, for a given crack of initial length, a , is defined as the difference in the total strain energy of the structure, ΔU , before and after a small crack extension, Δa , is introduced, that is,

$$G(a) = \lim_{\Delta a \rightarrow 0} \frac{\Delta U}{\Delta a} \quad (2.1)$$

2.1.2 Modified Crack Closure Approach

Irwin [14] contended that if a crack extends by a small amount, Δa , the energy released in the process is equal to the work required to close the crack back to its original length. This statement in equation form is

$$G(a) = \lim_{\Delta a \rightarrow 0} \frac{1}{2\Delta a} \int_0^{\Delta a} \vec{\sigma} \cdot \Delta \vec{u} \, da \quad (2.2)$$

where $\vec{\sigma}$ is the surface traction vector and $\Delta \vec{u}$ the displacement vector required to close the crack back to its original length.

The modified crack closure technique of Rybicki and Kannien [9] enables the direct evaluation of the crack closure integral (2.2) and thus the energy release rate through the use of a finite element model. The finite element model starts with the presence of an initial crack of length, a , Fig. (2.1a), with tip at node K . The finite element solution determines the displacement components, \vec{u}_k , (where $\vec{u}_k = (u_k,$

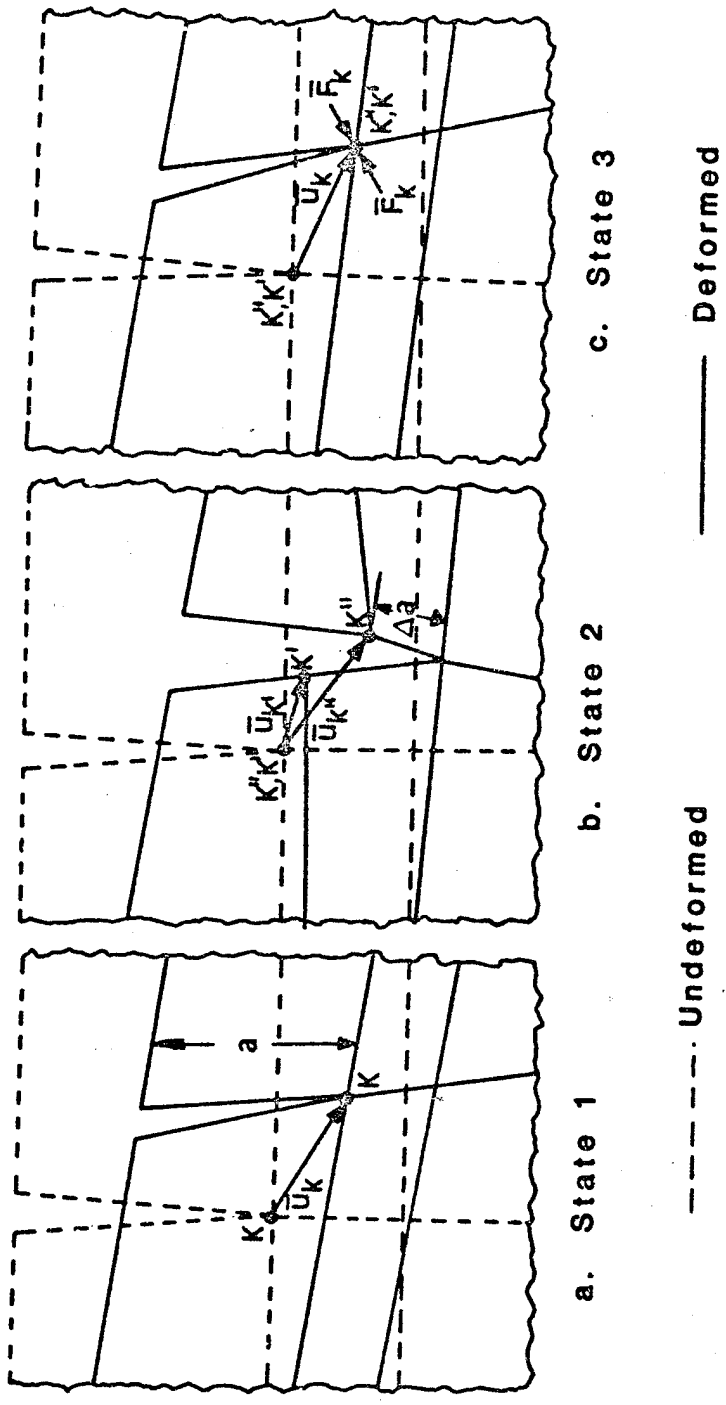


Figure 2.1 States Of Crack Closure

v_k, w_k) of the crack tip node K. An incremental crack extension Δa is introduced by replacing the crack tip node K with two separate nodes K' and K'' as shown in Fig. (2.1b). With this new crack geometry taken into account, the finite element solution for the nodal displacements \bar{u}_k' and \bar{u}_k'' are found for nodes K' and K'', respectively, under the same load. The crack extension is then closed by applying equal and opposite forces at nodes K' and K'' such that their common displacements match the displacements found earlier for node K, Fig. (2.1c). These nodal forces can be described by

$$\bar{F}_k \Rightarrow (F_{xk}, F_{yk}, F_{zk}) \quad (2.3)$$

The energy release rate is then given by [9],

$$G(a) = [F_{xk}(u_k' - u_k'') + F_{yk}(v_k - v_k'') + F_{zk}(w_k' - w_k'')] / 2\Delta a \quad (2.4)$$

By resolving the forces and displacements into a "crack coordinate system," Fig. (2.2), the respective fracture mode contributions to the total energy release rate can be determined. That is,

$$G_I(a) = \{ [F_{zk} \cos\phi - F_{yk} \sin\phi] [\cos\phi(w_k' - w_k'') - \sin\phi(v_k' - v_k'')] \} / 2\Delta a \quad (2.5a)$$

$$G_{II}(a) = \{ [F_{yk} \cos\phi + F_{zk} \sin\phi] [\cos\phi(v_k' - v_k'') + \sin\phi(w_k' - w_k'')] \} / 2\Delta a \quad (2.5b)$$

$$G_{III}(a) = \{ F_{xk}(u_k' - u_k'') \} / 2\Delta a \quad (2.5c)$$

ORIGINAL PAGE IS
OF POOR QUALITY,

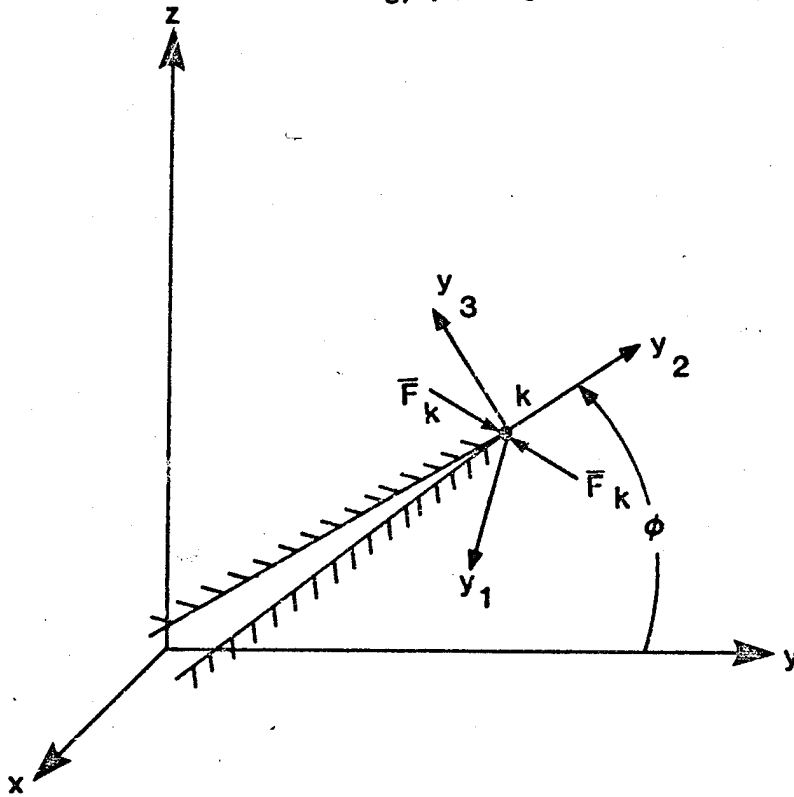


Figure 2.2 Crack Coordinate System

where G_I , G_{II} and G_{III} are the mode-I, mode-II and mode-III contributions to the total energy release rate, G , respectively, i.e.,

$$G(a) = G_I(a) + G_{II}(a) + G_{III}(a) \quad (2.5d)$$

2.1.3 Finite Element Considerations in Computing the Energy Release Rate

As previously mentioned, the energy release rate requires the evaluation of the nodal forces and displacements necessary to close a crack of extended length, $a + \Delta a$, back to its original length, a . The needed displacements are directly obtained from finite element solutions of the initial and extended crack states, Fig. (2.1a) and (2.1b), respectively. However, the calculation of the required forces are not as obvious. Rybicki and Kanninen [9] computed the forces by placing a very stiff "spring" between nodes K' and K'' , then computed the force components in the "spring." This procedure can lead to unnecessary approximation errors. An alternative approach will now be presented. Consider three separate states. State No. 1 represents the loaded initial state, Fig. (2.1a), where node K displaces (u_k, v_k, w_k) . The finite element equations (Appendix A) for State No. 1 can be written as,

$$[K_1]\{\delta_1\} = \{F_1\} \quad (2.6a)$$

where $[K_1]$ is the global stiffness matrix, $\{\delta_1\}$ is the global displacement vector and $\{F_1\}$ is the global force vector for State No. 1. Simi-

larly, State No. 2, Fig. (2.1b), represents the loaded extended state which can be expressed by,

$$[K_2]\{\delta_2\} = \{F_2\} \quad (2.6b)$$

and State No. 3, Fig. (2.1c), represents the loaded separated state with applied forces to hold nodes K' and K'' together - which may be written as,

$$[K_3]\{\delta_3\} = \{F_3\} \quad (2.6c)$$

Since the forces required to hold nodes K' and K'' together are contained within the $\{F_3\}$ vector it is necessary to compute $\{F_3\}$. Since the separated state with applied forces, State 3, Fig. (2.1c), is constrained to displace identical to that of the unseparated state, State 1, Fig. (2.1a), the displacement vector $\{\delta_1\}$ is the same as $\{\delta_3\}$ with the exception of the additional degrees of freedom (i.e., u, v and w displacements) for the new node created by separating the crack tip node into two nodes. Now, if $\{\delta_1'\}$ is defined as being the $\{\delta_1\}$ vector with the additional degrees of freedom it follows that

$$\{\delta_3\} = \{\delta_1'\} \quad (2.6d)$$

where the additional degrees of freedom are specified as being the same as for the initial crack tip node of State 1 since State 3 requires that

the displacements of the separated nodes match those of the unseparated state, State 1. Note that the new node created by separating the crack tip node was numbered as being the crack tip node number plus one and all node numbers greater than the crack tip node were re-numbered as being one plus the node numbers that they had in State 1. This re-numbering procedure guarantees that the half bandwidth will not increase by any more than 2 for plane stress or plane strain and by any more than 3 for generalized plane strain.

The undeformed mesh of the separated state, State 2, Fig. (2.1b) is identical to that of State 3, Fig. (2.1c), and since the stiffness matrices do not change for different loading conditions, it follows that

$$[k_3] = [k_2] \quad (2.6e)$$

Substituting Eqns. (2.6d) and (2.6e) into (2.6c), the solution for $\{F_3\}$ is found to be

$$[k_2]\{\delta_1'\} = \{F_3\} \quad (2.7)$$

Hence, for a growing crack problem, the forces necessary to close the current crack extension are found by simply multiplying the current stiffness matrix by the, modified, previous displacement vector - without the addition of extra steps or the introduction of unnecessary approximation errors. Note that it is not necessary to store the entire $[k_2]$ stiffness matrix. Since $[k_2]$ is a banded matrix, the only contri-

butions to the force necessary to close the crack will come from the elements containing the crack tip node K. Hence, the elemental contributions to the force at node K can simply be summed up to give the total force at node K.

2.2 Criteria for Predicting the Direction of Crack Extension

2.2.1 Modified Griffith Criterion

The Griffith or energy release rate criterion states that a crack will extend when the available energy release rate, $G(a)$, reaches or exceeds the critical energy release rate, G_c [13]. In a crack problem where the crack extension direction is unknown the criterion should be modified to state that crack extension will occur in the direction in which the available energy release rate, $G(a)$, first reaches the critical energy release rate, G_c .

If the critical energy release rate is assumed independent of direction then the direction of crack extension can be taken as the direction of maximum available energy release rate since this would be the direction which would first reach or exceed the critical energy release rate.

Two serious limitations of the modified Griffith criterion, as defined above, are that the critical energy release rate may have a dependence on the mode of fracture in isotropic problems and it also depends on which direction, relative to the material principal coordinates, the crack extends in fibrous materials. As an example of the latter of the two limitations, consider two different mode-I cracks

extending in an anisotropic material. The first crack, Fig. (2.3a), represents a mode-I crack growing parallel to the fibers and the second crack, Fig. (2.3b), represents a mode-I crack growing perpendicular to the fibers. Based on surface energy considerations [13], an approximate relation for the mode-I critical energy release rate, G_{IC} , for an isotropic material is given by

$$G_{IC} = \frac{\pi \sigma_c^2 a}{E} \quad (2.8)$$

where σ_c is the critical applied stress required to cause crack extension and E is Young's modulus. Substituting the ultimate strength of a composite material, (T300/5208 graphite-epoxy), in the transverse direction, Y_T , and the modulus in the transverse direction, E_2 , from Appendix C, into Eqn. (2.8), gives an approximate value for G_{IC} for extension parallel to the fibers, Fig. (2.3a), that is,

$$G_{IC} = \frac{\pi (Y_T)^2 a}{E_2} = 81.2a \quad (2.9a)$$

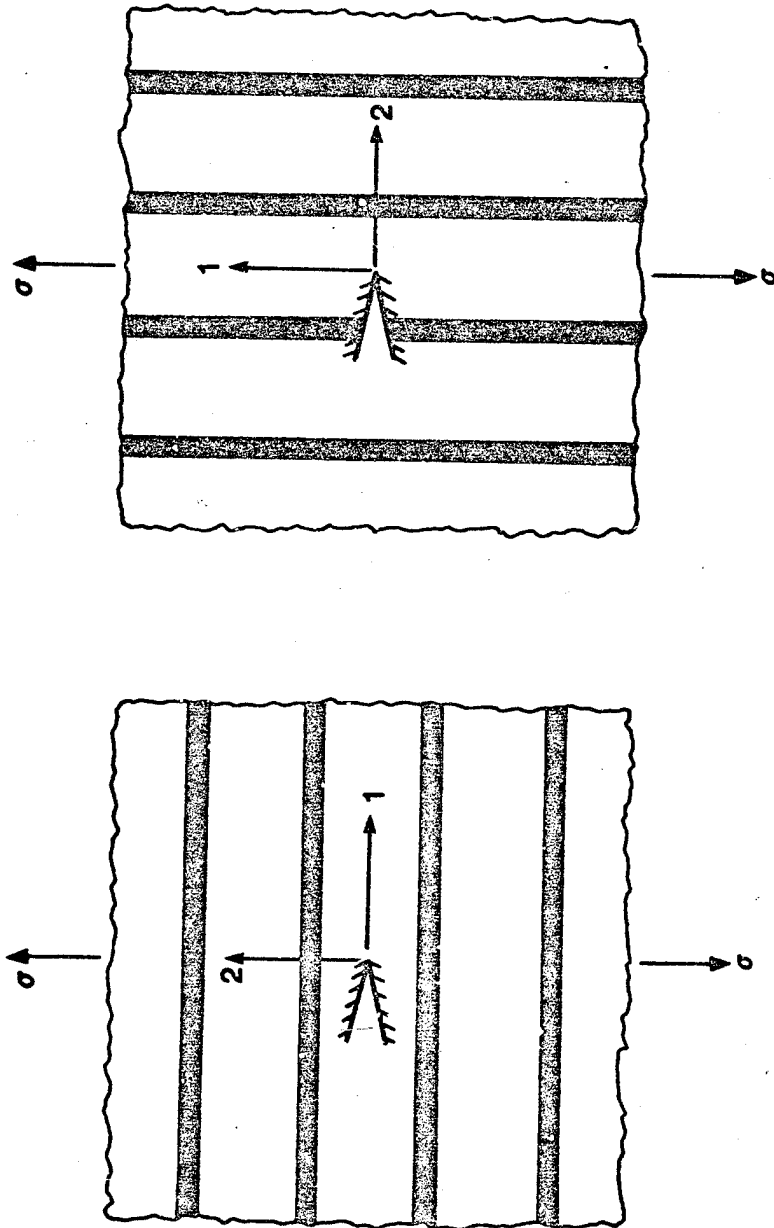
Similarly, for the crack growing perpendicular to the fibers, Fig. (2.3b),

$$G_{IC} = \frac{\pi (X_T)^2 a}{E_1} = 7883a \quad (2.9b)$$

Hence, the critical energy release rate for the crack growing perpendicular to the fibers is roughly two orders of magnitude greater than

ORIGINAL FACE IS
OF POOR QUALITY

20



a. Extension Parallel To Fibers b. Extension Perpendicular To Fibers

Figure 2.3 Mode-I Cracks In A Fibrous Material

that of the crack growing parallel to the fibers.

Another disadvantage of the modified Griffith criterion is that it requires an additional finite element solution for each possible direction that the crack can extend. Referring to Fig. (2.4), for the crack defined by oab there are seven possible directions of crack extension, from o to c, from o to d, from o to e, from o to f, from o to g, from o to h and from o to i. In order to use the modified Griffith criterion, seven independent finite element solutions would be required to compute the seven possible energy release rates. This is obviously time consuming and thus a costly procedure.

2.2.2 Sih Strain Energy Density Criterion

The strain energy density criterion [2, 15] is based on the local value of strain energy density in the vicinity of a crack tip, which is direction sensitive. Crack extension is postulated to occur in the direction of minimum strain energy density when the strain energy density factor, S , (to be defined), attains a critical value, S_c .

For a planar crack in an isotropic material under plane strain, Fig. (2.5), the strain energy density in the vicinity of the crack tip, $\frac{dU}{dV}$, is given as, [15]

$$\frac{dU}{dV} = \frac{1}{\pi r} (a_{11}k_I^2 + 2a_{12}k_I k_{II} + a_{22}k_{II}^2 + a_{33}k_{III}^2) + \text{non-singular terms} \quad (2.10)$$

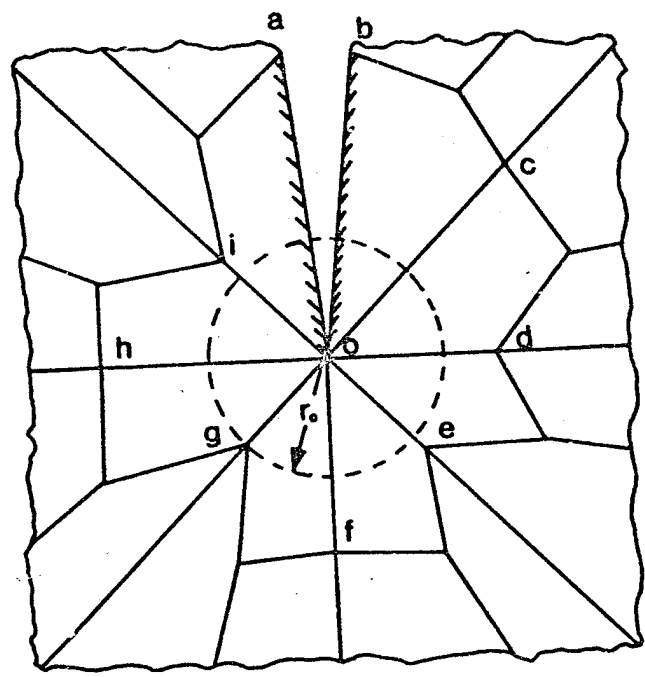


Figure 2.4 Finite Element Representation
Of A Crack With Seven Possible
Extension Directions

ORIGINAL PAGE IS
OF POOR QUALITY

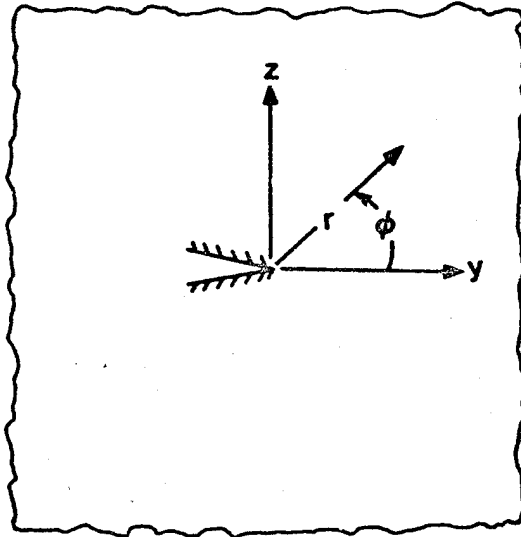


Figure 2.5 Crack Tip Coordinate System Of The
Strain Energy Density Theory

where k_I , k_{II} and k_{III} are the mode-I, mode-II and mode-III stress intensity factors, respectively,

$$a_{11} = \frac{1}{16G} [(3-4\nu-\cos\phi)(1+\cos\phi)] \quad (2.11a)$$

$$a_{12} = \frac{1}{16G} \cdot 2\sin\phi [\cos\phi - (1-2\nu)] \quad (2.11b)$$

$$a_{22} = \frac{1}{16G} [4(1-\nu)(1-\cos\phi) + (1+\cos\phi)(3\cos\phi-1)] \quad (2.11c)$$

$$a_{33} = \frac{1}{4G} \quad (2.11d)$$

and G is the shear modulus of elasticity and ν is Poisson's ratio.

Eqn. (2.10) demonstrates that the strain energy density function possesses a $(1/r)$ singularity at the crack tip. Hence the expression

$$S = (a_{11}k_I^2 + 2a_{12}k_Ik_{II} + a_{22}k_{II}^2 + a_{33}k_{III}^2)/\pi \quad (2.12)$$

represents the intensity of the strain energy density field in the vicinity of the crack tip. The fundamental hypotheses on crack growth in the Sih theory are as follows:

(1) Crack initiation takes place in a direction determined by the stationary value of the strain-energy density factor, i.e.,

$$\frac{\partial S}{\partial \phi} = 0, \quad \text{at } \phi = \phi_0 \quad (2.13)$$

(2) Crack extension occurs when the strain-energy density factor reaches a critical value, i.e.,

$$S_c = S(k_I, k_{II}, k_{III}), \quad \text{for } \phi = \phi_0 \quad (2.14)$$

Exact evaluation of the stresses and strains in the vicinity of the crack tip with the current finite element model is not guaranteed since there exists a geometric singularity at the crack tip which cannot be accurately modeled with the linear-elastic analysis formulated herein. Hence, it is not possible to use the Sih theory to determine when the crack will extend. However, the Sih theory can be used to determine the direction of crack propagation in isotropic materials.

From continuum mechanics [16] it is possible to write an alternative form of the strain energy density at a point in a stressed body, i.e.,

$$\frac{dU}{dV} = \frac{1}{2}(\sigma_{xx}\epsilon_{xx} + \sigma_{yy}\epsilon_{yy} + \sigma_{zz}\epsilon_{zz} + \tau_{yz}\gamma_{yz} + \tau_{xz}\gamma_{xz} + \tau_{xy}\gamma_{xy}) \quad (2.15)$$

Neglecting the non-singular terms in Eqn. (2.10) and substituting in the expression for the strain energy density factor of Eqn. (2.12) gives,

$$\frac{dU}{dV} = \frac{S}{r} \quad (2.16)$$

Combining Eqns. (2.15) and (2.16), an alternative equation for the strain energy density factor, S , is found to be:

$$S = \frac{r}{2} (\sigma_{xx} \epsilon_{xx} + \sigma_{yy} \epsilon_{yy} + \sigma_{zz} \epsilon_{zz} + \tau_{yz} \gamma_{yz} + \tau_{xz} \gamma_{xz} + \tau_{xy} \gamma_{xy}) \quad (2.17)$$

There is one serious limitation to the use of the strain energy density theory in the current study. This limitation is that the theory does not account for the anisotropic strength characteristics of the material. Since such properties must be accounted for in fibrous composites, the Sih strain energy density theory is limited to isotropic material applications. It should be noted that the strain energy density theory has been used in the past to predict crack growth characteristics in composite materials [2]. However, the success of such studies resulted from assuming that the crack was situated entirely within the isotropic matrix between fibers.

The procedure for implementing the strain energy density criterion in the finite element model is briefly described as follows: First, the possible directions of crack extension in the model are identified by the element sides containing the crack tip node, (node-0 in Fig. (2.4)). Second, the stresses and strains are calculated in the adjoining elements at the element corners, (points c thru i in Fig. (2.4)). Third, Eqn. (2.17) is used to calculate the strain energy density factor, S , at the respective points. Last, the crack is assumed to grow in the direction in which S is a minimum.

2.2.3 Tsai-Wu Failure Criterion

Tsai and Wu [11] postulated that a failure surface in stress space exists in the form:

$$F_i s_i + F_{ij} s_i s_j = 1 \quad i, j = 1, \dots, 6 \quad (2.18)$$

where F_i and F_{ij} are strength tensors of second and fourth order, respectively, and s_i represent a contracted form of the stress tensor components in material principal coordinates. For an orthotropic lamina under plane stress conditions, Eqn. (2.18) becomes:

$$\left(\frac{1}{X_T} + \frac{1}{X_C}\right) s_{11}^2 + \left(\frac{1}{Y_T} + \frac{1}{Y_C}\right) s_{22}^2 - \left(\frac{1}{X_T X_C}\right) s_{11}^2 - \left(\frac{1}{Y_T Y_C}\right) s_{22}^2 + \left(\frac{1}{S_{12}}\right) t_{12}^2 + 2F_{12} s_{11} s_{22} = 1 \quad (2.19)$$

where X_T and Y_T represent the tensile strength of the material in the fiber and transverse directions, respectively, X_C and Y_C represent the compressive strengths, S_{12} represents the shear strength in the 1-2 plane and F_{12} is an interaction term which must be determined from a biaxial strength test.

As a failure theory, the Tsai-Wu criterion has several advantages. These advantages include, (1) invariance under rotation of coordinates, (2) transformation via known tensor transformation laws; and (3) symmetry properties akin to those of the stiffnesses and compliances. However, for use in this study, it has two serious limitations. The

first is that it fails to account for differences in creating new fracture surfaces at various angles to the material principal coordinates and second is that it makes no distinction between tensile and compressive failure which could cause the Tsai-Wu criterion to choose a compressive direction of crack propagation.

The Tsai-Wu criterion was incorporated into the finite element model by assuming that the crack would extend in the direction where the value of the Tsai-Wu polynomial reached a maximum. Referring to Fig. (2.4), the stresses, σ_{ij} , are calculated at some fixed distance, r_0 , away from the crack tip at the various locations dictated by the element sides incorporating the crack tip node, (points c thru i in Fig. (2.4)). Next, the values of the Tsai-Wu polynomial were computed at these points through the use of Eqn. (2.19), (for the case of orthotropic plane stress). Last, the crack was assumed to extend in the direction for which the Tsai-Wu polynomial reached a maximum.

The choice of r_0 is arbitrary within certain limitations. These limitations are that r_0 should be greater than zero and less than the longest possible path that the crack extension could take and not extend through more than one element. Referring to Fig. (2.4), if the possible path of crack extension were as shown from node o to c, o to d, o to e, o to f, o to g, o to h or o to i, then r_0 would be limited to that of the segment from o to g since that is the direction of longest possible single element crack extension. Note that it would be impractical to use a distance greater than og since this would require using stresses from an element outside those adjacent to the crack tip.

2.2.4 Modified Point Stress and Hashin Criteria

The criteria for predicting the crack growth direction considered up to this point, in their present form, are all unsatisfactory for anisotropic materials. As pointed out in Sections 2.2.1-3, they all fail to account for differences in the work required to create a new area of crack surface at different directions in an anisotropic material. Since it is imperative that this distinction be accounted for in this study, two new criteria are proposed. The first criterion considered is a modification of the point stress criterion of Whitney and Nuismer [12], and the second is a modification of the Hashin criterion [10].

2.2.4.1 Modified Point Stress Criterion

The point stress criterion of Whitney and Nuismer [12] assumes that failure of a notched laminate occurs when the local stress at a certain distance, r_0 , from the notch tip reaches the strength of the unnotched laminate.

The modified point stress criterion of this study assumes that a crack will grow in the direction of the maximum ratio of normal stress to strength at a certain distance, r_0 , from the tip of an existing crack. Note that this is equivalent to assuming that a crack will grow perpendicular to the plane of maximum tensile stress in an isotropic material. Referring to Fig. (2.6), the normal stress, $\sigma_{\phi\phi}(r,\phi)$, is calculated at some fixed distance, r_0 , away from the crack tip. The stress, $\sigma_{\phi\phi}(r_0,\phi)$, is then divided by the tensile strength of the mate-

ORIGINAL PAGE IS
OF POOR QUALITY

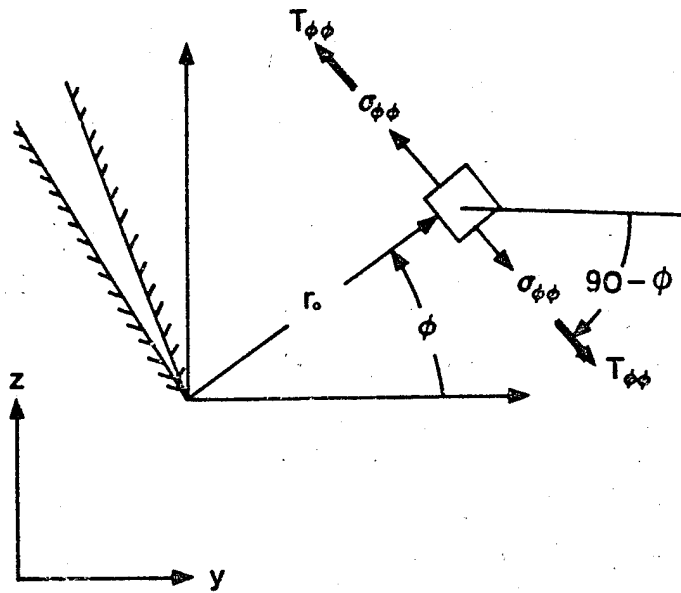


Figure 2.6 Modified Point Stress Parameters

rial, $T_{\phi\phi}(\phi)$, (to be defined), normal to the direction of crack extension. This ratio, $R(r_0, \phi)$, is then used to predict the direction of crack extension by assuming that the crack will extend in the direction for which $R(r_0, \phi)$ reaches a maximum. Quantitatively, the ratio is defined as:

$$R(r_0, \phi) = \frac{\sigma_{\phi\phi}(r_0, \phi)}{T_{\phi\phi}(\phi)} \quad (2.20)$$

The value of r_0 used in this criterion is subject to the same limitations as the value of r_0 in the Tsai-Wu criteria, Section 2.2.3. That is, r_0 should be greater than zero and less than or equal to the longest path of possible crack extension while not extending through more than one finite element.

2.2.4.2 Strength, $T_{\phi\phi}$, Along a Given Plane in Anisotropic Materials

The strength, $T_{\phi\phi}(\phi)$, normal to a given direction, is taken as the normal stress required to fail an infinitesimal element of anisotropic material along a given plane. In the finite element solution the finite element sides dictate the directions of possible crack extension.

$T_{\phi\phi}$ was taken in this form to account for differences in the energy required to create new crack surfaces at arbitrary angles with the material principal coordinate system. Such a definition is necessary in the proposed model to permit selection of the proper direction of crack growth. Further, as shown by Herakovich [7], for example, failure of individual lamina in a laminate can occur along planes which are neither

parallel to nor perpendicular to the fibers. It appears to be most difficult if not impossible to experimentally verify a relation for $T_{\phi\phi}(\phi)$ by testing unidirectional laminates since only one direction of crack extension would be present for a given laminate. However, three obvious conditions must be met by such an expression. The conditions are:

1. For an isotropic material, the strength, $T_{\phi\phi}(\phi)$, should be constant and equal to the ultimate strength of the material, σ_u , independent of ϕ .
2. For a crack extending parallel to the fibers in a unidirectional composite, $T_{\phi\phi}(\phi)$ should be equal to the transverse tensile strength of the material, Y_T .
3. For a crack extending perpendicular to the fibers, $T_{\phi\phi}(\phi)$ should be equal to the tensile strength of the material in the fiber direction, X_T .

For a unidirectional laminate under plane stress, as shown in Fig. (2.7), a simple relationship for $T_{\phi\phi}(\phi)$ can be postulated. Removing an infinitesimal element at (r_0, ϕ) , Fig. (2.8a), and defining the angle β as the difference between the fiber angle, θ , and the assumed crack extension angle, ϕ , that is

$$\beta = \theta - \phi \quad (2.21)$$

It is then possible to isolate yet another infinitesimal element, Fig. (2.8b), which gives the orientation of the crack extension relative to

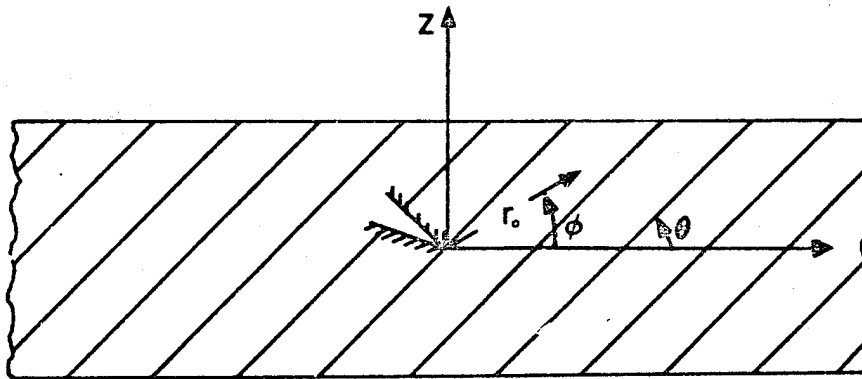
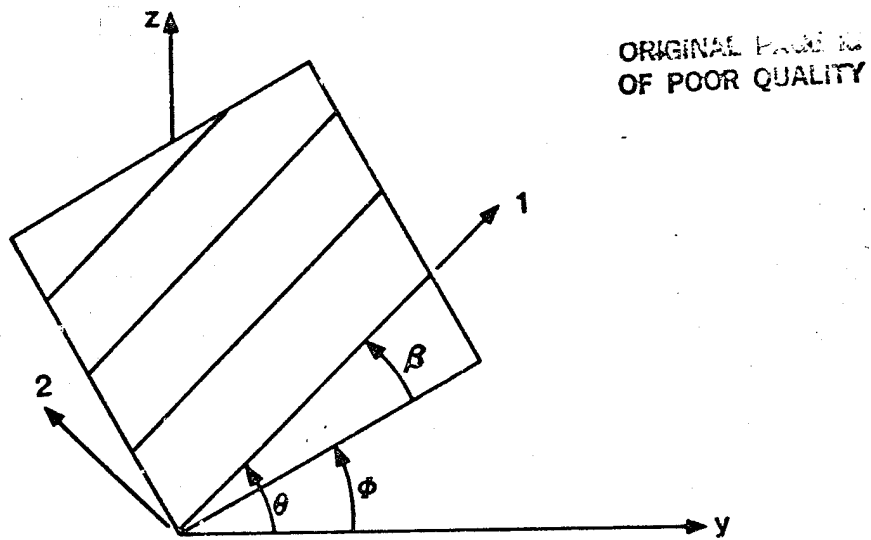
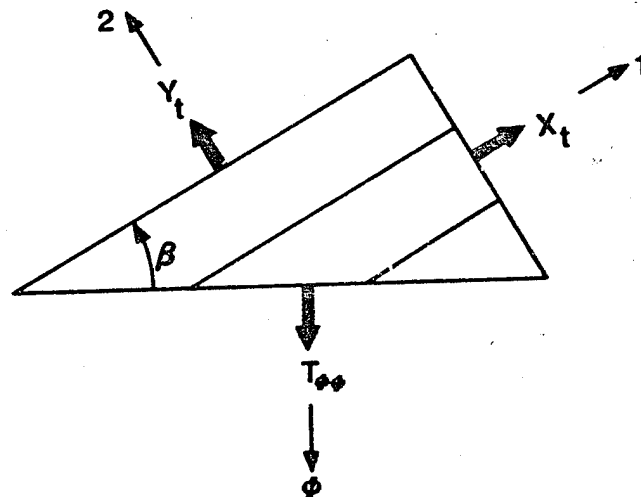


Figure 2.7 Unidirectional Laminate With An Arbitrary Crack Present

a. Defined Angles



b. Rotation Into Material Coordinates

Figure 2.8 Infinitesimal Stress Elements At (r, ϕ)

the material principal directions. Then, assuming that the strength, $T_{\phi\phi}(\phi)$, is balanced by only the transverse and longitudinal strength of the material Y_T and X_T , respectively, the relation for $T_{\phi\phi}(\phi)$ is obtained by summing forces in the ϕ direction as,

$$T_{\phi\phi}(\phi) = X_T \sin^2 \beta + Y_T \cos^2 \beta \quad (\text{plane stress}) \quad (2.22)$$

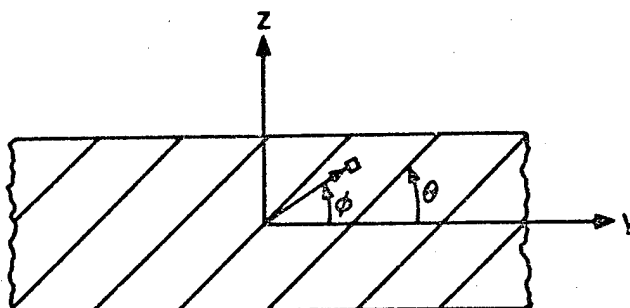
Testing Eqn. (2.22) against the three conditions,

$$\begin{aligned} \text{Isotropic material: } X_T &= Y_T = \sigma_u \\ T_{\phi\phi} &= \sigma_u \sin^2 \beta + \sigma_u \cos^2 \beta = \sigma_u \end{aligned} \quad (2.23a)$$

$$\begin{aligned} \text{Fracture parallel to fibers: } \beta &= 0^\circ \\ T_{\phi\phi} &= X_T \sin^2(0^\circ) + Y_T \cos^2(0^\circ) = Y_T \end{aligned} \quad (2.23b)$$

$$\begin{aligned} \text{Fracture perpendicular to fibers: } \beta &= 90^\circ \\ T_{\phi\phi} &= X_T \sin^2(90^\circ) + Y_T \cos^2(90^\circ) = X_T \end{aligned} \quad (2.23c)$$

The three conditions specified herein are satisfied. Hence, in principle, the expression is acceptable. A plot of $T_{\phi\phi}$ vs. ϕ for plane stress is shown in Fig. (2.9) for various values of θ for T300/5208 graphite-epoxy, (properties from Appendix C). The maximums in Fig. (2.9) represent the combinations of angles for which a crack grows perpendicular to fibers and the minimums represent crack growth parallel to fibers.

ORIGINAL PAGE IS
OF POOR QUALITY

———— $\theta = 0^\circ$

----- $\theta = 45^\circ$

- - - - $\theta = 90^\circ$

T300/5208

Graphite-Epoxy

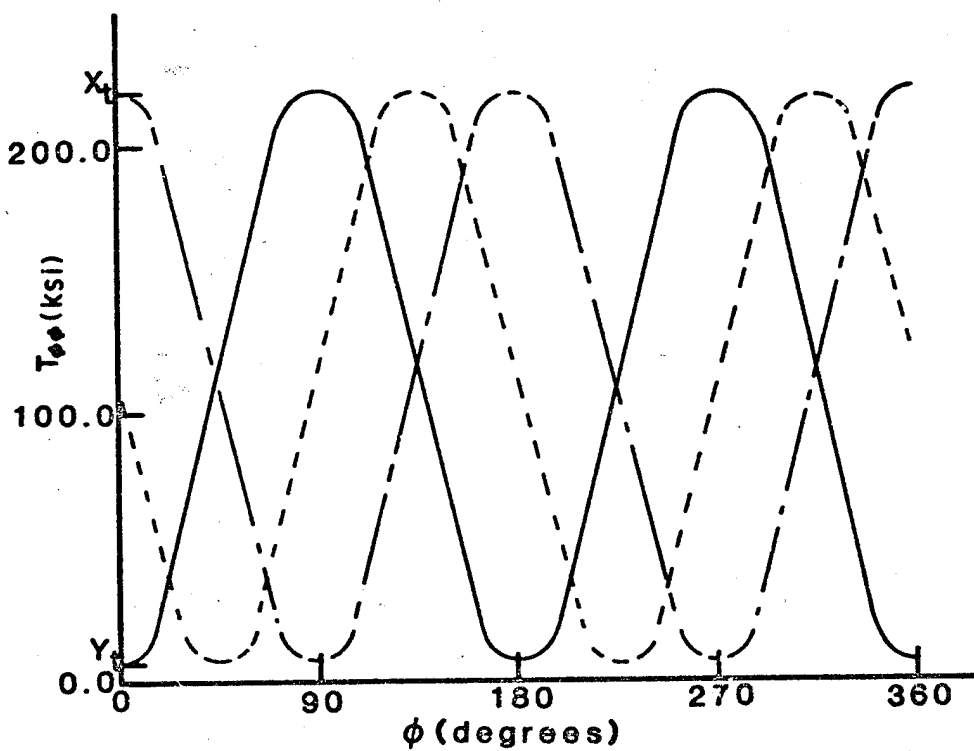


Figure 2.9 Plane Stress $T_{\phi\phi}$ vs. ϕ For Various Values Of θ

For a transverse crack extending through a laminate, Fig. (2.10), a similar relationship can be derived. Removing the lamina at the crack tip and rotating it about the z' axis into material principal coordinates, Fig. (2.11a), gives the geometry necessary to compute the strengths $T'_{xx}(\theta)$, $T'_{yy}(\theta)$ and $T'_{zz}(\theta)$ in the x' , y' , and z' directions, respectively. Removing an infinitesimal element, oab, from Fig. (2.11a), applying the normal strengths X'_T , Y'_T and T'_{xx} in the 1', 2' and x' directions, respectively, Fig. (2.11b), and summing forces in the x' -direction gives the relation for $T'_{xx}(\theta)$ as,

$$T'_{xx}(\theta) = Y'_T \sin^2 \theta + X'_T \cos^2 \theta \quad (2.24a)$$

Similarly, removing element, ocd, from Fig. (2.11a), applying strengths X'_T , Y'_T , and T'_{yy} , Fig. (2.11c), then summing forces in the y' -direction yields

$$T'_{yy}(\theta) = X'_T \sin^2 \theta + Y'_T \cos^2 \theta \quad (2.24b)$$

Since the z' and 3' axis in the lamina coordinate system are the same as in the laminate coordinate system,

$$T'_{zz}(\theta) = Z'_T \quad (2.24c)$$

The strength, $T'_{\phi\phi}(\phi)$, normal to a free edge crack extension, Fig. (2.12a), is found by removing an infinitesimal element, Fig. (2.12b),

ORIGINAL PAGE IS
OF POOR QUALITY

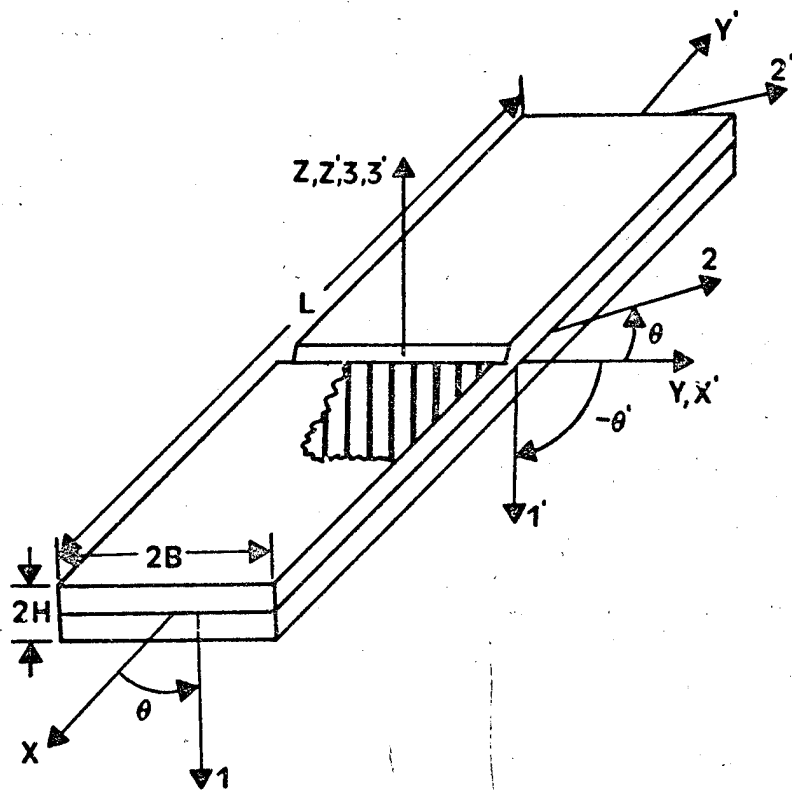


Figure 2.10 Free Edge Crack In
A Laminated Composite

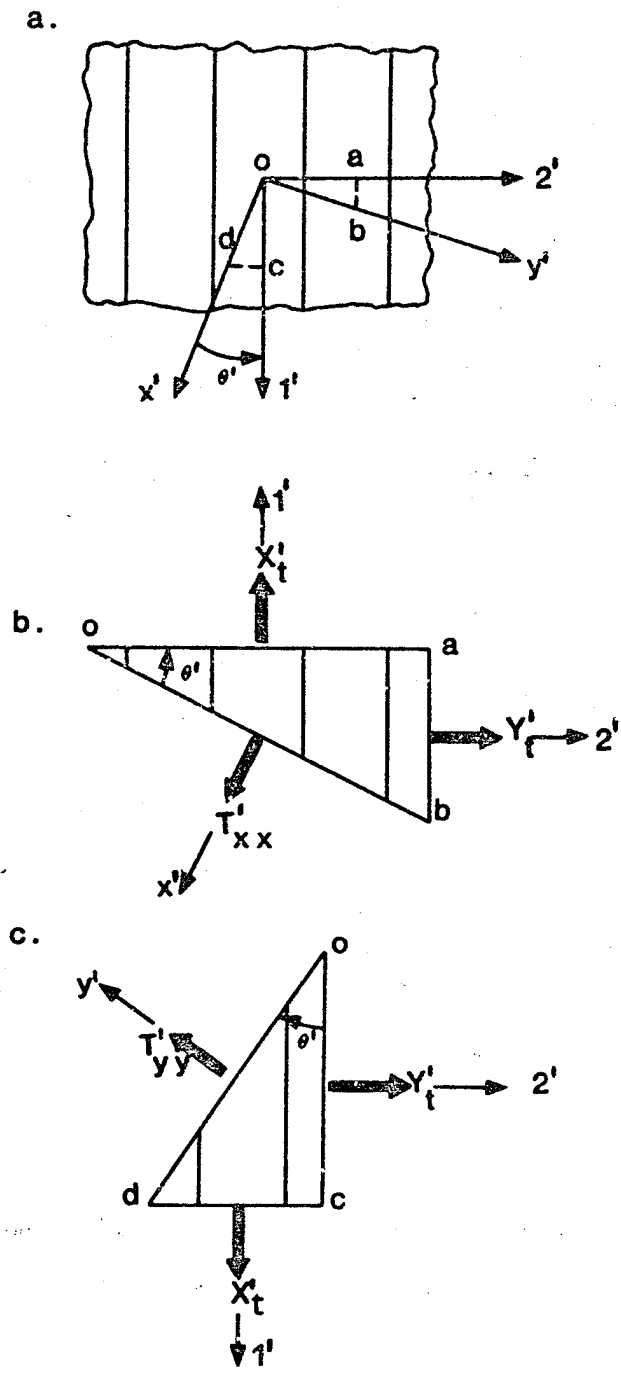
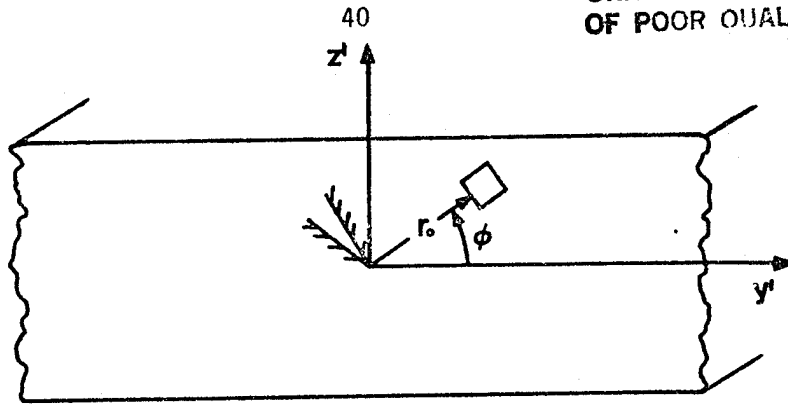
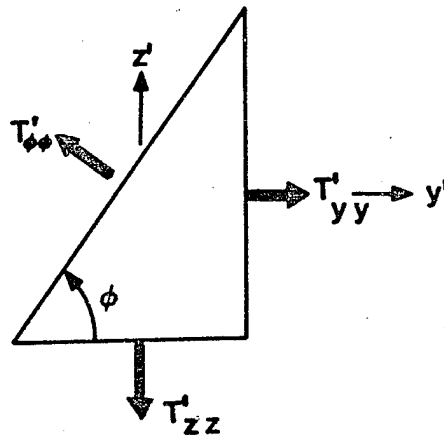


Figure 2.11 Local To Global Strength Transformations

ORIGINAL PAGE IS
OF POOR QUALITY



a. Free Edge Crack With Arbitrary Orientation



b. Stress Element At (r_0, ϕ)

Figure 2.12 Free Edge Crack Strength Transformation

applying the respective strengths and summing forces in the ϕ direction which gives

$$T'_{\phi\phi}(\phi) = T'_{yy}\sin^2\phi + T'_{zz}\cos^2\phi \quad (2.25)$$

Substituting Eqns. (2.24a), (2.24b) and (2.24c) into Eqn. (2.25) yields that

$$T'_{\phi\phi}(\phi) = (X'_T\sin^2\theta' + Y'_T\cos^2\theta')\sin^2\phi + Z'_T\cos^2\phi \quad (2.26)$$

Testing Eqn. (2.26) against the three conditions,

Isotropic material: $X'_T = Y'_T = Z'_T = \sigma_u$

$$T'_{\phi\phi} = (\sigma_u\sin^2\theta + \sigma_u\cos^2\theta)\sin^2\phi + \sigma_u\cos^2\phi = \sigma_u \quad (2.27a)$$

Fracture parallel to fibers: $\theta' = 0^\circ, \phi = 90^\circ$

$$T'_{\phi\phi} = (X'_T\sin^2(0^\circ) + Y'_T\cos^2(0^\circ))\sin^2(90^\circ) + Z'_T\cos^2(90^\circ) = Y'_T \quad (2.27b)$$

Fracture perpendicular to fibers: $\theta' = 90^\circ, \phi = 90^\circ$

$$T'_{\phi\phi} = (X'_T\sin^2(90^\circ) + Y'_T\cos^2(90^\circ))\sin^2(90^\circ) + Z'_T\cos^2(90^\circ) = X'_T \quad (2.27c)$$

Again, the three conditions are satisfied so, in principle, the relation is acceptable. A plot of $T'_{\phi\phi}$ vs. ϕ for free edge crack extension is

shown in Fig. (2.13) for various values of fiber orientation, θ' , for T300/5208 graphite-epoxy, (properties from Appendix C). As in the plane stress case, the values of ϕ , (for $\theta' = 90^\circ$), for which $T'_{\phi\phi}$ is a maximum represents crack extension perpendicular to fibers while a minimum $T'_{\phi\phi}$ represents crack extension parallel to fibers. The constant $T'_{\phi\phi}$ for $\theta' = 0^\circ$ represents matrix mode failure independent of ϕ . Last, the curve for $\theta' = 45^\circ$ has minimums at $T'_{\phi\phi} = Y'_T$, which represents matrix mode failure and the maximums never reach X'_T since some combination of fibers and matrix, thru the width, is always involved for the free edge cracks considered, Fig. (2.10).

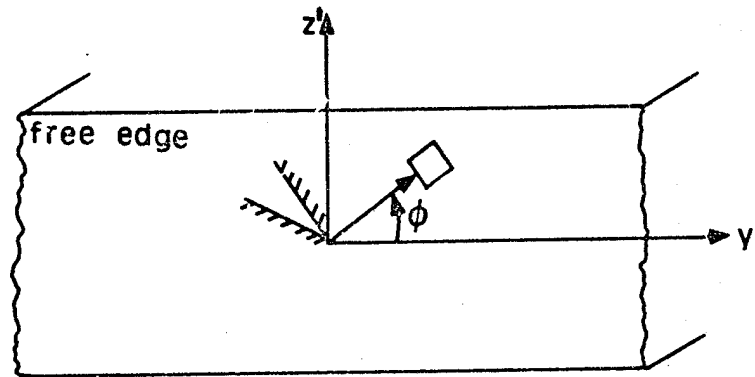
2.2.4.3 Modified Hashin Criterion

The Hashin failure criterion [10] assumes that failure of a transversely isotropic material will occur in a tensile fiber mode, $\sigma_{11} > 0$, when:

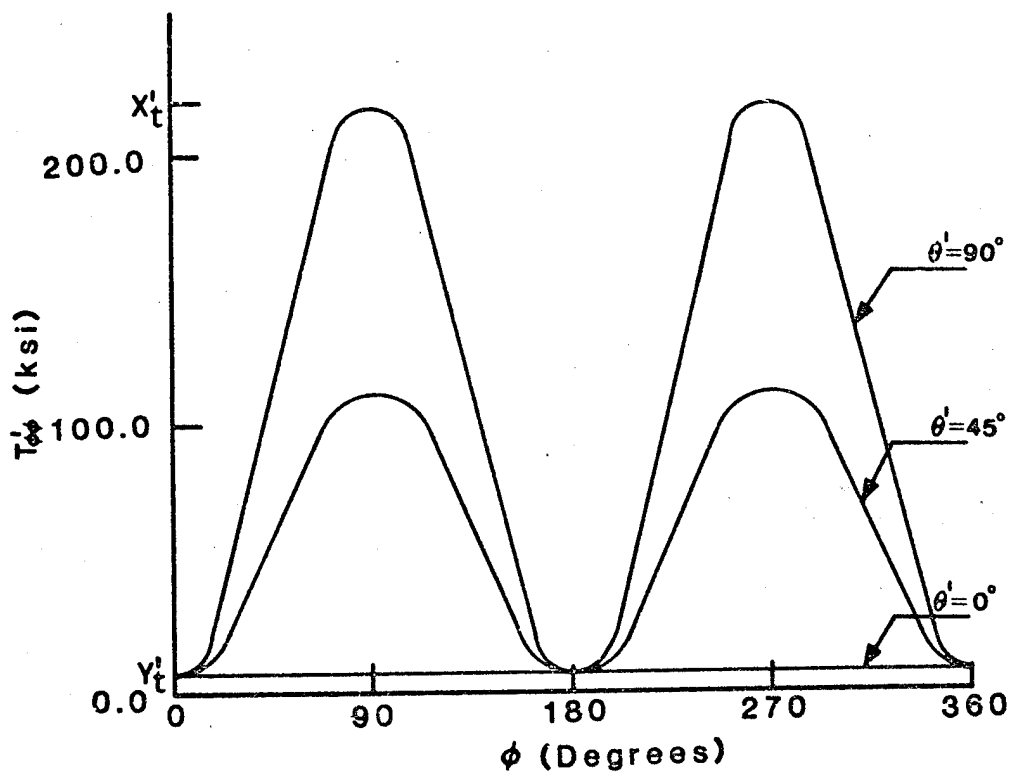
$$\left(\frac{\sigma_{11}}{X_T}\right)^2 + \frac{1}{S_{12}}(\sigma_{12}^2 + \sigma_{13}^2) = 1 \quad (2.28)$$

where X_T is the tensile failure stress in the fiber direction and S_{12} is the axial failure shear stress. The Hashin criterion also assumes failure to occur in a tensile matrix mode, $\sigma_{22} + \sigma_{33} > 0$, when:

$$\frac{1}{Y_T^2}(\sigma_{22} + \sigma_{33})^2 + \frac{1}{S_{23}^2}(\sigma_{23}^2 - \sigma_{22}\sigma_{33}) + \frac{1}{S_{12}^2}(\sigma_{12}^2 + \sigma_{13}^2) = 1 \quad (2.29)$$



T300/5208 Graphite Epoxy

Figure 2.13 Free Edge $T_{\phi\phi}'$ vs. ϕ For Various Values of θ'

where Y_T and S_{23} are the transverse tensile and shear strength of the material, respectively. For the case of plane stress in the 1-2 plane, the criterion for fiber mode tensile failure becomes:

$$\left(\frac{\sigma_{11}}{Y_T}\right)^2 + \left(\frac{\sigma_{12}}{S_{12}}\right)^2 = 1 \quad (2.30)$$

and for matrix mode tensile failure:

$$\left(\frac{\sigma_{22}}{Y_T}\right)^2 + \left(\frac{\sigma_{12}}{S_{12}}\right)^2 = 1 \quad (2.31)$$

where S_{12} is the shear strength of the material in the 1-2 plane.

The Hashin criterion does account for distinct differences in fiber and matrix mode failure. However, it does not account for an arbitrary combination of matrix and fiber mode failure. (In the actual failure of composite laminates this feature is necessary since as Herakovich [7], for example, has shown failure can occur on a plane which is neither parallel to nor perpendicular to the fibers.)

Hashin [10] proposed that a similar criterion for the failure of composite materials could be developed to include the plane on which failure occurred, ϕ_0 , Fig. (2.14). Such a criterion would predict failure when some function $g(\sigma_{ij}, \phi)$ satisfied the condition:

$$g(\sigma_{ij}, \phi) = 1 \quad (2.32)$$

ORIGINAL PAGE IS
OF POOR QUALITY

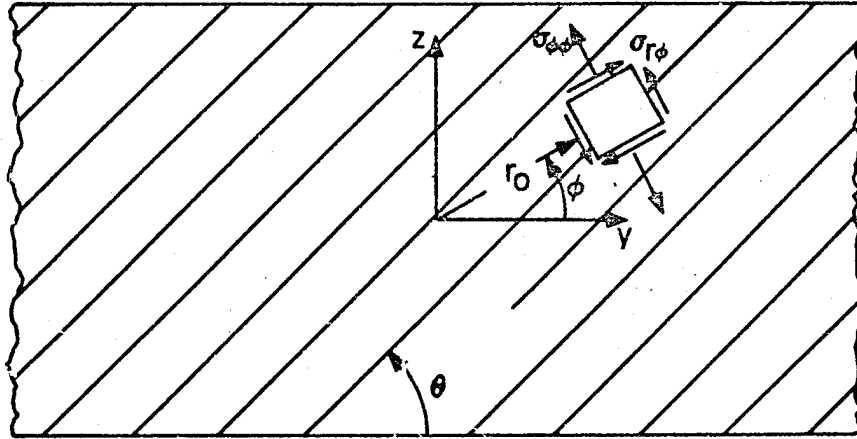


Figure 2.14 Composite Laminate With Modified Hashin Parameters

and that failure would occur on a plane defined by, ϕ_0 , for which (2.32) was first satisfied under monotonically increasing load.

The modified Hashin criterion of this study assumes that a given crack in a composite material will extend in the direction, ϕ_0 , in which the left side of Eqn. (2.32) reaches a maximum when evaluated at some fixed distance, r_0 , from the crack tip. (Note: r_0 is subject to the same limitations as in Sections 2.2.3 and 2.2.4.1).

The development of the modified Hashin criterion as used in this study is based on developing an expression for Eqn. (2.32). As in the case of the point stress criterion, it appears impossible to test such an expression experimentally. However, two obvious conditions should be met by such a criterion, they are:

- 1) For a crack extending parallel to the fibers, the criteria should give back the Hashin criterion for tensile matrix mode failure, Eqn. (2.31).
- 2) For a crack extending perpendicular to the fibers, the criteria should give back the Hashin criterion for tensile fiber mode failure, Eqn. (2.30).

Proceeding along the same line as Hashin [10], if the failure criterion is taken as,

$$\left(\frac{\sigma_{\phi\phi}}{T_{\phi\phi}}\right)^2 + \left(\frac{\sigma_{r\phi}}{T_{r\phi}}\right)^2 = 1, \quad \sigma_{\phi\phi} > 0 \quad (2.33)$$

where $T_{\phi\phi}$ and $T_{r\phi}$ are the normal and shear strengths and $\sigma_{\phi\phi}$ and $\sigma_{r\phi}$ are the normal and shear stresses, respectively, on the plane of crack

extension, Fig. (2.14), then the direction of crack extension is given by the value of ϕ for which the left side of Eqn. (2.33) reaches a maximum, provided that $\sigma_{\phi\phi}$ is greater than zero. (A $\sigma_{\phi\phi}$ less than zero would represent crack closure.) For the case of plane stress of a unidirectional composite laminate, Fig. (2.7), the normal strength, $T_{\phi\phi}(\phi)$, was derived in Section 2.2.4.2 and is given by Eqn. (2.22). If the shear strength, $T_{r\phi}(\phi)$, is simply taken as being S_{12} , that is

$$T_{r\phi} = S_{12} \quad (\text{plane stress}) \quad (2.34)$$

Then the failure criterion is complete. Testing the criteria of Eqn. (2.33) against the two conditions specified herein,

- (i) Fracture perpendicular to fibers: $\phi = 90 + \theta$, equilibrium of an element, Fig. (2.15a) gives

$$\sigma_{\phi\phi} = \sigma_{yy} \sin^2 \phi + \sigma_{zz} \cos^2 \phi - 2\tau_{yz} \sin \phi \cos \phi \quad (2.35a)$$

$$\sigma_{r\phi} = \cos \phi \sin \phi (\sigma_{zz} - \sigma_{yy}) + \tau_{yz} (\cos^2 \phi - \sin^2 \phi) \quad (2.35b)$$

substituting $\phi = 90 + \theta$,

$$\begin{aligned} \sigma_{\phi\phi} &= \sigma_{yy} \sin^2(90+\theta) + \sigma_{zz} \cos^2(90+\theta) - 2\tau_{yz} \sin(90+\theta) \cos(90+\theta) \\ &= \sigma_{yy} \cos^2 \theta + \sigma_{zz} \sin^2 \theta + 2\tau_{yz} \sin \theta \cos \theta \end{aligned} \quad (2.35c)$$

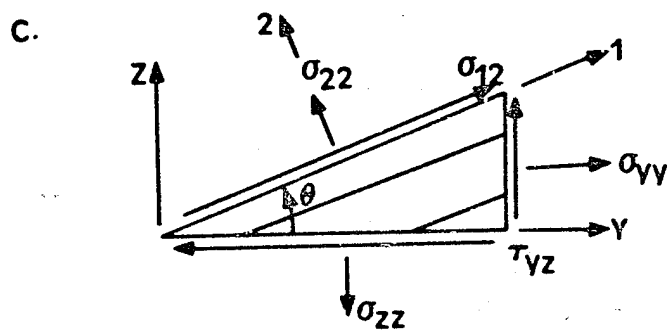
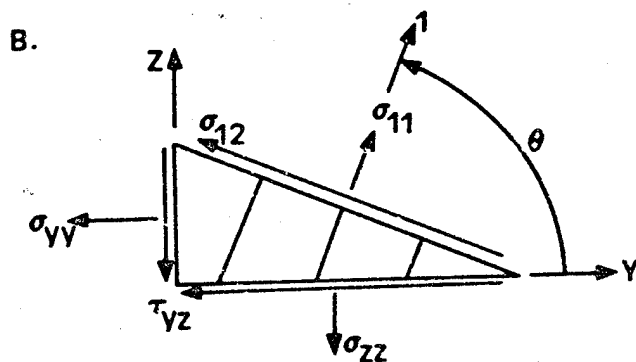
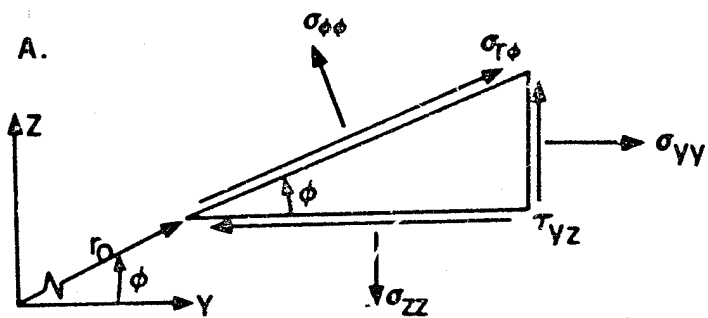


Figure 2.15 Two Dimensional Stress Transformations

and,

$$\begin{aligned}\sigma_{r\phi} &= \cos(90+\theta)\sin(90+\theta)(\sigma_{zz}-\sigma_{yy}) + \tau_{yz}[\cos^2(90+\theta)-\sin^2(90+\theta)] \\ &= -\sin\theta\cos\theta(\sigma_{zz}-\sigma_{yy}) + \tau_{yz}[\sin^2\theta-\cos^2\theta]\end{aligned}\quad (2.35d)$$

but, from Fig. (2.15b);

$$\sigma_{11} = \sigma_{yy}\cos^2\theta + \sigma_{zz}\sin^2\theta + 2\tau_{yz}\sin\theta\cos\theta \quad (2.35e)$$

$$\sigma_{12} = -[-\sin\theta\cos\theta(\sigma_{zz}-\sigma_{yy}) + \tau_{yz}[\sin^2\theta-\cos^2\theta]] \quad (2.35f)$$

comparing Eqns. (2.35e) and (2.35f) with (2.35c) and (2.35d), respectively,

$$\sigma_{\phi\phi} = \sigma_{11} \quad (2.35g)$$

and

$$\sigma_{r\phi} = -\sigma_{12} \quad (2.35h)$$

Also, for fracture perpendicular to the fibers, Eqn. (2.22) reduces to that of Eqn. (2.23c). Substituting Eqns. (2.23c), (2.34), (2.35g) and (2.35h) into Eqn. (2.33) yields,

$$\left(\frac{\sigma_{11}}{\chi_T}\right)^2 + \left(\frac{\sigma_{12}}{S_{12}}\right)^2 = 1 \quad (2.35i)$$

which is precisely the Hashin criterion for tensile fiber mode failure, Eqn. (2.30).

(ii) Fracture parallel to fibers: $\phi = \theta$ Substituting, $\phi = \theta$, into Eqns. (2.35a) and (2.35b) gives that:

$$\sigma_{\phi\phi} = \sigma_{yy} \sin^2 \theta + \sigma_{zz} \cos^2 \theta - 2\tau_{yz} \sin \theta \cos \theta \quad (2.36a)$$

and

$$\sigma_{r\phi} = \cos \theta \sin \theta (\sigma_{zz} - \sigma_{yy}) + \tau_{yz} (\cos^2 \theta - \sin^2 \theta) \quad (2.36b)$$

but from Fig. (2.15c):

$$\sigma_{22} = \sigma_{yy} \sin^2 \theta + \sigma_{zz} \cos^2 \theta - 2\tau_{yz} \sin \theta \cos \theta \quad (2.36c)$$

and

$$\sigma_{12} = \cos \theta \sin \theta (\sigma_{zz} - \sigma_{yy}) + \tau_{yz} (\cos^2 \theta - \sin^2 \theta) \quad (2.36d)$$

Comparing Eqns. (2.36c) and (2.36d) with (2.36a) and (2.36b), respectively,

$$\sigma_{\phi\phi} = \sigma_{11} \quad (2.36e)$$

and

$$\sigma_{r\phi} = \sigma_{12} \quad (2.36f)$$

Also, for fracture parallel to the fibers, Eqn. (2.22) reduces to that of Eqn. (2.23b). Substituting Eqns. (2.23b), (2.34), (2.36e) and (2.36f) into Eqn. (2.33) yields,

$$\left(\frac{\sigma_{22}}{Y_T}\right)^2 + \left(\frac{\sigma_{12}}{S_{12}}\right)^2 = 1 \quad (2.36g)$$

which is precisely the Hashin criterion for tensile matrix mode failure, Eqn. (2.31). Since the relation developed gives back the Hashin criteria for tensile fiber mode and tensile matrix mode failure it is in principle acceptable.

2.2.4.4 Finite Element Considerations in Implementing the Modified Point Stress and Hashin Criteria

The steps in the implementation of the modified point stress and Hashin criteria are similar to those in implementing the Sih and Tsai-Wu criteria. Briefly:

- (i) Determine the elements containing the crack tip node. This gives the possible directions of crack extension.
- (ii) Find the minimum element side length. This gives r_0 .
- (iii) Compute the stresses along the element sides, which define the possible directions of crack extension, at r_0 .
- (iv) Use Eqn. (2.20) for the point stress criterion or Eqn. (2.33) for the Hashin criterion and assume crack extension in the direction which makes (2.20), for point stress, or (2.33), for the Hashin criterion, a maximum.

Chapter 3

RESULTS

3.1 Isotropic Cases

3.1.1 Mode-I Crack in an Infinite Plate

The classical problem of a mode-I crack in an infinite plate, Fig. (1.2a), was run as a test of the energy release rate formulation. Results for two different finite element meshes, one being much finer than the other, were generated for comparison. The computed energy release rates were converted to stress intensity factors for ease of comparison with theory.

The boundary condition for the fine mesh, a 306 element x 338 node mesh, Fig. (D.1) considered a full crack model assumed specified displacement loading. Referring to Fig. (3.1a), the boundary conditions were:

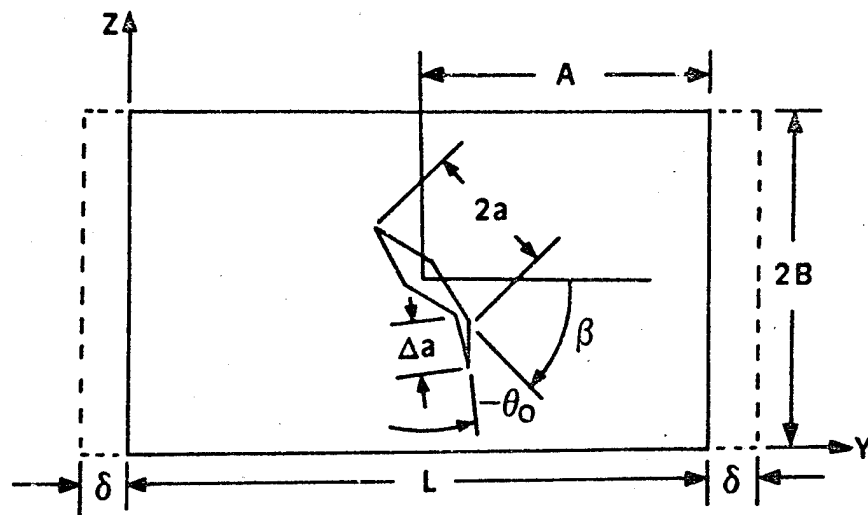
$$\text{at } y = 0: v(y = 0, z) = -\delta \quad (3.1a)$$

$$\text{at } y = L: v(y = L, z) = \delta \quad (3.1b)$$

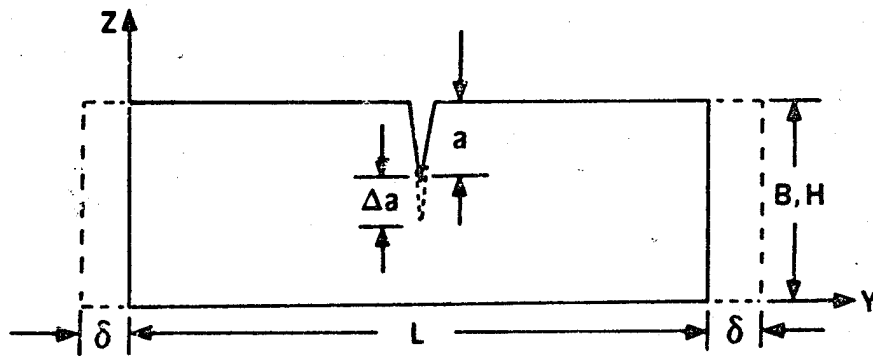
$$\text{at } z = 0, 2B: \text{traction free} \quad (3.1c)$$

The input parameters; a , δ , L , B , A and β were taken as,

$$\begin{aligned} a &= 0.5'' , \Delta a = 0.2a, L = 40a, B = 10a \\ A &= L/2, \delta = .002a, \beta = 90^\circ \end{aligned} \quad (3.2)$$



a. Full Crack Model



b. Mid-Plane Symmetry Model

Figure 3.1 Finite Element Crack Models

The problem was treated as a case of plane strain, constitutive equation given by Eqn. (B.18), with material properties listed in Appendix C. The crack was assumed to be a virtual crack, i.e., having a width equal to zero.

The coarse mesh, a 68 element x 82 node mesh, Fig. (D.2), assumed symmetry about the midplane and also used specified displacement loading. Referring to Fig. (3.1b), the boundary conditions were:

$$\text{at } y = 0: v(y = 0, z) = -\delta \quad (3.3a)$$

$$\text{at } y = L: v(y = L, z) = \delta \quad (3.3b)$$

$$\text{at } z = 0: \text{Traction free} \quad (3.3d)$$

$$\text{at } z = B: w(y, z = B) = 0 \quad (3.3d)$$

The input parameters were taken the same as for the fine mesh, Eqn. (3.2).

The theoretical stress intensity factor, K_I , for a mode-I crack in an infinite plate, Fig. (3.1), is given by [17] as,

$$K_I = \bar{\sigma}(\pi a)^{1/2} \quad (3.4)$$

and the relation between the mode-I stress intensity factor, K_I , and the mode-I energy release rate, G_I , for plane strain is given by [17] as,

$$K_I = \left(\frac{G_I E}{1-\nu^2} \right)^{1/2} \quad (3.5)$$

where E is Young's modulus and ν is Poisson's ratio. Since the theoretical stress intensity factor, Eqn. (3.4), is computed using the remote stress, $\bar{\sigma}$, the applied displacement, δ , must be converted to an equivalent stress. From Eqn. (B.18) this relation is given by

$$\bar{\sigma} = \delta_{,yy} = \frac{E\epsilon_{yy}}{1-\nu^2} \quad (3.6)$$

where

$$\epsilon_{yy} = \frac{2\delta}{L} \quad (3.7)$$

The finite element results for the two meshes considered are presented in Table (3.1). The stresses, $\bar{\sigma}$, were computed using Eqns. (3.6) and (3.7). The comparisons of the predicted stress intensity factors with the theoretical stress intensity factors is shown in Table (3.2). The results indicated pure mode-I crack extension, i.e., $-\theta_0 = 0^\circ$ in Fig. (3.1a), as expected. Note that theoretical values for two different initial crack lengths, a , are shown. The first crack length represents the actual, initial, crack length and the second represents the actual, initial, crack length plus the crack extension. The two crack lengths were considered to demonstrate the error incurred in using a finite crack extension. That is, the theoretical energy release rate, Eqn. (2.1), is based on an infinitesimal crack extension, i.e., limit $\Delta a \rightarrow 0$, whereas the finite element model introduces a finite crack extension, Δa . The results of Table (3.2) indicated that the fine mesh gave better results than the coarse mesh and that using the crack length

ORIGINAL PAGE 13
OF POOR QUALITY

**Table 3.1 Finite Element Energy Release Rate Predictions
For A Mode-I Crack In An Infinite Plate**

mesh size	$\bar{\sigma} \left(\frac{\text{lbs}}{\text{in}^2} \right)$	$G_I \left(\frac{\text{in. lbs}}{\text{in}^2} \right)$
68 elmt. x 82 node	3125	0.4703
306 elmt. x 338 node	3125	0.6123

ORIGINAL PAGE IS
OF POOR QUALITY

Table 3.2 Comparisons Of The Theoretical And Finite Element Predicted
Stress Intensity Factors For A Mode-I Crack In An Infinite Plate

mesh size	finite element* $k_I \left(\frac{lb}{in^{3/2}} \right)$	theoretical	
		a (in)	$k_I \left(\frac{lb}{in^{3/2}} \right)$
68 elmt. x 82 node	3834	0.5	3917
		0.6	4290
306 elmt. x 338 node	4374	0.5	3917
		0.6	4290

*a = 0.5 (in), $\Delta a = 0.1$ (in)

plus the extension in the theoretical stress intensity factor compared better with the finite element results.

3.1.2 Mixed Mode Fracture of an Infinite Isotropic Plate

The problem of a mixed mode crack in an infinite isotropic plate, Fig. (1.2b), was run as a test of the crack growth direction. Results were compared with the results predicted by the Sih strain energy density theory [2]. The mesh used consisted of 306 elements and 338 nodes, Fig. (E.1).

The boundary conditions used were identical to those of the fine mesh for the mode-I crack in an infinite plate, i.e., Eqns. (3.1a), (3.1b) and (3.1c). Referring to Fig. (3.1a), the input parameters; a , δ , L , B , and A were taken as,

$$\begin{aligned} a &= \frac{0.50''}{\sin\beta}, \quad L = 40a, \quad B = 10a \\ \delta &= 0.001'', \quad A = L/2 \end{aligned} \quad (3.8)$$

while the crack inclination angle, β , was varied from 30 to 90 degrees.

While simple relations for the mode-I stress intensity factor, K_I , and the mode-II stress intensity factor, K_{II} , exist for the mixed mode problem of Fig. (1.2b), reference [17] points out that there is no known relation between the energy release rates and stress intensity factors for such a problem. Hence, discussion of the results for the mixed-mode crack problem of Fig. (1.2b) will be limited to the crack extension direction.

The theoretical crack extension direction, θ_0 , was computed from the Sih strain energy density theory [18], by solving for θ_0 from Eqn. (3.9), below:

$$2(1-\nu)\sin(\theta_0-2\beta) - \{2\sin[2(\theta_0-\beta)]\} - \sin 2\theta_0 = 0 \quad (3.9)$$

Finite element results were generated for various crack inclination angles, β , through the use of the modified Griffith criterion, Section 2.2.1, the Sih strain energy density theory, Section 2.2.2, and the modified point stress and Hashin criterion, Section 2.2.4. A plot of the theoretical and finite element crack extension direction, θ , as a function of the crack inclination angle, β , is shown in Fig. (3.2).

The results for the modified Griffith criterion were generated by evaluating the value of the crack closure integral, through the use of Eqn. (2.4), for all possible paths of crack extension present, e.g., see Fig. (2.4), and assuming that crack extension would occur in the direction of a maximum energy release rate. The results consistently predicted crack extension in a direction in which the mode-I energy release rate, $G_I(a)$, made up 99% or more of the total energy release rate.

The results for the Sih strain energy density criterion were evaluated using Eqns. (2.13) and (2.17). The strain energy density factor was considered as the sum of two components [18], one due to a change in volume, S_v , and one due to a change in shape, S_d ,

$$S = S_v + S_d \quad (3.10)$$

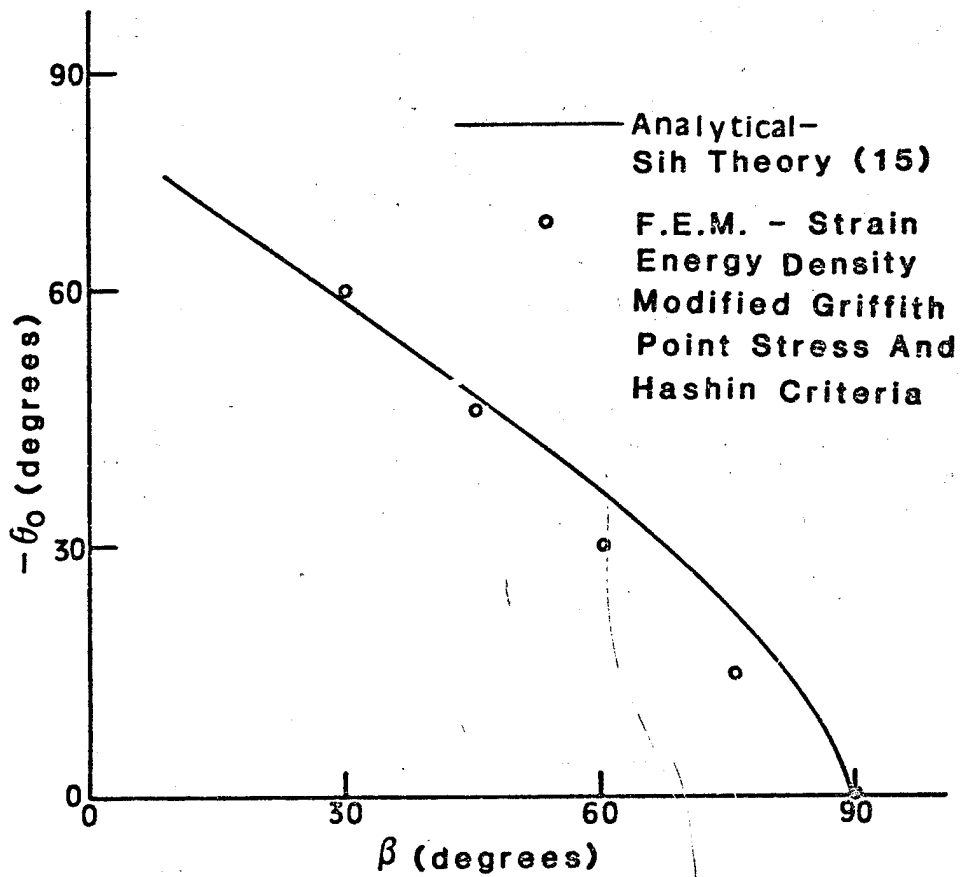
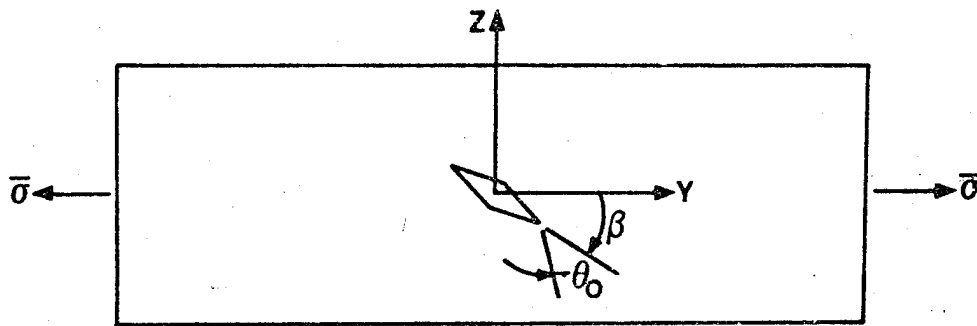


Figure 3.2 Crack Extension Angle, $-\theta_0$, vs. Crack Inclination Angle, β , For Isotropic Mixed Mode Fracture

The results always predicted crack extension in a direction in which $S_v \gg S_d$. This conforms with the concept [18] that fracture occurs along a plane where $S_v > S_d$.

The modified point stress cases were evaluated using Eqns. (2.20) and (2.22) with

$$X_T = Y_T = \sigma_u \quad (3.11)$$

The crack was assumed to extend in the direction for which, $R(\phi)$, Eqn. (2.20) was a maximum.

The results for the modified Hashin criterion were generated through the use of Eqn. (2.33), with

$$T_{\phi\phi} = T_{r\phi} = \sigma_u \quad (3.12)$$

Crack extension was assumed to occur in the direction which maximized the left hand side of Eqn. (2.33).

All of the tested theories gave identical results, as indicated in Fig. (3.2). The small differences between the theoretical and finite element predicted values was attributed to there being only a finite number of crack extension paths available in the finite element model compared to an infinite number in the analytical Sih theory. However, the finite element model always predicted crack extension along the closest available crack extension path to that of the theoretical crack extension direction.

3.2 Off-Axis, Unidirectional Composite Tension Specimens.

A tension test of a unidirectional coupon with a small crack present, Fig. (1.3a), was simulated as a test of the crack extension direction. The mesh used consisted of 306 elements and 338 node points, Fig. (D.1). Referring to Fig. (3.1a) and (2.7), the boundary conditions were chosen to simulate the grips of a tension test machine and are given by:

$$\text{at } y = 0: \quad v(y = 0, z) = -\delta, \quad w(y = 0, z) = 0 \quad (3.13a)$$

$$\text{at } y = 2L: \quad v(y = L, z) = \delta, \quad w(y = L, z) = 0 \quad (3.13b)$$

$$\text{at } z = 0, 2B: \quad \text{traction free} \quad (3.13c)$$

The dimensions were chosen to be similar to a typical tensile coupon, (Reference [19] suggests $L > 30B$ be used.), and were taken as,

$$B = 0.25'' \quad (3.14a)$$

$$L/2B = 15 \quad (3.14b)$$

The applied displacement load was chosen to be,

$$\delta = 0.001'' = \frac{L}{3750}(\text{in}) \quad (3.14c)$$

The initial half-crack length was chosen as,

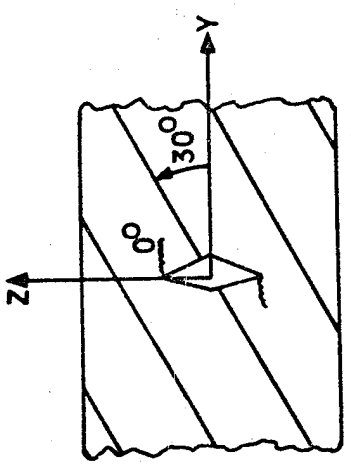
$$a = \frac{0.005 \text{ in}}{\sin \theta} \quad (3.14d)$$

and the other parameters, the fiber direction, θ , the crack inclination angle, β , and the crack position, A , were varied to simulate various conditions. The problem was treated as being a case of orthotropic plane stress with the constitutive relation being that of Eqn. (B.13). The material system chosen was T300/5208 graphite-epoxy, properties listed in Appendix C. The crack was assumed to be a virtual crack, i.e., having zero initial width.

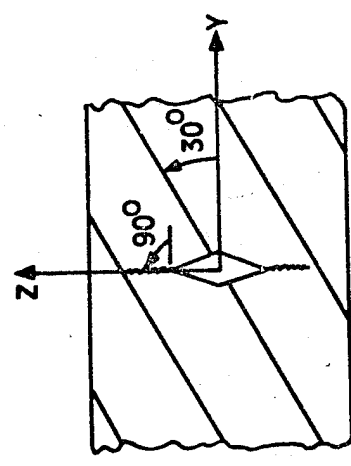
3.2.1 Comparison of the Crack-Extension Direction Theories for a 30° Lamina

The theories for predicting the crack extension direction, i.e., the modified Griffith theory, Section (2.2.1), the Sih strain energy density theory, Section (2.2.2), the Tsai-Wu theory, Section (2.2.3), the modified point stress theory, Section (2.2.4), and the modified Hashin theory, Section (2.2.4), were compared against the expected crack extension path for a 30°, off-axis, unidirectional tensile specimen with a crack orientated along the z axis, i.e., $\beta = 90^\circ$ in Fig. (3.1a).

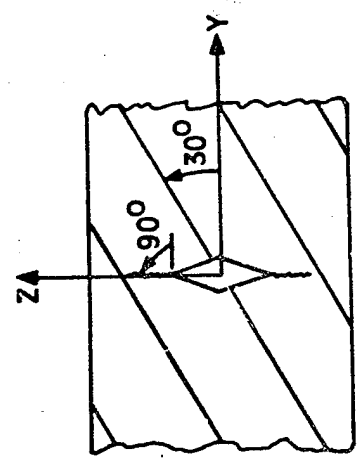
The predicted crack extension path for the modified Griffith theory is shown in Fig. (3.3a), the Sih strain energy density criterion in Fig. (3.3b), the Tsai-Wu theory in Fig. (3.3c), the modified point stress theory in Fig. (3.3d) and the modified Hashin theory in Fig. (3.3e). The experimentally observed direction is shown in Fig. (3.3f). Experimental results for graphite-epoxy [6, 7 and 8], Boron-aluminum [20], and graphite polyimide [21], unidirectional composites all indicated that failure of unnotched specimens and fracture of notched specimens



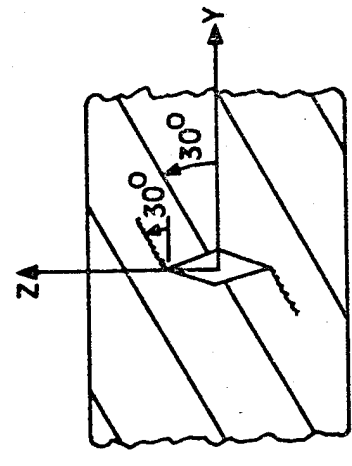
c. Tsai-Wu



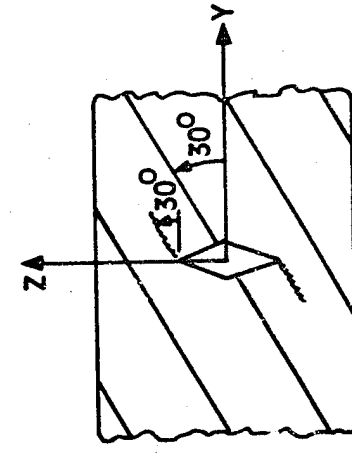
b. Strain Energy Density



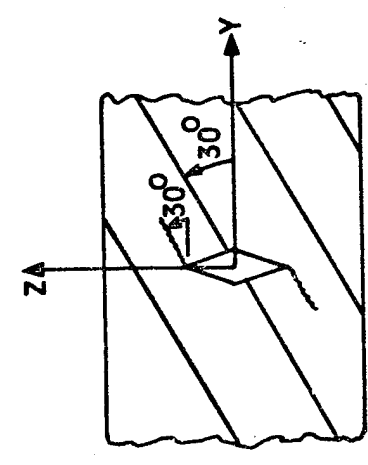
a. Modified Griffith



f. Experimental (6,7,8,20,21)



e. Modified Hashin



d. Modified Point Stress

Figure 3.3 Predicted And Experimental Crack Extensions For A 30°, Unidirectional, Laminate

occurred along planes parallel to the fibers. Fig. (3.3a) thru (3.3e) indicate that the modified point stress and the modified Hashin theories were the only theories that predicted the correct crack extension path.

The reason that the modified Griffith, the strain energy density and the Tsai-Wu theories predicted incorrect crack extension paths was because none of these theories account for the differences in the energy required to create crack extension surfaces at arbitrary angles to the fibers.

Since the modified point stress and Hashin criteria were the only criteria to yield accurate results, further case studies were limited to these two criteria.

3.3.2 Variation of the Modified Point Stress and Hashin Functions for a 30° Lamina.

The modified point stress function, $R(r_0, \phi)$, was given by Eqn. (2.20) as

$$R(r_0, \phi) = \frac{\sigma_{\phi\phi}}{T_{\phi\phi}} \quad (3.15)$$

where $\sigma_{\phi\phi}$ was taken as the normal stress and $T_{\phi\phi}$, defined by Eqn. (2.22), the strength normal to a plane of possible crack extension. The modified Hashin function can be defined as $H(r_0, \phi)$, where from Eqn. (2.33),

$$H(r_0, \phi) = \left(\frac{\sigma_{\phi\phi}}{T_{\phi\phi}} \right)^2 + \left(\frac{\sigma_{r\phi}}{T_{r\phi}} \right)^2 \quad (3.16)$$

where $\sigma_{r\phi}$ was the shear stress and $T_{r\phi}$ the shear strength, Eqn. (2.34), on the plane of possible crack extension.

Finite element predictions of $R(r_0, \phi)$ and $H(r_0, \phi)$ were computed as a function of ϕ for three different values of r_0 for the 30° lamina of Section 3.2.1. (The finite element mesh, the boundary conditions and the crack geometry were identical to those of the problem considered in Section 3.2.1). The values for the $R(r_0, \phi)$ function were normalized to their maximum values and plotted in Fig. (3.4) for three different normalized values of r_0 . The r_0 values were normalized with respect to r_0^{\max} , where r_0^{\max} was the limiting value of r_0 for the finite element mesh used, (e.g., see Section 2.2.4.4). The values for the $H(r_0, \phi)$ function of the modified Hashin theory were also normalized to their maximum value and were plotted in Fig. (3.5) for the same three normalized r_0 values.

The results of Fig. (3.4) and (3.5) achieve maximum values at $\phi = 210^\circ$ for all of the various r_0/r_0^{\max} values. Since the criteria both assume crack extension in the direction where $R(r_0, \phi)$ or $H(r_0, \phi)$ reach a maximum, both criteria choose the expected value of $\phi = 210^\circ$, (e.g., see Section 3.2.1). Figure (3.4) and (3.5) also indicate that the trends remain unchanged though the values differ slightly for the three r_0/r_0^{\max} values. This indicates that the prediction of the crack extension direction is fairly insensitive to the value chosen for r_0 . Note that in the case of the modified point stress theory, Fig. (3.4), the maximum value of R/R_{\max} increased with increasing distance from the crack tip. This trend was just the opposite of what was expected since the stresses

ORIGINAL PAGE IS
OF POOR QUALITY

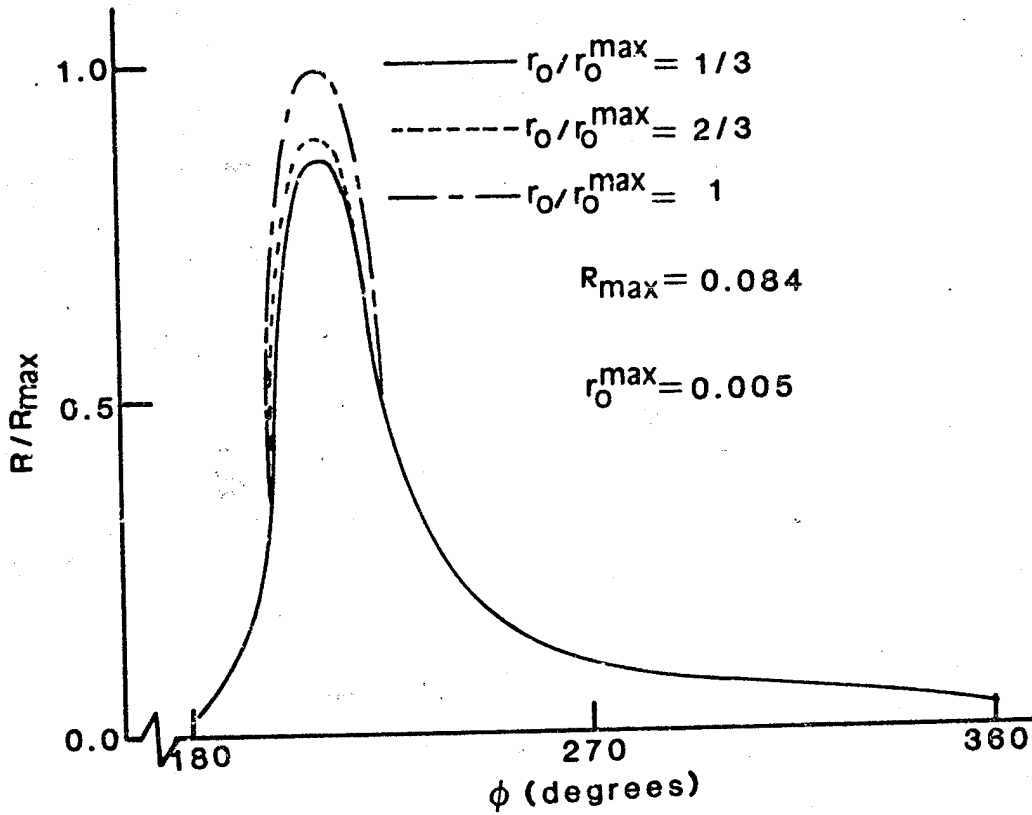
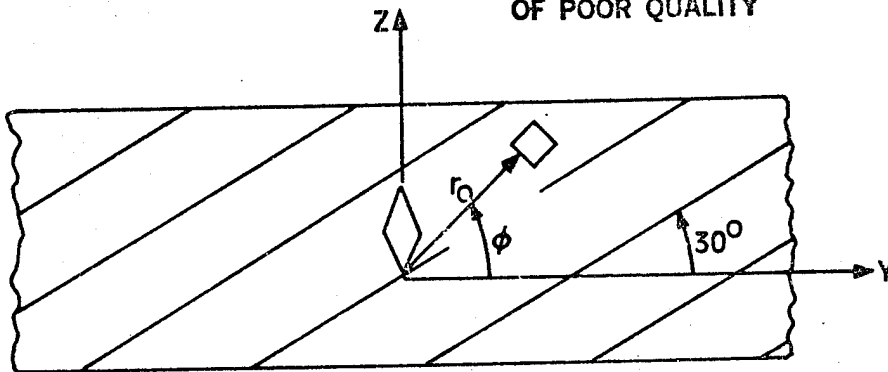
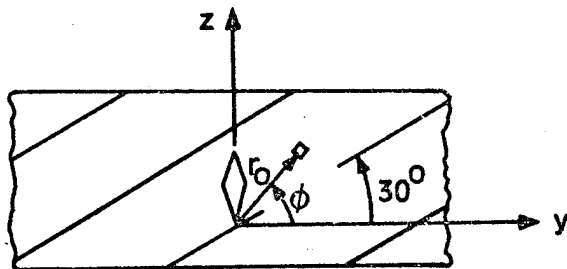


Figure 3.4 Normalized Modified Point Stress Ratio vs. ϕ
For A 30° Unidirectional, Laminate

ORIGINAL PAGE IS
OF POOR QUALITY



- $r_0/r_0^{\max} = 1/3$
- - - - - $r_0/r_0^{\max} = 2/3$
- · - · - $r_0/r_0^{\max} = 1$

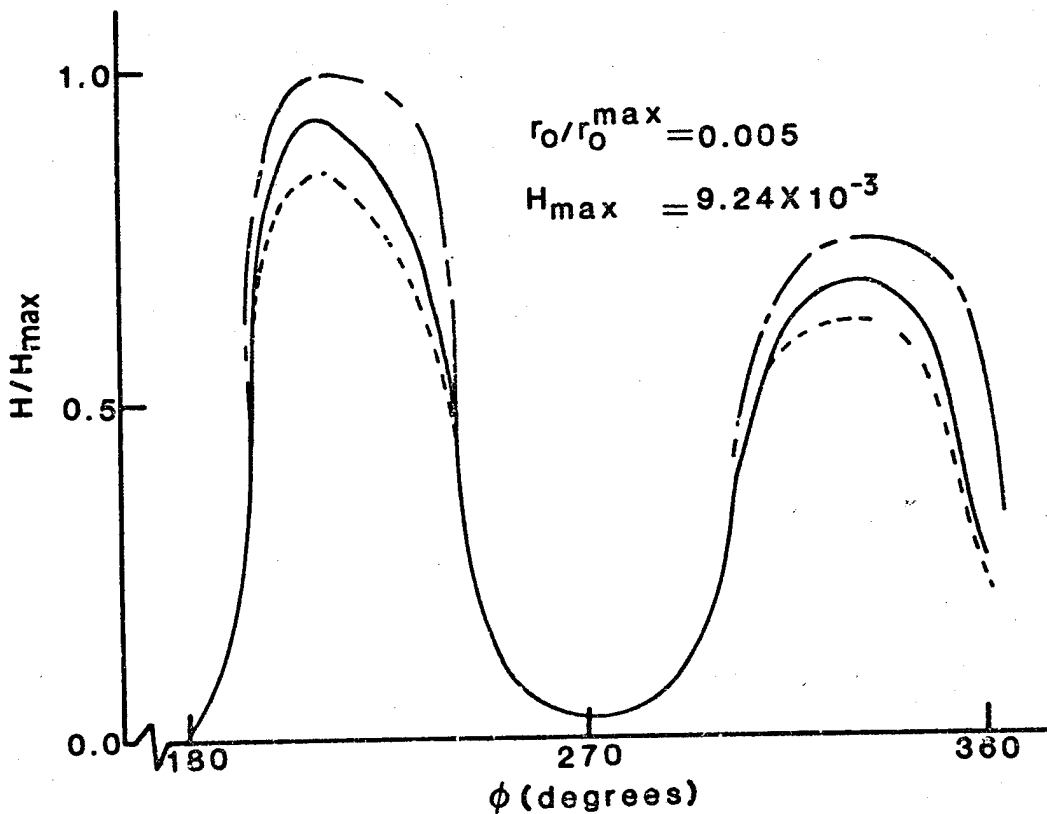


Figure 3.5 Normalized Modified Hashin Function vs. ϕ
For A 30° Unidirectional , Laminate

are actually singular at the crack tip, i.e., at $r_0 = 0$. The reason for this discrepancy is that as r_0/r_0^{\max} approaches unity, the stresses are computed nearer the element corners which introduces numerical errors in the stress computation. This stands as a good example of why such criteria are limited to the prediction of crack extension direction and not the load which would cause crack extension. The values for the normalized modified point stress ratio, Fig. (3.4) and the normalized modified Hashin ratio, Fig. (3.5), for $0^\circ < \phi < 180^\circ$ were not shown because of numerical difficulties in the computation of the stresses in this regime. However, the modified point stress results seemed to indicate a slight increase in $R(r_0, \phi)$ for $0^\circ < \phi < 30^\circ$ and some negative values between $\phi = 30^\circ$ and $\phi = 180^\circ$. Similarly for the modified Hashin ratio, Fig. (3.5), the values for $0^\circ < \phi < 180^\circ$ seemed to indicate slight increases in $H(r_0, \phi)$ around $\phi = 30^\circ$ and $\phi = 120^\circ$ with some negative values for $\sigma_{\phi\phi}$ between $\phi = 30^\circ$ and $\phi = 180^\circ$. Comparison of the modified point stress ratio, $R(r_0, \phi)$, Eqn. (3.15), and the modified Hashin ratio, $H(r_0, \phi)$, Eqn. (3.16), reveal that

$$H(r_0, \phi) = [R(r_0, \phi)]^2 + \left(\frac{\sigma_{r\phi}}{\tau_{r\phi}}\right)^2 \quad (3.17)$$

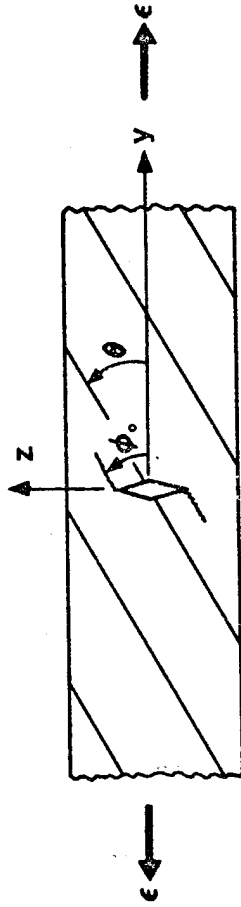
Hence, the differences in Fig. (3.4) and (3.5) represent the effects of squaring the point stress ratio, $R(r_0, \phi)$, plus the shear effect of including the square of the shear ratio, $\sigma_{r\phi}/\tau_{r\phi}$.

3.2.3 Crack Extension in Unidirectional Laminates

The modified point stress and the modified Hashin criteria were used to predict the crack extension direction and the modified crack closure technique was used to predict the energy release rate for several different unidirectional laminates. The reason the study of crack extension in unidirectional laminates was limited to the modified point stress and Hashin criteria was because they were the only criteria which accounted for differences in the energy required to create new fracture surfaces at arbitrary angles to the material principal system-- as demonstrated for a 30° lamina in section 3.2.1. The mesh, boundary conditions and material system were identical to those explained at the beginning of section 3.2. A virtual crack, i.e., one having zero initial width, was assumed. The orientation of the crack was assumed to be $\beta = 90^\circ$ and $A = L/2$, Fig. (3.1a).

The results are shown in Table (3.3) where θ is the material principle coordinate system orientation, ϕ_0 the orientation of the plane of crack extension, G is the total energy release rate, Eqn. (2.4), and the % mode-I and % mode-II values represent the mode-I and mode-II contributions to the total energy release rate, G . The expected crack extension directions were based on experimental results for graphite-epoxy [6, 7], Boron-aluminum [20], and graphite polyimide [21] composites. The results of these experiments all indicated that failure of unnotched specimens and fracture of notched specimens occurred along planes parallel to the fibers and that ϕ_0 was always greater than 180° except in the case of $\theta = 0^\circ$, where extension could occur in either a $\phi_0 = 0^\circ$

**Table 3.3 Finite Element Crack Extension Predictions
For Unidirectional Laminates**



θ (degrees)	ϕ_0 (degrees) experimental [6,7,20,21]	modified point stress ϕ_0 (degrees)	modified Hashin ϕ_0 (degrees)	G ($\frac{\text{in. lbs}}{\text{in}^2}$)	% mode-I	% mode-II
0	0, 180	0, 180	0, 180	0.0335	0.10	99.9
10	10	10	10	0.0152	9.40	90.6
30	30	30	30	0.0083	60.4	39.6
45	45	45	45	0.0055	77.3	22.7
60	60	60	60	0.0050	93.8	6.2
90	90	90	90	0.0052	100.0	0.0

or $\phi_0 = 180^\circ$ direction. The results of Table (3.3) indicate that both the modified point stress and Hashin criteria choose the correct path of crack extension in all of the cases considered. The fact that both criteria also choose dual values of $\phi_0 = 0^\circ, 180^\circ$ for the $\theta = 0^\circ$ specimens was also promising since this is what would be expected. While no direct comparison of the computed energy release rates could be made, the computed values were similar to and in the same range as experimental values obtained by Wang and Crossman [6] for double side notched graphite-epoxy specimens. The % mode-I and the % mode-II values were also compared with the results of Wang and Crossman [6] and were found to exhibit the same trends and range of results.

3.2.4 Effects of Crack Orientation on the Fracture Characteristics of Unidirectional Laminates

The finite element model was used to predict the fracture characteristics of a 30° , unidirectional laminate. The cases considered were:

1. Influence of crack position, referring to Fig. (3.1a), a crack near the grip of the tensile machine was simulated by specifying that $\frac{A}{L} = 0.1$ with $\beta = 90^\circ$.
2. Influence of specimen aspect ratio, referring to Fig. (3.1a), a short specimen was modeled having length $L/2B = 2$ with $\beta = 90^\circ$.
3. Influence of crack orientation, referring to Fig. (3.1a), specimens with $\beta = 30^\circ$, $\beta = 60^\circ$, and $\beta = 90^\circ$ were considered.

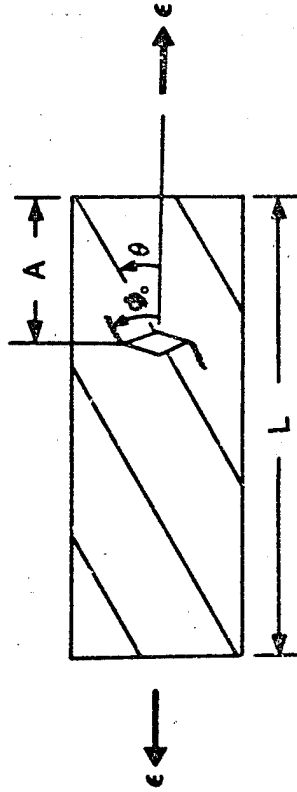
All of the cases assumed that a virtual crack existed and used the same mesh, boundary conditions, loading, material and geometry, unless stated otherwise above, as described at the beginning of section 3.2.

The results of case 1, Table (3.4), indicated that the crack direction for the crack near the grip, $A/L = 0.1$, extended in the same direction, ϕ_0 , as did the center cracked specimen, $A/L = 0.5$, while the energy release rates, G , and the % mode-I and % mode-II contributions to the total energy release rate differed by 10-20%.

The case 2 results, Table (3.5), indicated that the crack extension direction, ϕ_0 , was insensitive to the specimen aspect ratio and that the resulting energy release rates differed by about 20%. However, the type of fracture that occurred was the opposite for the two cases. That is, the long specimen, $L/2B = 15$, fractured in a mainly mode-I fashion while the short specimen, $L/2B = 2$, fractured in a mainly mode-II fashion. This trend is not surprising since Nemeth, et al. [19] have shown that a completely different stress state exists in short specimens, i.e., $L/2B = 5$, as compared to long specimens, i.e., $L/2B = 15$.

The results of case 3, Table (3.6) predicted the same crack extension directions, ϕ_0 , and similar energy release rates and fracture modes for the three crack inclination angles, β , considered. These results are consistent with the experimental results of [6], [7], [20], and [21] which indicate that fracture of unidirectional laminates always occurs on planes parallel to the fibers.

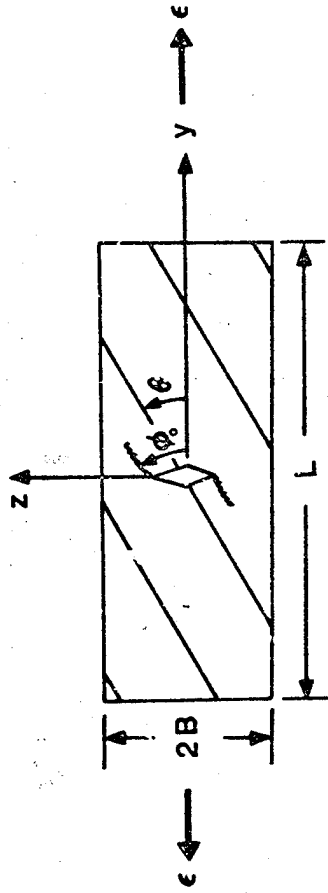
Table 3.4 Influence Of Crack Position On The Fracture Characteristics Of 30° Unidirectional , Laminates



a/L	θ (degrees)	ϕ_0 (degrees)	G($\frac{\text{in. lbs}}{\text{in}^2}$)	% mode-I	% mode-II
0.1	30	30	0.0072	74.7	25.3
0.5	30	30	0.0083	60.4	39.6

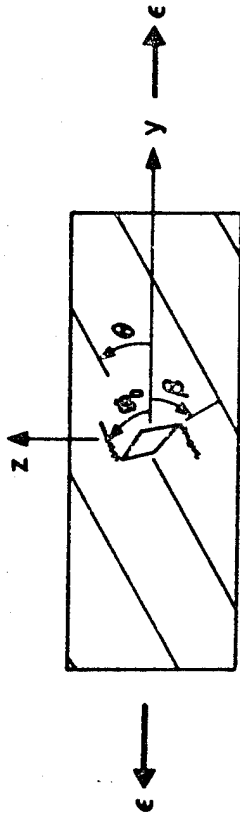
ORIGINAL PAGE IS
OF POOR QUALITY

Table 3.5 Influence Of Specimen Aspect Ratio On The Fracture Of 30° Unidirectional, Laminates



$L/2B$	θ (degrees)	ϕ_0 (degrees)	$G/_{yy}$ ($\frac{\text{in. lbs}}{\text{in}^2}$)	% mode-I	% mode-II
2	30	30	12.25	25.9	74.1
15	30	30	15.56	60.4	39.6

Table 3.6 Influence Of Crack Orientation On The Fracture Characteristics Of 30° Unidirectional, Laminates



β (degrees)	ϵ (degrees)	ϕ_0 (degrees)	G (in.lbs/in ²)	% mode-I	% mode-II
30	30	30	0.0089	66.1	33.9
60	30	30	0.0087	62.7	37.3
90	30	30	0.0083	50.4	39.6

3.3 Free Edge Crack Growth in Laminated Composite Tensile Specimens

Cracks located at the free edge of laminated tension specimens, Fig. (2.10), were considered. The crack extension paths and the resulting energy release rate vs. crack length curves were considered.

The solution procedure consisted of obtaining a generalized plane strain solution of the front face, i.e., the y - z plane, under an applied load of ϵ_{xx} then, using the results of the front face solution as applied loads, obtain a fracture mechanics solution to the free edge, i.e., the y' - z' plane, via subsequent generalized plane strain solutions. (The generalized plane strain formulation is described in Appendix A.)

The generalized plane strain solution of the front face was obtained using a 132 element by 150 node finite element mesh, Fig. (D.3). Referring to Fig. (2.10) and Eqn. (A.4), the boundary conditions and geometry used were:

$$B = 0.25'', \quad H = 0.02'', \quad \epsilon_{xx} = 0.001 \quad (3.18a)$$

$$\text{at } y = 0, \quad U(y = 0, z) = V(y = 0, z) = 0 \quad (3.18b)$$

$$\text{at } y = B, \quad \text{traction free} \quad (3.18c)$$

$$\text{at } z = 0, \quad W(y, z = 0) = 0 \quad (3.18d)$$

$$\text{at } z = H, \quad \text{traction free} \quad (3.18e)$$

where quarter symmetry was assumed.

Since the generalized plane strain solution assumes stresses and strains to be independent of the out of plane coordinate, the study of

the free edge crack growth problem can be modeled exactly only when there is no variation of these quantities in both the x and x' directions. Since the x -direction is the out of plane direction, Fig. (3.6a), for the front face problem and the x' -direction is the out of plane direction, Fig. (3.6b), for the free edge problem, the study is limited to cases which exhibit x and x' independence. The only laminates which exhibit this quality are unidirectional laminates because of the absence of edge effects. However, if the thru the thickness variables of the free edge problem, Fig. (3.6b), are assumed constant and equal to the values at the free edge of the front face problem, i.e., at $y = B$ in Fig. (3.6a), then the corresponding free edge boundary conditions become Fig. (2.10), (3.6a), (3.6b),

$$\text{at } y' = 0, \quad W'(y' = 0, z') = W(y = B, z) \quad (3.19a)$$

$$V'(y' = 0, z') = -[U(y = B, z) + \epsilon_{xx} \cdot (x = C)] \quad (3.19b)$$

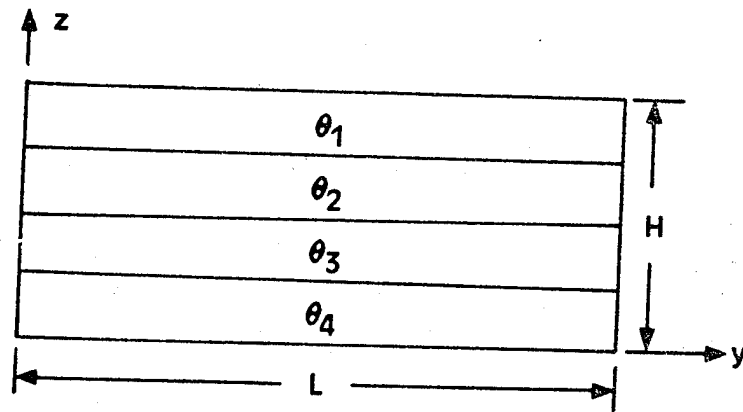
$$\text{at } y' = b, \quad W'(y' = 2C, z') = W(y = B, z) \quad (3.19c)$$

$$V'(y' = 2C, z') = -[U(y = B, z) + \epsilon_{xx} \cdot (x = -C)] \quad (3.19d)$$

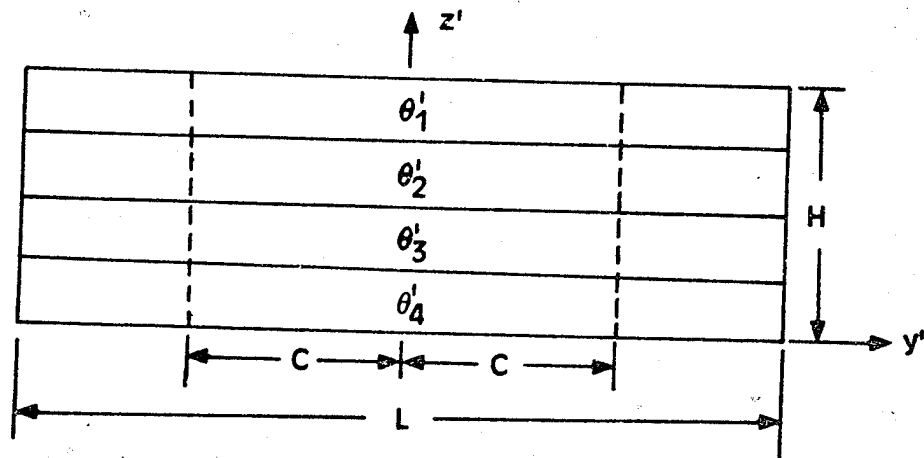
where $2C$ is the free edge modeled length.

$$\text{at } z' = 0, \quad W'(y', z' = 0) = 0 \quad (3.19e)$$

$$\text{at } z' = H, \quad \text{traction free} \quad (3.19f)$$



a. Front Face



b. Free Edge

Figure 3.6 Laminate Geometry

with:

$$U'(y', z') = 0 \quad (3.19g)$$

$$\epsilon_{xx}' = \epsilon_{xx}'(z') = -\frac{1}{B}V(y = B, z) \quad (3.19h)$$

and:

$$\theta_i' = \theta_i - 90^\circ \quad (3.19i)$$

Several laminate configurations were considered as candidates for the analysis of free edge crack growth. Tests were performed to find which laminate configurations could best be modeled as generalized plane strain problems on both the front face and the free edge. The tests consisted of first obtaining the front face solution then applying the corresponding boundary conditions, Eqns. (3.19a-i), to an uncracked free edge model. The results of the tests were analyzed to determine which laminates gave the best correspondence between the stresses and strains at the free edge as well as approximated independence of the displacements in the x and x' directions, Fig. (2.10), for the front face and free edge problems. The results indicated that both angle-ply and cross-ply laminate configurations gave a reasonable correspondence of free edge stresses and strains. However, only the cross-ply configurations approximated independence of both x and x' , Fig. (2.10), under the applied load. Hence, the analysis of free edge crack growth in this study was limited to cross-ply laminates.

Experimental results [6, 22] indicate that laminates which contain 90° plies along with other plies where $\theta \neq 90^\circ$ can exhibit transverse

crack growth in the 90° plys and delaminations between the 90° and $\theta \neq 90^\circ$ plys. As an example of the quasi-three dimensional capabilities of the finite element model the nature of crack growth in a $[90_2/0_2]_S$, T300/5208, graphite-epoxy tensile specimen was considered. Referring to Fig. (3.7), both transverse crack growth and delamination crack growth were considered and the results of the two analysis were compared. The method of analysis consisted of testing two cases. Case 1 was to trace the crack growth of an initial transverse crack and case 2 was to trace the crack growth of an initial delamination. Both cases used the boundary conditions of Eqns. (3.19a-c). The transverse crack case used the crack geometry of Fig. (3.1b) and the delamination case used the crack geometry of Fig. (3.8). Both cases were modeled as the free edge of an 8-ply tensile specimen with

$$B = 0.25\text{in}, H = 0.01\text{in}, C = 2H, a = 0.77H \quad (3.20)$$

and an applied normal strain of, Fig. (2.10),

$$\epsilon_{xx} = 0.001 \quad (3.21)$$

The modified point stress criterion, Section 2.2.4.1, was used to predict the direction of crack extension and the modified crack closure method was used to compute the energy release rates.

The resulting crack growth sequence for the initial transverse crack, case 1, is presented in Fig. (3.9). The case 1 results indicated

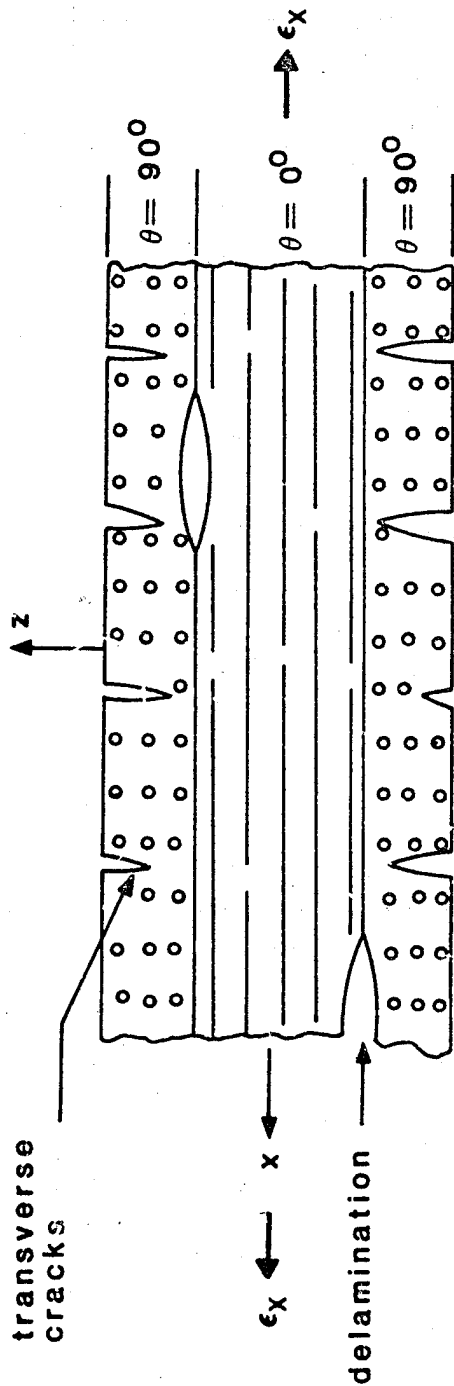


Figure 3.7 Possible Crack Types On The Free Edge
Of A Cross-Ply Laminate

ORIGINAL PAGE IS
OF POOR QUALITY

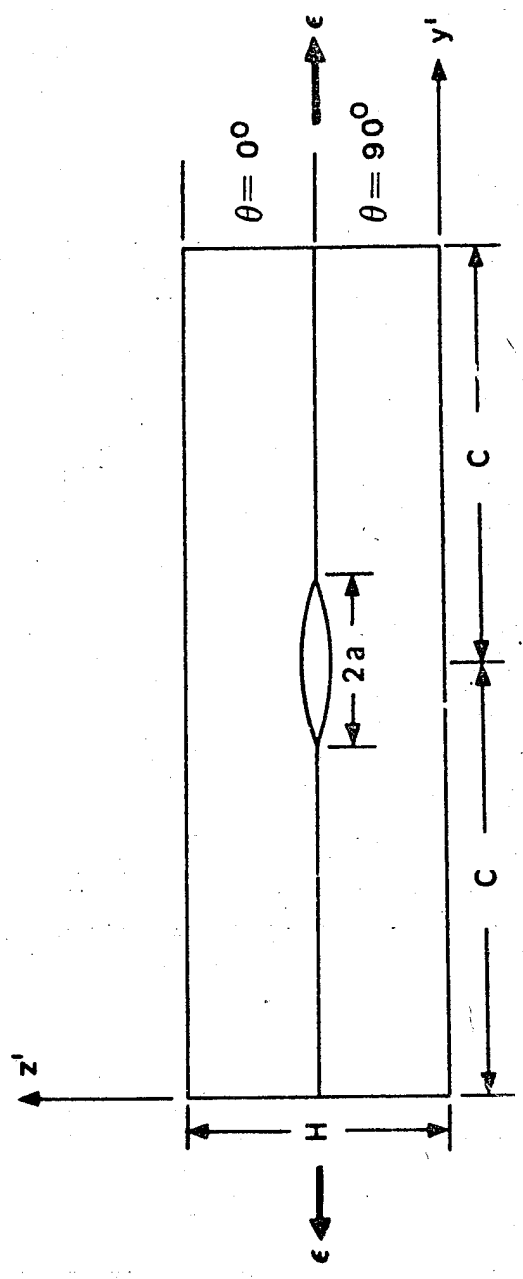


Figure 3.8. Delamination Crack Growth Model

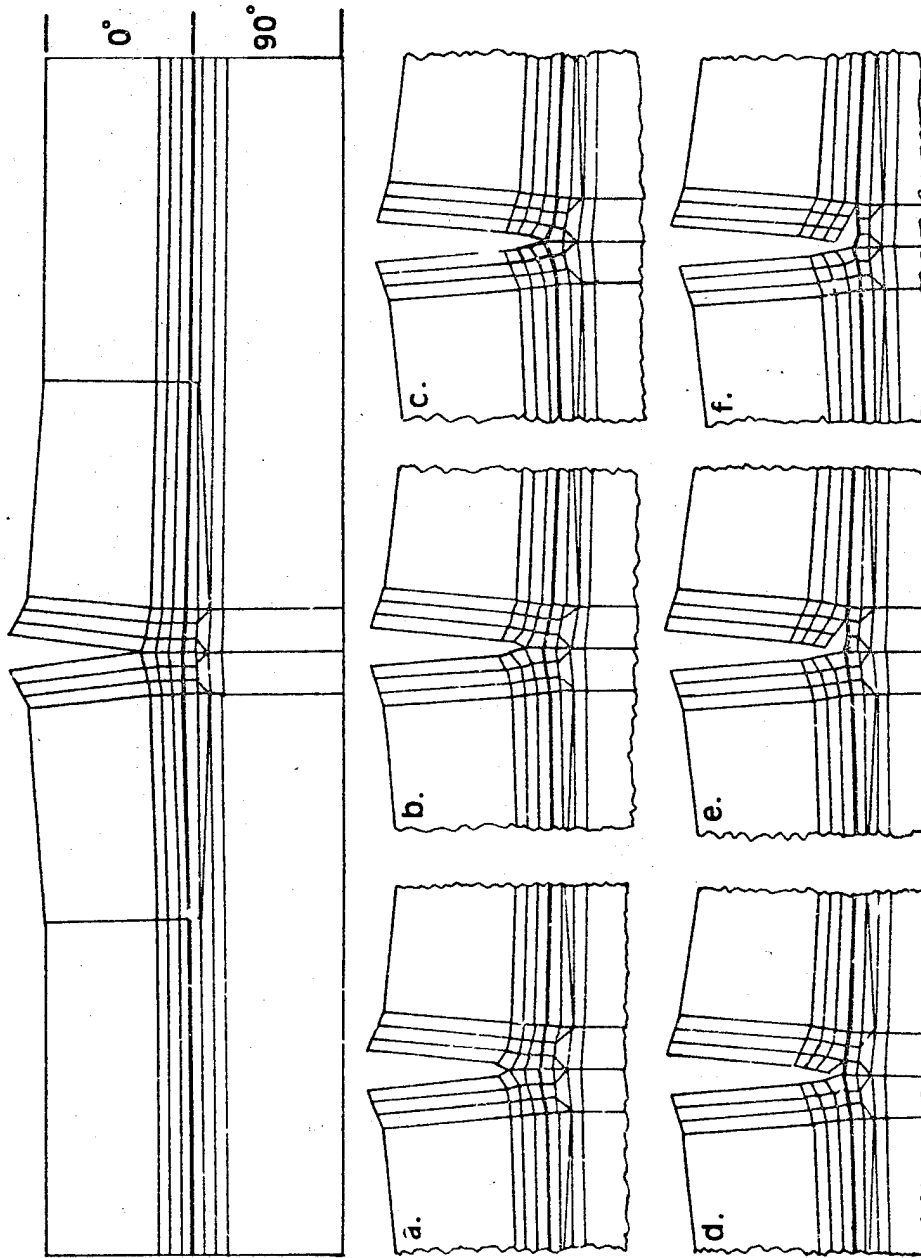


Figure 3.9 Cross-Ply Transverse Crack Growth Sequence

that the transverse crack extended through the 90° ply down to the 0° ply when it turned into a delamination. Note that this does not necessarily indicate that a transverse crack will turn into a delamination but just that, if the transverse crack was the only crack present and if it was to continue to extend that it would extend as a delamination before extending through the $\theta = 0^\circ$ plys. The plot of the corresponding energy release rate vs. crack length is shown in Fig. (3.10). Point A represents the initial crack length and point B represents the point at which the transverse crack turned into a delamination. The critical energy release rate for such a crack, is given by Wang and Crossman [6] for a mode-I transverse crack in graphite-epoxy as

$$G_{IC} = 0.9 \frac{\text{in. lbs}}{\text{in}^2} \quad (3.22)$$

Since the available energy release rate curve, Fig. (3.10), was less than $0.6 \frac{\text{in. lbs}}{\text{in}^2}$ for the entire crack extension sequence, the crack would not have extended at the applied load level of $\epsilon_{xx} = 0.001$. However, if the load were increased the G vs. a curve would have translated up, retaining the exact same shape, [6], C-D in Fig. (3.10) for example, and would have predicted crack growth until the crack length was such that the available energy release fell below the critical energy release rate. Regardless of applied load, however, the shape of the G vs. a curve, Fig. (3.10), indicates that G is decreasing with increasing a. Hence, there exists a certain range of ϵ_{xx} values for which the transverse crack would grow then arrest when G falls below G_c . This trend is

ORIGINAL PAGE IS
OF POOR QUALITY

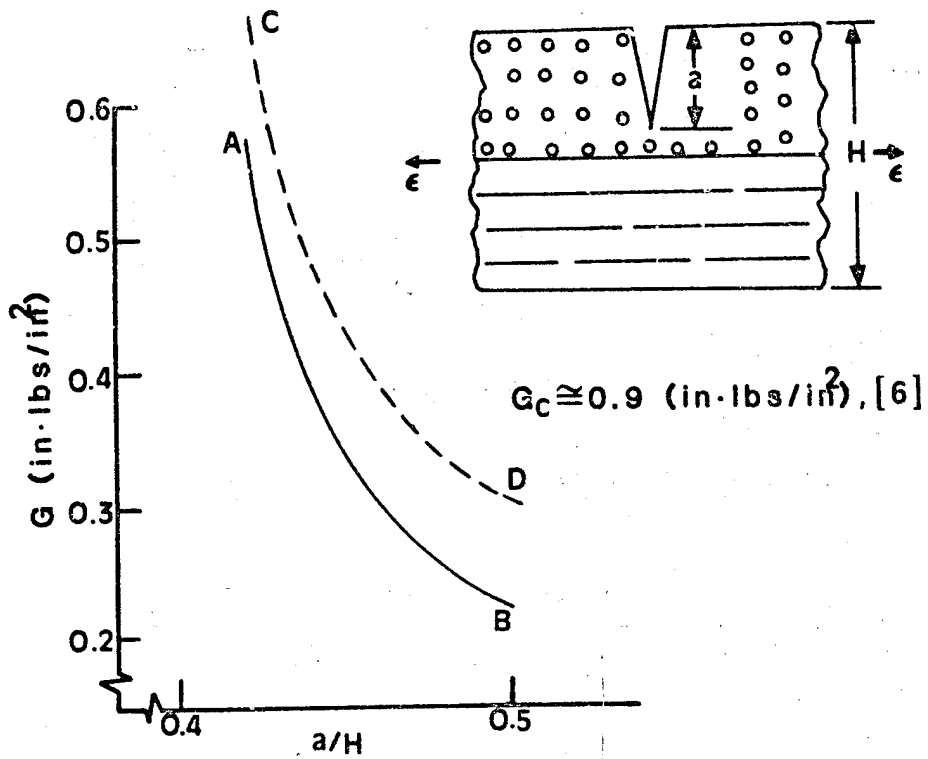


Figure 3.10 G vs. a For Transverse Crack Growth
In A Cross-Ply Laminate

supported by many experimental results of [6, 22], for example, which show that transverse cracks will grow through the 90° plys, arrest and form other transverse cracks at regular spacings.

The results for the initial delamination crack, case 2, indicated that the initial delamination would immediately turn into a transverse mode. In comparing the point stress ratios of the initial delamination crack with the initial transverse crack at the point it turned into a delamination, it was found that the point stress ratio was roughly two times larger for the delamination turning into a transverse crack than for the transverse crack turning into a delamination. This indicates that if both a delamination and a transverse crack were present in a given specimen, the delamination would turn and grow into a transverse crack before the initial transverse crack would extend. This trend is supported by the experimental results of Harris and Orringer [22], which indicate that transverse cracks can branch off from delaminations.

Chapter 4

CONCLUSIONS

The present investigation has been concerned with predicting the direction of crack extension as well as the load to cause extension in composite materials. The results of the present study indicate that failure criteria can be used to predict the direction of crack extension and that an energy release rate approach, implemented through the use of a modified crack closure integral, can be used to determine when a crack extends and if crack arrest will occur. The finite element models presented herein were formulated for two-dimensional and quasi three-dimensional analysis. However, the procedures and methods developed can be applied to full three-dimensional analyses as well.

It was found that criteria for predicting the direction of crack extension should account for differences in the energy required to create crack surfaces at arbitrary angles to the material principal system. The Griffith criterion, the Tsai-Wu failure criterion and the Sih strain energy density theory all were unsatisfactory in this regard; but the modified point stress and Hashin criteria provided good predictions for crack growth direction. It was also found that since the procedure developed herein assumes that crack extension will occur along the element sides adjacent to the crack tip node, an incorrect direction of extension can be chosen if no element sides coincide with the actual direction of extension. However, the model always chooses the closest direction available to the actual direction of extension. This problem

can easily be overcome by first finding an approximate direction of extension using a coarse mesh then refining the mesh in the area of the direction chosen by the coarse mesh.

The present investigation has also shown that future research is warranted in the following areas:

1. The extension of the current work into a full three-dimensional model. A full three-dimensional model should be formulated to account for the three-dimensional crack growth characteristics of many laminates.
2. Experimental work in the area of critical energy release rates. Experimental work should be performed to determine the effect on the critical energy release rate of cracks extending at arbitrary angles to the material principal system so that the load to cause failure can be accurately defined.

REFERENCES

1. Smith, C. W., "Limitations of Fracture Mechanics as Applied to Composites," Inelastic Behavior of Composite Materials, AMD - Vol. 13, (Herakovich, ed.), The American Society of Mechanical Engineers, New York, 1975, pp. 157-175.
2. Sih, G. C., "Fracture Mechanics of Composite Materials," Fracture of Composite Materials, Proceedings of first USA-USSR Symposium on Fracture of Composite Materials, Sijthoff and Noordhoff, The Netherlands, 1979, pp. 111-130.
3. Adams, D. F., "Elastoplastic Crack Propagation in a Transversely Loaded Unidirectional Composite," Journal of Composite Materials, Vol. 8, January 1974, pp. 38-54.
4. Atluri, S. N., Kobayashi, A. S., and Nakagaki, M., "A Finite Element Program for Fracture Analysis of Composite Materials," Fracture Mechanics of Composites, ASTM STP 593, American Society for Testing and Materials, 1975, pp. 86-98.
5. Benzley, S. E., "Representation of Singularities with Isoparametric Finite Elements," International Journal for Numerical Methods in Engineering, Vol. 8, 1974, pp. 537-545.
6. Wang, A. S. D., Crossman, F. W., "Fracture Mechanics of Transverse Cracks and Edge Delamination in Graphite-Epoxy Composite Laminates," Final Technical Report, Air Force Office of Scientific Research, March 1982.
7. Herakovich, C. T., "Influence of Layer Thickness on the Strength of Angle-Ply Laminates," Journal of Composite Materials, Vol. 16, 1982, pp. 216-227.
8. Herakovich, C. T., "On the Relationship Between Engineering Properties and Delamination of Composite Materials," Journal of Composite Materials, Vol. 15, 1975, pp. 336-348.
9. Rybicki, E. F. and Kannien, M. F., "A Finite Element Calculation of Stress Intensity Factors by a Modified Crack Closure Integral," Engineering Fracture Mechanics, Vol. 9, 1977, pp. 931-938.
10. Hashin, Z., "Failure Criteria for Unidirectional Fiber Composites," Journal of Applied Mechanics, Vol. 47, June 1980, pp. 329-334.
11. Tsai, S. W. and Wu, E. M., "A General Theory of Strength for Anisotropic Materials," Journal of Composite Materials, January 1971, pp. 58-80.

12. Whitney, J. M. and Nuismer, R. J., "Stress Fracture Criteria for Laminated Composites Containing Stress Concentrations," Journal of Composite Materials, Vol. 8, 1974, pp. 253-265.
13. Griffith, A. A., "The Theory of Rupture," Proceedings of the First International Congress of Applied Mechanics, Biezeno and Burgers, eds., Waltman, 1925, pp. 55-63.
14. Irwin, G. R., "Fracture," Handbuch Der Physik, Vol. 6, 1958, p. 551.
15. Sih, G. C., "Methods of Analysis and Solutions of Crack Problems," Mechanics of Fracture, Vol. I, Noordhoff, Leiden, 1973.
16. Frederick, D. and Chang, T. S., Continuum Mechanics, Scientific Publishers, Inc., Cambridge, 1972, p. 158.
17. Parker, A. P., The Mechanics of Fracture and Fatigue, E. and F. N. Spon Ltd., New York, 1981, pp. 23-46.
18. Sih, G. C., "Some Basic Problems in Fracture Mechanics and New Concepts," Engineering Fracture Mechanics, Vol. 5, 1973, pp. 365-377.
19. Nemeth, M. P., Herakovich, C. T. and Post, D., "On the Off-Axis Tensile Test for Unidirectional Composites," Composites Technology Review, ASTM, to be published in 1983.
20. Hancock, J. R., "Fatigue of Metal-Matrix Composites," Composite Materials Fracture and Fatigue, Vol. 5, Academic Press, New York, 1974, pp. 371-414.
21. Pindera, M. J., Herakovich, C. T., "An Endochronic Theory for Transversely Isotropic Fibrous Composites," VPI-E-81-27, College of Engineering, Virginia Polytechnic Institute and State University, Blacksburg, Virginia, 1981.
22. Harris, A. and Orringer, O., "Investigation of Angle-Ply Delamination Specimen for Interlaminar Strength Test," Journal of Composite Materials, Vol. 12, 1978, pp. 285-299.
23. Segerlind, L. J., Applied Finite Element Analysis, John Wiley and Sons, Inc., New York, 1976, pp. 80-84, 314-316.
24. Jones, R. M., Mechanics of Composite Materials, SCRIPTA Book Co., Washington, DC, 1975, pp. 32-53.

25. Nagarkar, A. P., Herakovich, C. T., "Nonlinear Temperature Dependent Failure Analysis of Finite Width Composite Laminates," VPI-E-79-36, Virginia Polytechnic Institute and State University, Blacksburg, VA, 1979.

APPENDIX A

Linear Elastic Finite Element Relationships

The finite element used is shown in Fig. (A.1). The element is a four node, general quadrilateral, isoparametric element. The element uses linear interpolation as described by Segerlind [23]. The details of the finite element concept are also given in reference [23]. The technique involves mapping a distorted shape in the Cartesian (y,z) Coordinate System into a square in the Local (ξ, η) Coordinate System where ξ and η range from -1 to +1. The relationship between the global Cartesian and the local coordinates is

$$\begin{aligned} Y &= N_1 Y_1 + N_2 Y_2 + N_3 Y_3 + N_4 Y_4 = N_i Y_i & i &= 1,4 \\ Z &= N_1 Z_1 + N_2 Z_2 + N_3 Z_3 + N_4 Z_4 = N_i Z_i & i &= 1,4 \end{aligned} \quad (\text{A.1})$$

where the $N_i(\xi, \eta)$ are the interpolation functions for the four node points and Y_i, Z_i are the Cartesian coordinates of the nodes. The interpolation functions are given by

$$\begin{aligned} N_1 &= \frac{1}{4}(1-\xi)(1-\eta), & N_2 &= \frac{1}{4}(1+\xi)(1-\eta) \\ N_3 &= \frac{1}{4}(1+\xi)(1+\eta), & N_4 &= \frac{1}{4}(1-\xi)(1+\eta) \end{aligned} \quad (\text{A.2})$$

For an isoparametric element, the same interpolation functions are used for the assumed displacements as for the geometry. Hence, for plane

ORIGINAL PAGE IS
OF POOR QUALITY

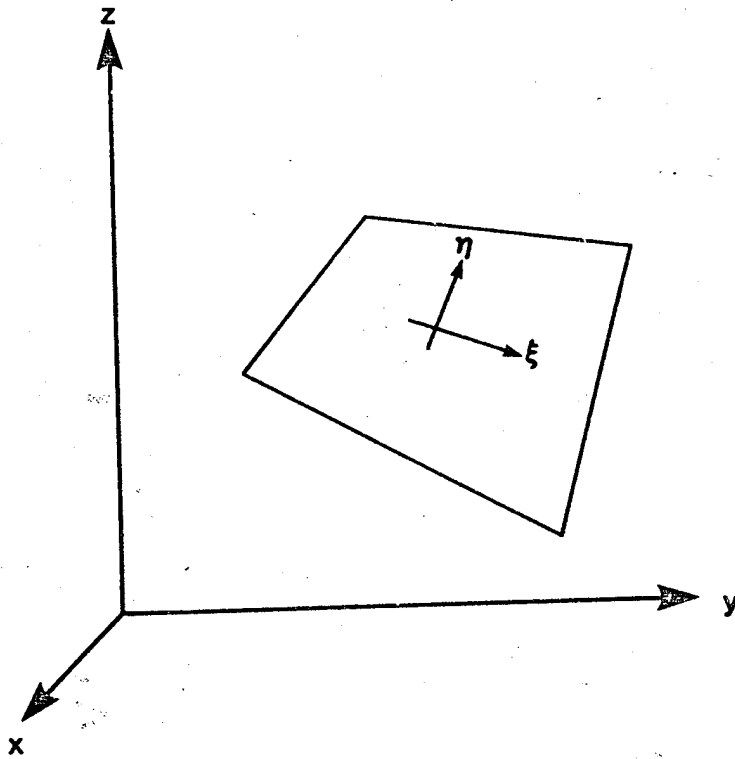


Figure A.1 Global And Local Coordinate System -
4 Node , Isoparametric Element

stress or plane strain, where there exists two unknown degrees of freedom per node, the interpolation becomes

$$\begin{aligned} v(y,z) &= N_i v_i & i &= 1,4 \\ w(y,z) &= N_i w_i & i &= 1,4 \end{aligned} \quad (\text{A.3})$$

For generalized plane strain, where there are three degrees of freedom per node, the interpolation is given by

$$\begin{aligned} u(x,y,z) &= U(y,z) + \epsilon_{xx} \cdot x = N_i u_i + \epsilon_{xx} \cdot x & i &= 1,4 \\ v(x,y,z) &= V(y,z) = N_i v_i & i &= 1,4 \\ w(x,y,z) &= W(y,z) = N_i w_i & i &= 1,4 \end{aligned} \quad (\text{A.4})$$

where u , v and w are the x , y and z displacements, respectively. u_i , v_i and w_i are the unknown values at the i th node and are functions of y and z only, and ϵ_{xx} is the total strain in the x direction, which is assumed to be constant and either known or unknown.

The strain-displacement relationships are derived based on the small strain - small displacement theory. For the three dimensional (generalized plane strain) case, these relationships may be written as

$$\begin{Bmatrix} \epsilon_{xx} \\ \epsilon_{yy} \\ \epsilon_{zz} \\ \gamma_{yz} \\ \gamma_{xz} \\ \gamma_{xy} \end{Bmatrix} = \begin{bmatrix} \frac{\partial}{\partial x} & 0 & 0 \\ 0 & \frac{\partial}{\partial y} & 0 \\ 0 & 0 & \frac{\partial}{\partial z} \\ 0 & \frac{\partial}{\partial z} & \frac{\partial}{\partial y} \\ \frac{\partial}{\partial z} & 0 & \frac{\partial}{\partial x} \\ \frac{\partial}{\partial y} & \frac{\partial}{\partial x} & 0 \end{bmatrix} \begin{Bmatrix} u \\ v \\ w \end{Bmatrix} \quad (\text{A.5})$$

And for plane strain or plane stress these relationships become

$$\begin{Bmatrix} \epsilon_{yy} \\ \epsilon_{zz} \\ \gamma_{yz} \end{Bmatrix} = \begin{bmatrix} \frac{\partial}{\partial y} & 0 \\ 0 & \frac{\partial}{\partial z} \\ \frac{\partial}{\partial z} & \frac{\partial}{\partial y} \end{bmatrix} \begin{Bmatrix} v \\ w \end{Bmatrix} \quad (\text{A.6})$$

Substituting (A.4) into (A.5), for generalized plane strain,

$$\begin{Bmatrix} \epsilon_{xx} \\ \epsilon_{yy} \\ \epsilon_{zz} \\ \gamma_{yz} \\ \gamma_{xz} \\ \gamma_{xy} \end{Bmatrix} = \begin{bmatrix} \frac{\partial}{\partial x} & 0 & 0 \\ 0 & \frac{\partial}{\partial y} & 0 \\ 0 & 0 & \frac{\partial}{\partial z} \\ 0 & \frac{\partial}{\partial z} & \frac{\partial}{\partial y} \\ \frac{\partial}{\partial z} & 0 & \frac{\partial}{\partial x} \\ \frac{\partial}{\partial y} & \frac{\partial}{\partial x} & 0 \end{bmatrix} [IN_1 | IN_2 | IN_3 | IN_4] \{q\} + \begin{Bmatrix} \epsilon_{xx} \\ 0 \\ 0 \\ 0 \\ 0 \\ 0 \end{Bmatrix} \quad (\text{A.7})$$

where

I is the 3 x 3 identity matrix

{q} is the 12 x 1 vector of nodal displacements

given by

ORIGINAL PAGE IS
OF POOR QUALITY

$$\{q\} = \begin{Bmatrix} u_1 \\ v_1 \\ w_1 \\ u_2 \\ v_2 \\ w_2 \\ u_3 \\ v_3 \\ w_3 \\ u_4 \\ v_4 \\ w_4 \end{Bmatrix} \quad (A.8)$$

Substituting (A.3) into (A.6), for plane stress or plane strain,

$$\begin{Bmatrix} \epsilon_{yy} \\ \epsilon_{zz} \\ \gamma_{yz} \end{Bmatrix} = \begin{bmatrix} \frac{\partial}{\partial y} & 0 \\ 0 & \frac{\partial}{\partial z} \\ \frac{\partial}{\partial z} & \frac{\partial}{\partial y} \end{bmatrix} [\bar{I}N_1 | \bar{I}N_2 | \bar{I}N_3 | \bar{I}N_4] \{\bar{q}\} \quad (A.9)$$

where

\bar{I} is the 2 x 2 identity matrix

$\{\bar{q}\}$ is the 8 x 1 vector of nodal displacements given by

ORIGINAL PAGE IS
OF POOR QUALITY

$$\{\bar{q}\} = \begin{Bmatrix} v_1 \\ w_1 \\ v_2 \\ w_2 \\ v_3 \\ w_3 \\ v_4 \\ w_4 \end{Bmatrix} \quad (\text{A.10})$$

The [B] matrix (strain-displacement relationships) for generalized plane strain can be defined as

$$\{\epsilon\} = [B]\{q\} + \begin{Bmatrix} \epsilon_{xx} \\ 0 \\ 0 \\ 0 \\ 0 \\ 0 \end{Bmatrix} \quad (\text{A.11})$$

(6x1) (6x12)(12x1)

where by comparing (A.11) and (A.7), for generalized plane strain,

$$[B] = \begin{bmatrix} \frac{\partial}{\partial x} & 0 & 0 \\ 0 & \frac{\partial}{\partial y} & 0 \\ 0 & 0 & \frac{\partial}{\partial z} \\ 0 & \frac{\partial}{\partial z} & \frac{\partial}{\partial y} \\ \frac{\partial}{\partial z} & 0 & \frac{\partial}{\partial x} \\ \frac{\partial}{\partial y} & \frac{\partial}{\partial x} & 0 \end{bmatrix} [IN_1|IN_2|IN_3|IN_4] \quad (A.12)$$

For plane strain or plane stress, the $[B]$ matrix can be written as

$$\begin{matrix} \{\epsilon\} = [B]\{\bar{q}\} & (A.13) \\ (3 \times 1) & (3 \times 8)(8 \times 1) \end{matrix}$$

Comparing (A.13) and (A.9), for plane stress or plane strain,

$$[B] = \begin{bmatrix} \frac{\partial}{\partial y} & 0 \\ 0 & \frac{\partial}{\partial z} \\ \frac{\partial}{\partial z} & \frac{\partial}{\partial y} \end{bmatrix} [IN_1|IN_2|IN_3|IN_4] \quad (A.14)$$

Recall from (A.2) that the N_i are functions of the local coordinates ξ and η . In order to determine the elements of the $[B]$ matrix a relationship between the derivatives in the global (y,z) and the local (ξ, η) coordinate systems is needed. This relationship is given by the Jacobian matrix $[J]$ of the transformation where

$$\begin{Bmatrix} \frac{\partial N_i}{\partial y} \\ \frac{\partial N_i}{\partial z} \end{Bmatrix} = [J]^{-1} \begin{Bmatrix} \frac{\partial N_i}{\partial \xi} \\ \frac{\partial N_i}{\partial \eta} \end{Bmatrix} \quad (i = 1, 2, 3, 4) \quad (\text{A.15a})$$

and

$$[J] = \begin{bmatrix} \frac{\partial y}{\partial \xi} & \frac{\partial z}{\partial \xi} \\ \frac{\partial y}{\partial \eta} & \frac{\partial z}{\partial \eta} \end{bmatrix} \quad (\text{A.15b})$$

Substituting (A.1) into (A.15)

$$[J] = \begin{bmatrix} \frac{\partial N_1}{\partial \xi} & \frac{\partial N_2}{\partial \xi} & \frac{\partial N_3}{\partial \xi} & \frac{\partial N_4}{\partial \xi} \\ \frac{\partial N_1}{\partial \eta} & \frac{\partial N_2}{\partial \eta} & \frac{\partial N_3}{\partial \eta} & \frac{\partial N_4}{\partial \eta} \end{bmatrix} \begin{bmatrix} y_1 & z_1 \\ y_2 & z_2 \\ y_3 & z_3 \\ y_4 & z_4 \end{bmatrix} \quad (\text{A.16})$$

The stress-strain relationships are derived in Appendix B. For general purposes they can be written as

$$\{\sigma\} = [D]\{\epsilon\} \quad (\text{A.17})$$

For generalized plane strain, $\{\sigma\}$ and $\{\epsilon\}$ are 6×1 vectors, and are given in Appendix B by Eqns. (B.9) and (B.10), respectively.

For generalized plane strain, the $[D]$ matrix takes on the values of the $[\bar{C}]$ matrix as given by Eqn. (B.8). For plane stress or plane

strain $\{\sigma\}$ and $\{\epsilon\}$ are the 3 x 1 vectors given by Eqns. (B.14) and (B.15), respectively. For orthotropic plane stress the $[D]$ matrix takes on the value of the 3 x 3 $[\bar{D}]$ matrix of Eqn. (B.13), while for isotropic plane strain the $[D]$ matrix becomes the 3 x 3 $[\bar{C}]$ matrix of Eqn. (B.18).

The total potential energy, π , of a given finite element is the sum of the strain energy, U , and the work of external loads, W . The strain energy, U , of the element is

$$U = \frac{1}{2} \int_V \{\sigma\} \{\epsilon\}^T dV \quad (\text{A.18})$$

and the work of external loads, W , is

$$W = -\{q\} \{F\}^T \quad (\text{A.19})$$

where $\{F\}$ is applied mechanical load, (traction), vector.

Hence, the total potential energy of the element is given by

$$\pi = U + W \quad (\text{A.20})$$

Substitution into (A.20) in terms of the matrices and vectors described herein and minimizing with respect to the unknowns yields the finite element equations

$$[K]\{q\} = \{F\} \quad (\text{A.21})$$

where $[K]$ is the elemental stiffness matrix given by

$$[K] = \int_V [B]^T [D] [B] dV \quad (A.22)$$

when mapped into the ξ, η coordinate system

$$dV = |J| d\xi d\eta \quad (A.23)$$

where $|J|$ is the determinate of the Jacobian matrix. The limits of integration are -1 to $+1$ in both ξ and η . Hence, Eqn. (A.22) becomes

$$[K] = \int_{-1}^1 \int_{-1}^1 [B]^T [D] [B] |J| d\xi d\eta = \int_{-1}^1 \int_{-1}^1 G(\xi, \eta) d\xi d\eta \quad (A.24)$$

In order to evaluate the stiffness matrix, $[K]$, a numerical integration is necessary. Using a 2×2 Gauss rule Eqn. (A.24) can be evaluated as

$$[K] = \sum_{i=1}^2 \sum_{j=1}^2 H_i H_j G(a_i, b_j) \quad (A.25)$$

$$\text{where } G(\xi, \eta) = [B]^T [D] [B] |J| \quad (A.26)$$

(a_i, b_j) are the coordinates of the four Gauss points given by

$$a_i = \sqrt{\frac{1}{3}}, \sqrt{\frac{1}{3}} \quad (A.27)$$

$$b_j = \sqrt{\frac{1}{3}}, \sqrt{\frac{1}{3}}$$

and (H_i, H_j) are the corresponding weight functions given by

$$\begin{aligned} H_i &= 1,1 \\ H_j &= 1,1 \end{aligned} \tag{A.28}$$

The elemental matrices are then assembled into a global system of equations, the prescribed boundary conditions are imposed and the system of equations is solved for the unknown displacements. (This procedure is explained in most finite element books [23].)

The strains can be found at any ξ, η location within an element through the use of Eqn. (A.7) for generalized plane strain and through Eqn. (A.9) for plane stress or plane strain. The strains can be converted to stresses by using the stress strain relation of Eqn. (A.17) where $[D]$ takes on the values of the appropriate constitutive relation (Appendix B).

ORIGINAL PAGE IS
OF POOR QUALITY

APPENDIX B

CONSTITUTIVE RELATIONS

The constitutive relation for an orthotropic material in the principal material directions, Fig. (B.1), is given by Jones [24] as

$$\{\sigma\}_1 = [C]\{\epsilon\}_1 \quad (\text{B.1})$$

where

$$[C] = \begin{bmatrix} C_{11} & C_{12} & C_{13} & 0 & 0 & 0 \\ & C_{22} & C_{23} & 0 & 0 & 0 \\ & & C_{33} & 0 & 0 & 0 \\ & & & C_{44} & 0 & 0 \\ \text{(symmetric)} & & & & C_{55} & 0 \\ & & & & & C_{66} \end{bmatrix} \quad (\text{B.2})$$

$$\{\sigma\}_1 = \begin{bmatrix} \sigma_{11} \\ \sigma_{22} \\ \sigma_{33} \\ \tau_{23} \\ \tau_{13} \\ \tau_{12} \end{bmatrix} \quad (\text{B.3})$$

ORIGINAL PAGE IS
OF POOR QUALITY

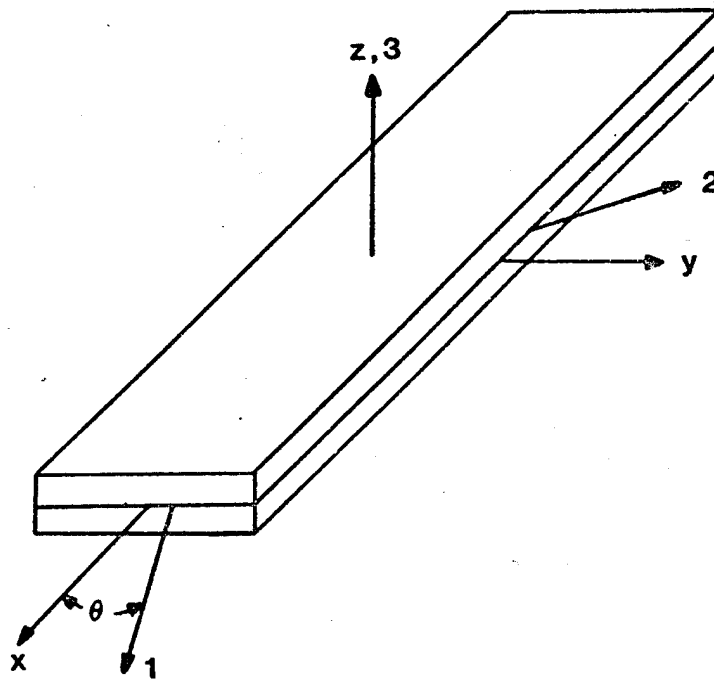


Figure B.1 Material And Global Coordinate System
For A General Laminate

ORIGINAL PAGE IS
OF POOR QUALITY

$$\{\epsilon\}_1 = \begin{Bmatrix} \epsilon_{11} \\ \epsilon_{22} \\ \epsilon_{33} \\ \gamma_{23} \\ \gamma_{13} \\ \gamma_{12} \end{Bmatrix} \quad (\text{B.4})$$

$$C_{11} = \frac{1-\nu_{23}\nu_{32}}{E_{22}E_{33}\Delta}, \quad C_{12} = \frac{\nu_{12}+\nu_{32}\nu_{13}}{E_{11}E_{33}\Delta}, \quad C_{13} = \frac{\nu_{13}+\nu_{12}\nu_{23}}{E_{11}E_{22}\Delta}$$

$$C_{22} = \frac{1-\nu_{13}\nu_{31}}{E_{11}E_{33}\Delta}, \quad C_{23} = \frac{\nu_{23}+\nu_{21}\nu_{13}}{E_{11}E_{22}\Delta}, \quad C_{33} = \frac{1-\nu_{12}\nu_{21}}{E_{11}E_{22}\Delta} \quad (\text{B.5})$$

$$C_{44} = G_{23}, \quad C_{55} = G_{13}, \quad C_{66} = G_{12}$$

$$\Delta = \frac{1-\nu_{12}\nu_{21}-\nu_{23}\nu_{32}-\nu_{31}\nu_{13}-2\nu_{21}\nu_{32}\nu_{13}}{E_{11}E_{22}E_{33}}$$

and

$$\frac{\nu_{12}}{E_{11}} = \frac{\nu_{21}}{E_{22}}$$

$$\frac{\nu_{13}}{E_{11}} = \frac{\nu_{31}}{E_{33}} \quad (\text{B.6})$$

$$\frac{\nu_{23}}{E_{22}} = \frac{\nu_{32}}{E_{33}}$$

For a θ rotation about the 3, (z), axis, Fig. (B.1), the constitutive relation becomes

$$\{\sigma\} = [\bar{C}]\{\epsilon\} \quad (B.7)$$

where

$$[\bar{C}] = \begin{bmatrix} \bar{C}_{11} & \bar{C}_{12} & \bar{C}_{13} & 0 & 0 & \bar{C}_{16} \\ & \bar{C}_{22} & \bar{C}_{23} & 0 & 0 & \bar{C}_{26} \\ & & \bar{C}_{33} & 0 & 0 & \bar{C}_{36} \\ \text{(Symmetric)} & & & \bar{C}_{44} & \bar{C}_{45} & 0 \\ & & & & \bar{C}_{55} & 0 \\ & & & & & \bar{C}_{66} \end{bmatrix} \quad (B.8)$$

$$\{\sigma\} = \begin{bmatrix} \sigma_{xx} \\ \sigma_{yy} \\ \sigma_{zz} \\ \tau_{yz} \\ \tau_{xz} \\ \tau_{xy} \end{bmatrix} \quad (B.9)$$

$$\{\epsilon\} = \begin{bmatrix} \epsilon_{xx} \\ \epsilon_{yy} \\ \epsilon_{zz} \\ \gamma_{yz} \\ \gamma_{xz} \\ \gamma_{xy} \end{bmatrix} \quad (B.10)$$

If $m = \cos \theta$ and $n = \sin \theta$ then the components of the $[\bar{C}]$ matrix are given by

$$\begin{aligned}
 \bar{C}_{11} &= m^4 C_{11} + 2m^2 n^2 (C_{12} + 2C_{66}) + n^4 C_{22} \\
 \bar{C}_{12} &= m^2 n^2 (C_{11} + C_{22} - 4C_{66}) + (m^4 - n^4) C_{12} \\
 \bar{C}_{13} &= m^2 C_{13} + n^2 C_{23} \\
 \bar{C}_{16} &= mn [m^2 (C_{11} - C_{12} - 2C_{66}) + n^2 (C_{12} - C_{22} + 2C_{66})] \\
 \bar{C}_{22} &= n^4 C_{11} + 2m^2 n^2 (C_{12} + 2C_{66}) + m^4 C_{22} \\
 \bar{C}_{23} &= n^2 C_{13} + m^2 C_{23} \\
 \bar{C}_{26} &= mn [n^2 (C_{11} - C_{12} - 2C_{66}) + m^2 (C_{12} - C_{22} + 2C_{66})] \\
 \bar{C}_{33} &= C_{33} \\
 \bar{C}_{36} &= mn (C_{13} - C_{23}) \\
 \bar{C}_{44} &= m^2 C_{44} + n^2 C_{55} \\
 \bar{C}_{45} &= mn (C_{55} - C_{44}) \\
 \bar{C}_{55} &= n^2 C_{44} + m^2 C_{55} \\
 \bar{C}_{66} &= m^2 n^2 (C_{11} - 2C_{12} + C_{22}) + C_{66} (m^2 - n^2)^2
 \end{aligned} \tag{B.11}$$

For an orthotropic material under a state of plane stress with a θ rotation about the 3, (x) axis, Fig. (B.2), Jones [24] gives the constitutive relation as

$$\{\sigma\} = [\bar{Q}]\{\epsilon\} \tag{B.12}$$

ORIGINAL PAGE IS
OF POOR QUALITY

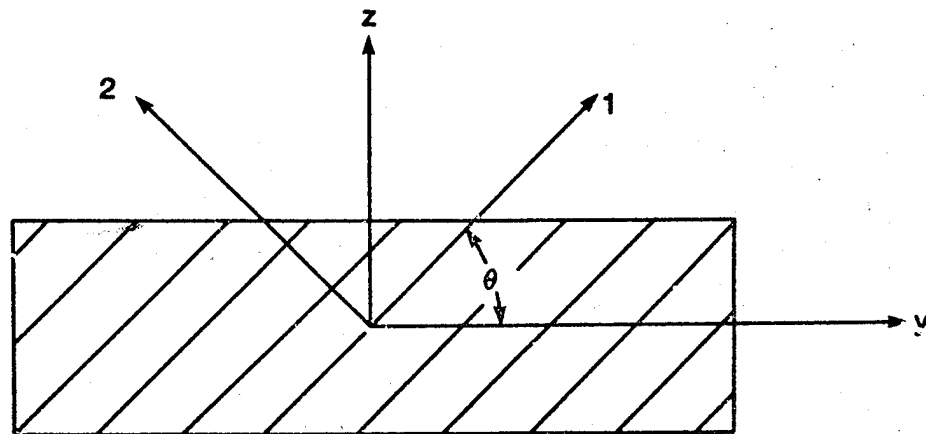


Figure B.2 Material And Global Coordinate System
For A Two-Dimensional Lamina

ORIGINAL PAGE IS
OF POOR QUALITY

where

$$[Q] = \begin{bmatrix} \bar{Q}_{11} & \bar{Q}_{12} & \bar{Q}_{16} \\ \bar{Q}_{12} & \bar{Q}_{22} & \bar{Q}_{26} \\ \bar{Q}_{16} & \bar{Q}_{26} & \bar{Q}_{66} \end{bmatrix} \quad (B.13)$$

$$\{\sigma\} = \begin{Bmatrix} \sigma_{yy} \\ \sigma_{zz} \\ \tau_{yz} \end{Bmatrix} \quad (B.14)$$

$$\{\epsilon\} = \begin{Bmatrix} \epsilon_{yy} \\ \epsilon_{zz} \\ \gamma_{yz} \end{Bmatrix} \quad (B.15)$$

and the \bar{Q}_{ij} terms of Eqn. (B.13) are given in terms of the \bar{C}_{ij} terms of Eqn. (B.11) by

$$\bar{Q}_{ij} = \bar{C}_{ij} - \frac{\bar{C}_{i3}\bar{C}_{j3}}{\bar{C}_{33}} \quad (B.16)$$

For an isotropic material under plane strain, Frederick and Chang [16] lists the constitutive relation as

$$\{\sigma\} = [\bar{C}]\{\epsilon\} \quad (B.17)$$

where

$$[\bar{C}] = \frac{E(1-\nu)}{(1+\nu)(1-2\nu)} \begin{bmatrix} 1 & \frac{\nu}{1-\nu} & 0 \\ \frac{\nu}{1-\nu} & 1 & 0 \\ 0 & 0 & \frac{1-2\nu}{2(1-\nu)} \end{bmatrix} \quad (\text{B.18})$$

$$\{\sigma\} = \begin{Bmatrix} \sigma_{yy} \\ \sigma_{zz} \\ \tau_{yz} \end{Bmatrix} \quad (\text{B.19})$$

$$\{\epsilon\} = \begin{Bmatrix} \epsilon_{yy} \\ \epsilon_{zz} \\ \gamma_{yz} \end{Bmatrix} \quad (\text{B.20})$$

and

$$\sigma_{zz} = \nu(\sigma_{yy} + \sigma_{zz}) \quad (\text{B.21})$$

APPENDIX C
MATERIAL PROPERTIES

The material properties for graphite-epoxy T300/5208 are given by Nagar-
kar and Herakovich [25] as

Elastic Moduli

$$E_{11} = 19.2 \times 10^6 \text{ psi}, \quad E_{22} = 1.56 \times 10^6 \text{ psi}, \quad E_{33} = 1.56 \times 10^6 \text{ psi}$$

Shear Moduli

$$G_{23} = 0.487 \times 10^6 \text{ psi}, \quad G_{13} = 0.820 \times 10^6 \text{ psi}, \quad G_{12} = 0.820 \times 10^6 \text{ psi}$$

Possion's Ratios

$$\nu_{23} = 0.490, \quad \nu_{13} = 0.238, \quad \nu_{12} = 0.238$$

Strength Parameters

$$\begin{aligned} X_T &= 219.5 \times 10^3 \text{ psi}, & Y_T &= 6.35 \times 10^3 \text{ psi}, & Z_T &= 6.35 \times 10^3 \text{ psi} \\ X_C &= -246.0 \times 10^3 \text{ psi}, & Y_C &= -23.85 \times 10^3 \text{ psi}, & Z_C &= -23.85 \times 10^3 \text{ psi} \\ S_{23} &= 9.8 \times 10^3 \text{ psi}, & S_{13} &= 12.6 \times 10^3 \text{ psi}, & S_{12} &= 12.6 \times 10^3 \text{ psi} \end{aligned}$$

The material properties for the isotropic problems considered were
chosen to be

$$E = 30 \times 10^6 \text{ psi}, \quad \nu = 0.20, \quad \sigma_u = 50 \times 10^3 \text{ psi}$$

where σ_u is the ultimate strength of the material.

APPENDIX D
FINITE ELEMENT MESHES

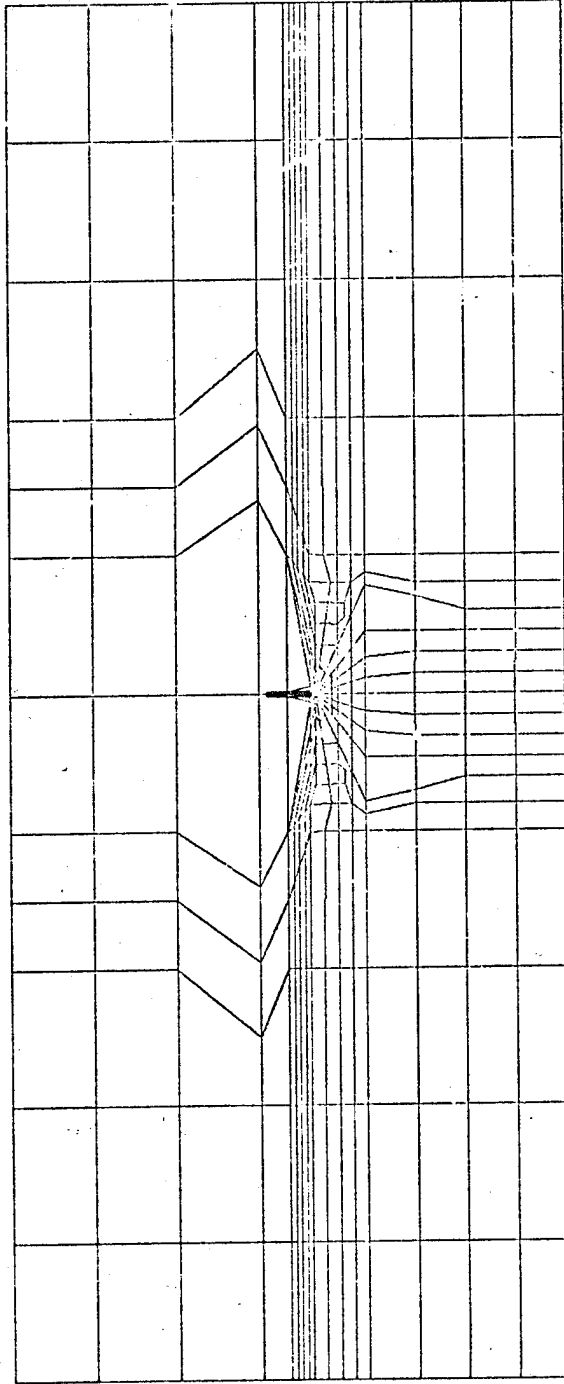


Figure D.1 306 Element X 338 Node Finite Element Mesh

ORIGINAL FACE IS
OF POOR QUALITY

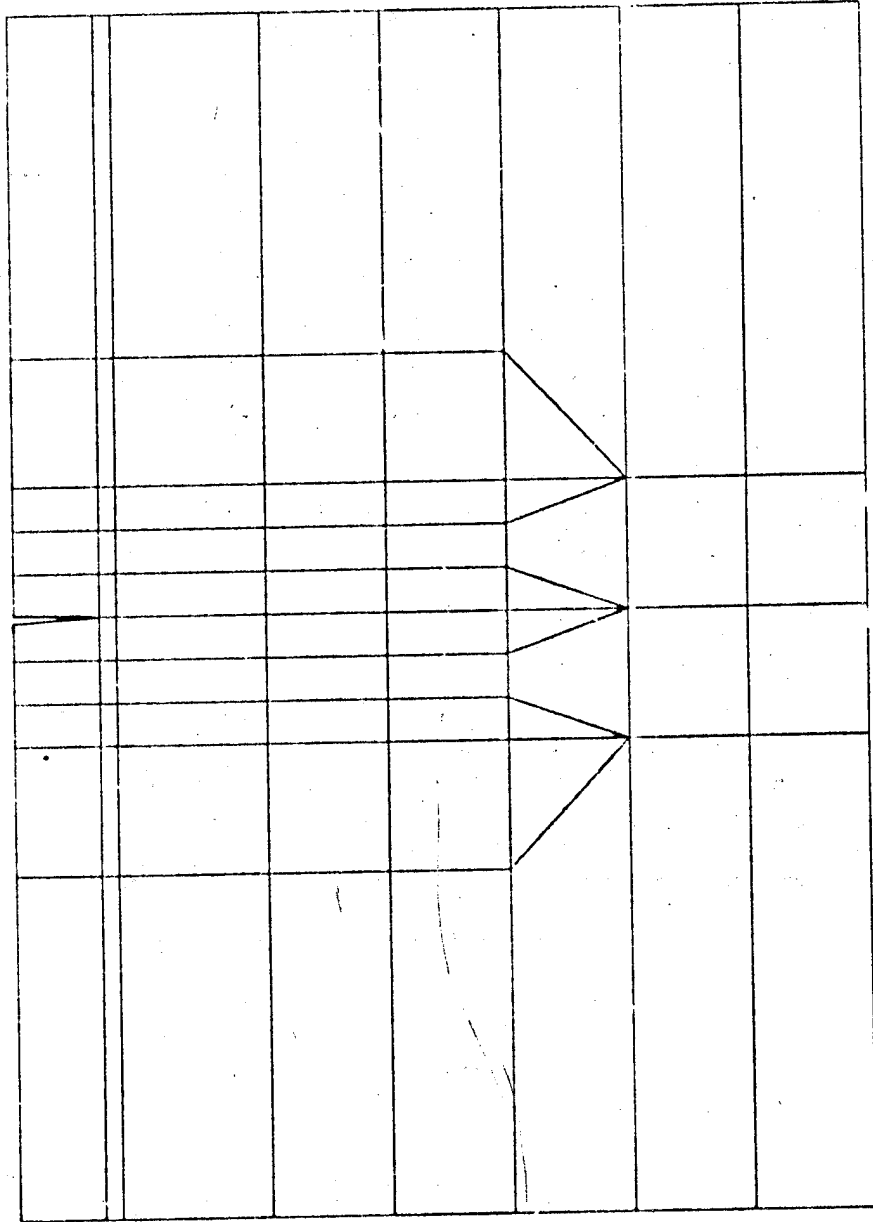


Figure D.2 68 Element X 82 Node Finite Element Mesh

ORIGINAL PAGE IS
OF POOR QUALITY

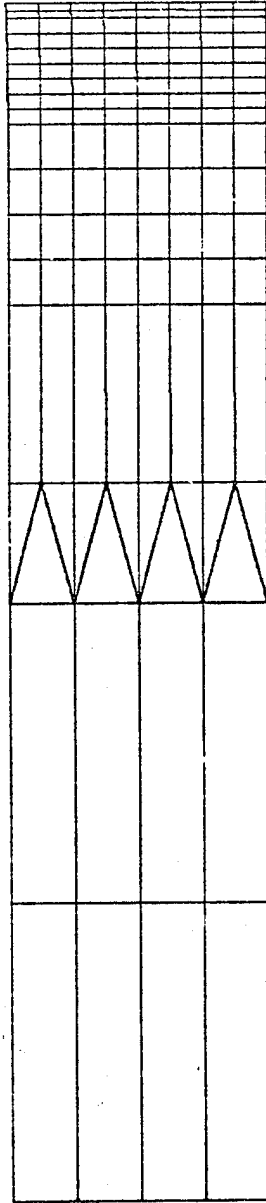


Figure D.3 132 Element X 150 Node Finite Element Mesh

APPENDIX E

ON THE RELATIONSHIP BETWEEN FREE-EDGE STRESSES AND THE DIRECTION OF CRACK EXTENSION IN ANGLE-PLY LAMINATES

It was originally thought that the free-edge stress state could be used to predetermine the direction of crack extension.

Herakovich [7, 8], for example, has demonstrated that the crack types present on the free-edge of tension specimens seem to exhibit distinct crack growth patterns direction of extension for different angle-ply laminates. To account for this effect it was thought that the orientation of the principal stress plane on the free edge would follow along the same path as the crack plane when traced through the laminate thickness. To test this premise, the orientation of the crack plane, ϕ_p , through the laminate thickness was compared with the through the thickness variation of the principal stress plane. A generalized plane strain solution of the front face, Fig. (3.6a), was obtained using the same geometry, loading and boundary conditions as given in Section 3.3. Only the stresses in the plane of the free edge were considered, i.e., σ_{xx} , σ_{zz} and τ_{xz} , in Fig. (2.10). It was assumed that the thermal curing stresses were balanced by the hygroscopic stresses in the laminate so that only mechanical loading be considered. The material considered and experimental crack plane orientation was that of Herakovich [7] (the material was the same T300/5208 graphite-epoxy of this report--with properties listed in Appendix C). The orientation of the principal

plane, ϕ_p , was calculated through

$$\phi_p = 270^\circ - \frac{1}{2} \tan^{-1} \left[\frac{2\tau_{xz}}{\sigma_{xx} - \sigma_{zz}} \right] \quad (E.1)$$

The results for four laminate configurations are presented in Fig. (E.1a-d). The multi-valued angles, ϕ_p , at $z/H = 0.5$ represent the effect of a crack turning into a delamination at that point. Fig. (E.1a-d) indicate that only in the $[90_2/0_2]_S$ case did the theory agree with the experiment. Hence, it was concluded that the direction of crack extension could not be predicted through the crack free stress state but that an actual crack must be introduced.

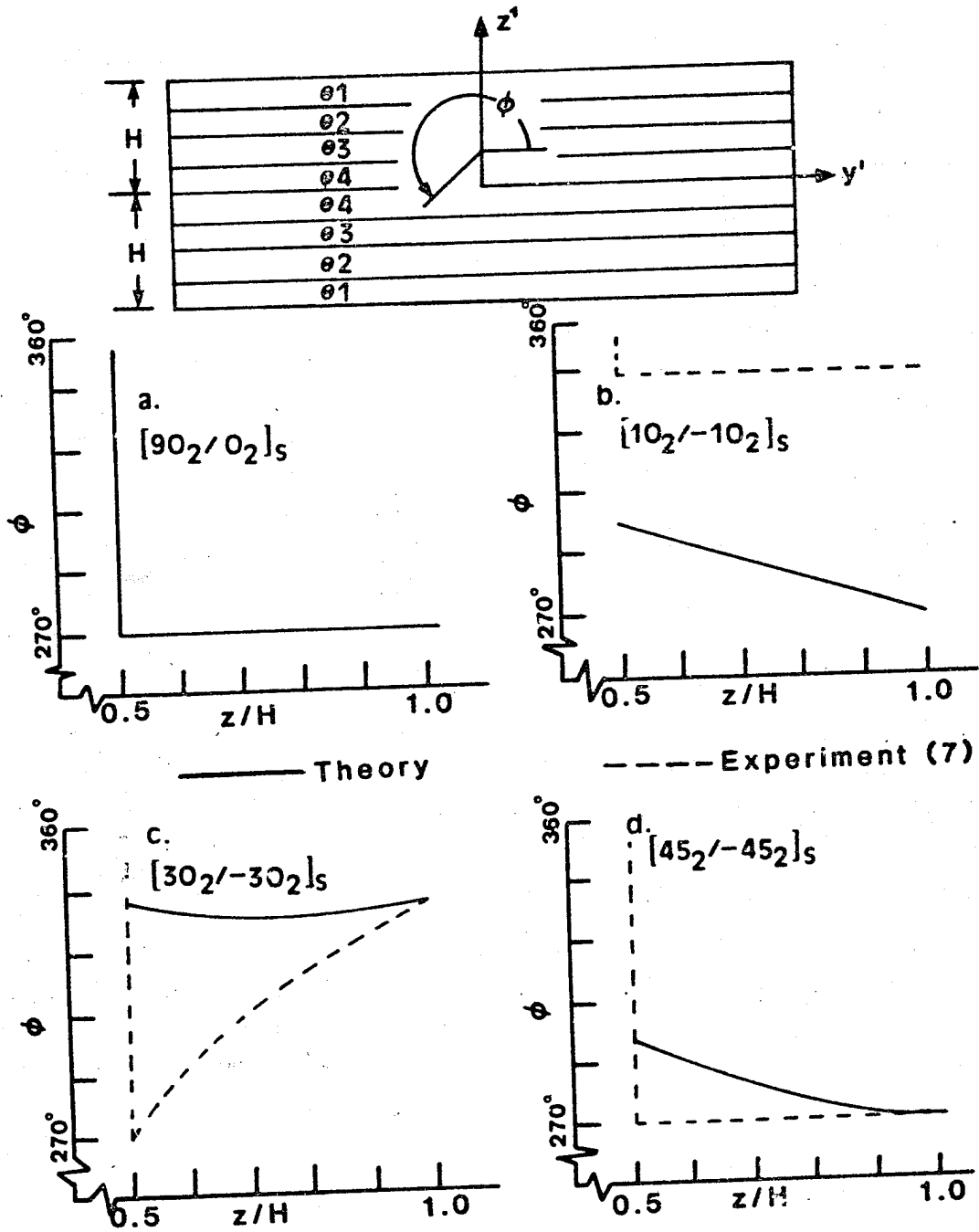


Figure E.1 Principal Plane Orientation vs. Plane Of Crack Extension For Angle-Ply Laminates

APPENDIX F
 COMPOSITE LAMINATE FRACTURE MECHANICS (CLFM2D)
 INPUT DATA SEQUENCE

Cards 1 & 2: title cards (20A4)

<u>Column</u>	<u>Contents</u>
1-80 ITITLE (I,J)	Title

Card 3: Control card (11IS)

<u>Column</u>	<u>Contents</u>
1-5 NPR0B	Problem type (1 = generalized plane strain, 2 = skewed plane stress, 3 = orthotropic plane stress, 4 = isotropic plane strain)
6-10 NEM	Number of elements in mesh
11-15 NODS	Number of nodes in mesh
16-20 NANG	Number of different angles - must be > 1
21-25 NSDF	Number of specified degrees of freedom
26-30 NSBF	Number of specified forces (tractions)
31-35 NEXX	Number of different E_{xx} - must be > 1.

36-40	NFX	Fracture mechanics key NFX = 0, no fracture analysis NFX \neq 0, fracture mechanics problem
41-45	NPLOTT	Plot key NPLOT = 0, no plot NPLOT = 1, undeformed plot only NPLOT = 2, deformed plot only NPLOT = 3, both deformed and undeformed plots
46-50	NT1	Dump file for displacements NT1 = 0, no dump NT1 \neq 0, dumps displacements to unit NT1
51-55	NT2	Dump file for strains, stresses and strain energies NT2 = 0, no dump NT2 \neq 0, dumps to unit NT2
56-60	NCHECK	Data check option (NCHECK \neq 0 - data check only)

Card 4: Scale factors (2D10.5)

<u>Column</u>	<u>Contents</u>
1-10 SCAV	Y-scale factor
11-20 SCAZ	Z-scale factor

Card 5: Printer control card (6I5)

<u>Column</u>		<u>Contents</u>
1-5	KEY (1)	Key for printing element data
6-10	KEY (2)	Key for printing nodal data
11-15	KEY (3)	Key for printing specified displacement data
16-20	KEY (4)	Key for printing specified force data
21-25	KEY (5)	Key for printing nodal displacements
26-30	KEY (6)	Key for printing strains, stresses and strain energies

Note: If KEY (I) \neq 0, print

Card 6: Plotter scale factors (4D10.5) - skip if NPLOT = 0

<u>Column</u>		<u>Contents</u>
1-10	PVSCl	Plot Y-scale factor
11-20	PZSCL	Plot Z-scale factor
21-30	VMAX	Maximum Y-displacement
31-40	WMAX	Maximum Z-displacement

Card 7: Material property card 1 (6D10.5)

<u>Column</u>		<u>Contents</u>
1-10	PROP (1)	E ₁₁
11-20	PROP (2)	E ₂₂
21-30	PROP (3)	E ₃₃
31-40	PROP (4)	G ₂₃

41-50	PROP (5)	G_{13}
51-60	PROP (6)	G_{12}

Card 8: Material property card 2 (6D10.5)

<u>Column</u>		<u>Contents</u>
1-10	PROP (7)	v_{23}
11-20	PROP (8)	v_{13}
21-30	PROP (9)	σ_{12}
31-40	PROP (10)	α_{11}
41-50	PROP (11)	α_{22}
51-60	PROP (11)	α_{33}

Card 9: Angles (8D10.5)

<u>Column</u>		<u>Contents</u>
1-10	ANG (1)	Angle No. 1 (in degrees)
11-20	ANG (2)	Angle No. 2 (in degrees)
.	.	.
.	.	.
.	.	.
	ANG (NANG)	Angle No. "NANG" (in degrees)

Card 10: Element data (5x, 1415) repeat "NEM" times

<u>Column</u>	<u>Contents</u>
1-5	Blank (can put in element numbers)
6-10 NOD (I,1)	Node No. 1 of element I ¹
11-15 NOD (I,2)	Node No. 2 of element I ¹
16-20 NOD (I,3)	Node No. 3 of element I ¹
21-25 NOD (I,4)	Node No. 4 of element I ¹
26-30 IANG(I)	Angle number of element I ²
31-35 IEPS (I,1)	ϵ_{xx} number at local node 1 ³
36-40 IEPS (I,2)	ϵ_{xx} number at local node 2 ³
41-45 IEPS (I,3)	ϵ_{xx} number at local node 3 ³
46-50 IEPS (I,4)	ϵ_{xx} number at local node 4 ³
51-55 ISTRS (I,1)	Stress output location 1 ⁴
56-60 ISTRS (I,2)	Stress output location 2 ⁴
61-65 ISTRS (I,3)	Stress output location 3 ⁴
66-70 ISTRS (I,4)	Stress output location 4 ⁴
71-75 ISTRS (I,5)	Stress output location 5 ⁴

1. Refer to Fig. (F.1) for node numbering sequence.
2. Refer to Fig. (F.2) for angle orientation.
3. ϵ_{xx} numbers correspond to those of Card 16.
4. Stress output locations shown in Fig. (F.1).

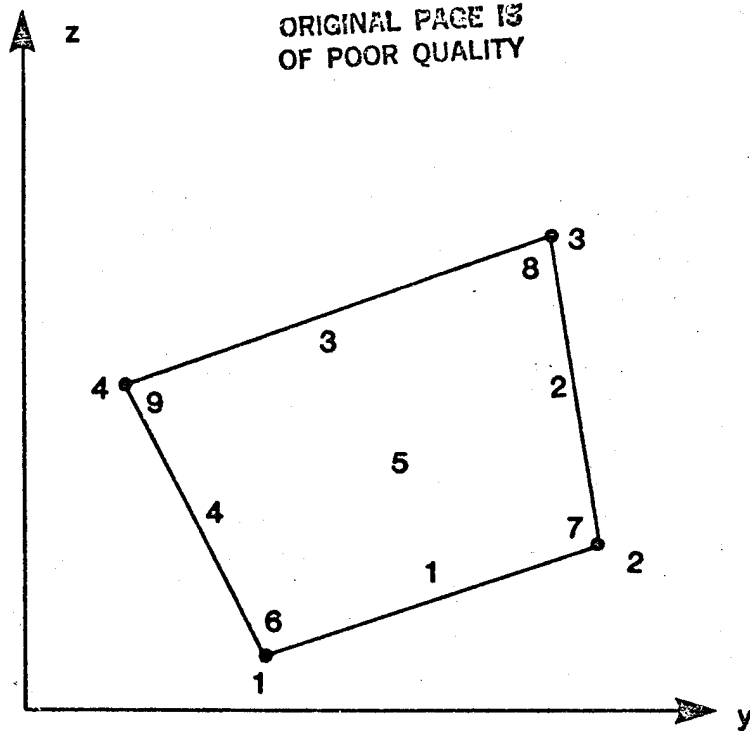


Figure F.1 Local Node Numbers And Stress-Strain Output Locations

ORIGINAL PAGE IS
OF POOR QUALITY

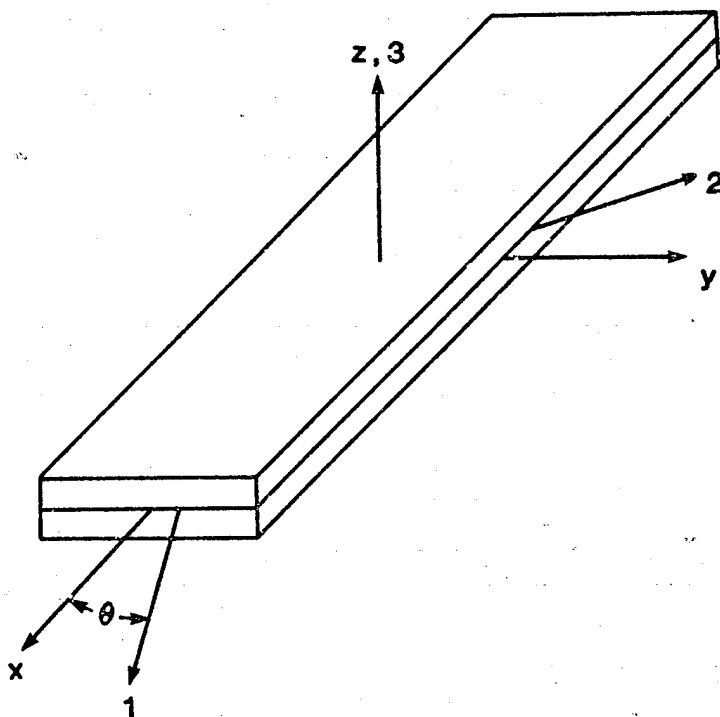


Figure F.2 Coordinate System And Orientation
Of Material Principal System.

Card 11: Nodal data (5x,2D10.5) - repeat "NODS" times.

<u>Column</u>	<u>Contents</u>
1-5	Blank (can put in node numbers)
6-15 Y(I)	Y coordinate of node I
16-25 Z(I)	Z coordinate of node I

Card 12: Specified displacement data (1I5,D10.5) - repeat "NSDF" times
and skip if NSDF = 0.

<u>Column</u>	<u>Contents</u>
1-5 ND	Node number
6-10 IDR	Direction (1 = x, 2 = y, 3 = z)
11-20 UBDF(I)	Specified displacement value

Card 13: Specified force data (2I5, D10.5) - repeat "NSBF" times
and skip if NSBF = 0.

<u>Column</u>	<u>Contents</u>
1-5 ND	Node number
6-10 IDR	Direction (1 = x, 2 = y, and 3 = z)
11-20 UVSF(I)	Specified force value

Card 15: Temperature data (1D10.5)

<u>Column</u>	<u>Contents</u>
1-10 TEMP	Temperature change

Card 16: Normal (x-direction) strain data (8D10.5)

<u>Column</u>	<u>Contents</u>
1-10 EPSX(1)	ϵ_{xx} value No. 1
11-20 EPSX(2)	ϵ_{xx} value No. 2
.	.
.	.
.	.
EPSX(NEXX)	ϵ_{xx} value No. "NEXX"

*if NFX = 0, end of data

Card 17: Fracture control card (6I5,2010.5)

<u>Column</u>	<u>Contents</u>
1-5 NODE	Initial crack tip node number ¹
6-10 NODE1	Secondary node No. 1 ¹
11-15 NODE2	Secondary node No. 2 ¹
16-20 NSE	Number of stop elements (must be > 1)
21-25 NSN	Number of skip nodes (must be > 1)
26-30 NCRT	Fracture criteria NCRT = 1 Griffith NCRT = 2 Sih-strain energy density NCRT = 3 3-D point stress NCRT = 4 2-D point stress
31-40 ANOT	Initial crack length
41-50 TMAX	Maximum run time (CPU-seconds)

1. Refer to Fig. (F.3) for crack nodes description.

ORIGINAL PAGE IS
OF POOR QUALITY

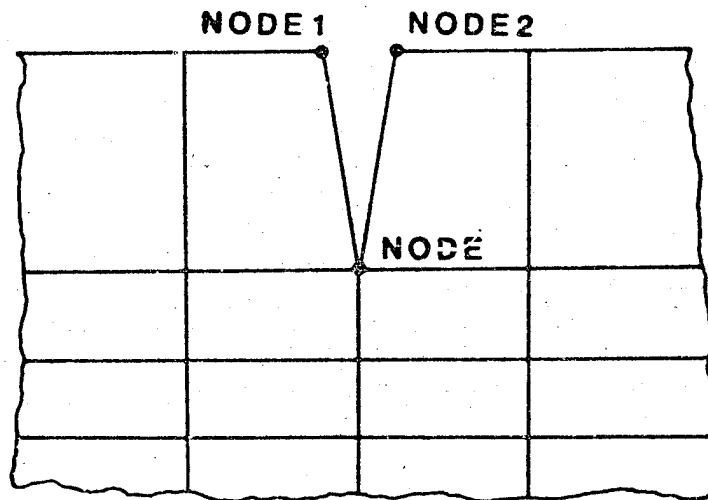


Figure F.3 Nodes Defining Crack Tip

Card 18: Stop element data¹ (1615)

<u>Column</u>		<u>Contents</u>
1-5	NSTOP (1)	Stop element No. 1
6-10	NSTOP (2)	Stop element No. 2
	.	.
	.	.
	.	.
	NSTOP (NSE)	Stop element No. "NSE"

Card 19: Skip node data² (1615)

<u>Column</u>		<u>Contents</u>
1-5	NSKIP (1)	Skip No. 1
6-10	NSKIP (2)	Skip node No. 2
	.	.
	.	.
	.	.
	NSKIP (NSN)	Skip node No. "NSN"

1. Stop elements terminate the solution when they are reached - used to prevent tear through.
2. Skip nodes are used to eliminate the designated nodes as crack growth possibilities - used to prevent tear through and the crack from growing back on itself.

Card 20: Strength properties (3D10.5)

<u>Column</u>		<u>Contents</u>
1-10	STRENG (1)	X _T
11-20	STRENG (2)	Y _T
21-30	STRENG (3)	Z _T
-----end of data-----		